Effects of Metal Ions from Implantable Biomaterials on Glycolytic Flux in Murine Bone Marrow-Derived Macrophages

by

Kyla Wilson

Thesis submitted to the University of Ottawa
in partial fulfilment of the requirements for the degree of
Master of Applied Science in Biomedical Engineering

Ottawa-Carleton Institute for Biomedical Engineering
University of Ottawa
Ottawa, Ontario, Canada

Acknowledgements

Firstly, I would like to extend a special thanks to Orthopaedic Bioengineering Laboratory (OBL) team members, Zeina Salloum and Jennifer Archibauld, for their knowledge, supportive attitudes and perpetual kindness.

I would also like to express my appreciation and gratitude to Dr. Mary-Ellen Harper and the members of her lab, David Patten, Chantal Pileggi, and Nidhi Kuksal, for their contributions and technical expertise in the application of the high performance liquid chromatography to my experiment model. I am grateful to Dr. Mary-Ellen Harper for use of the equipment and materials in her lab, and to her and all members of her lab for allowing me to feel welcome in the supportive and positive environment that can be found in their lab.

I would also like to convey my sincerest appreciation to Dr. Baddour for her support and guidance throughout the writing and completion of my thesis. The support of Dr. Baddour and Dr. Harper during this process has been invaluable, for which I would like to express a heartfelt thank you.

Last but not least, I would like to thank my family for their undying support throughout this journey and without whom I would not have been able to complete this thesis. In particular, I would like to thank my dad (Tyler), my mom (Penny), my brother (Ryley), my best friend (Jax, my loving Great Pyrenees), and my partner (Curtis). To all of you, I am eternally grateful.

Again, I would like to offer my utmost appreciation and thanks to everyone who made this thesis possible.

Thesis Organization

Chapter 1 introduces the context of the work.

Chapter 2 is the literature review focusing on biomaterials and orthopaedics, specifically hip implants; implant biomaterials, properties and mechanisms of failure; metal ions and metal ion toxicity; reactive oxidative species and oxidative stress; and, finally, macrophage metabolism and the immune response to metal ions.

Chapter 3 is the rationale of the work and describes the aims, objectives and hypothesis of this thesis.

Chapter 4 details the material and methods for the methodologies of the glycolytic flux assay (extracellular acidification rates [ECAR] and proton efflux rates [PER]) and the glutathione determination (high performance liquid chromatography [HPLC]).

Chapter 5 presents the results for the glycolytic flux assay and discussion of the results, as well as technical considerations for the work.

Chapter 6 presents the results on the improvement of BMDM recovery after exposure to metal ions for future reduced and oxidized glutathione determination by HPLC.

Chapter 7 is the overall thesis summary, which includes conclusions from the work and suggestions for future studies.

References list the scholarly works referred to in this thesis.

Appendix contains supplementary information for data collected during CO_2 Contribution Factor (CCF) experiments.

Abstract

Total joint replacement surgeries are currently the most cost effective method for joint restoration. However, approximately 10% are expected to fail in the first 10-15 years post-implantation. Failure occurs primarily due to aseptic loosening resulting from bone loss around the implant (i.e., periprosthetic osteolysis), which, itself, is caused primarily by an inflammatory response to implant wear and corrosion products. Some metal ions from implant wear and corrosion have been shown to decrease oxidative phosphorylation (OXPHOS) and alter redox status in macrophages. This metal ion-induced decrease in OXPHOS may be associated with increased glycolytic flux to help maintain energy homeostasis and cellular redox status. Consequently, the primary objective of this thesis was to analyze the effects of Co^{2+}, Cr^{3+} and Ni^{2+} on glycolytic flux parameters in BMDMs. Additionally, BMDM harvest after exposure to Co^{2+}, Cr^{3+} and Ni^{2+} was optimized to ultimately measure reduced and oxidized glutathione by HPLC to evaluate cellular redox status. Murine BMDMs prepared from C57BL/6NCrl mice were exposed to various concentrations of Co^{2+}, Cr^{3+} or Ni^{2+}, and glycolytic flux was measured using an extracellular flux analyzer. Overall, results demonstrate that Co^{2+} and Ni^{2+}, but not Cr^{3+}, lead to an increase in glycolytic flux in BMDMs. These results, together with a previous study showing that Co^{2+} and Ni^{2+} decrease OXPHOS in murine BMDM, suggest that Co^{2+} and Ni^{2+} (but not Cr^{3+}) can induce a metabolic shift away from OXPHOS towards glycolysis in macrophages. This metabolic shift may play a critical role in the inflammatory response induced by Co^{2+} and Ni^{2+} in the periprosthetic environment. This research will improve our understanding of the mechanisms underlying implant failure, and potentially facilitate the development of therapeutic approaches to increase implant longevity in the future.

Table of Contents

Acknowledgements ..... **ii**

Thesis Organization ..... **iii**

Abstract ..... **iv**

List of Figures ..... **viii**

List of Abbreviations ..... **ix**

1 Introduction **1**

1.1 Background 1

1.2 Objectives of the thesis 2

1.3 Contributions of the thesis 2

2 Literature Review **3**

2.1 Total Joint Replacements 3

2.2 Medical Applications of Orthopaedic Joint Implants 3

2.3 Implant Failure and Biocompatibility 4

2.4 Hip Implant Design 5

2.4.1 Articulating Surface and Wear 5

2.5 Implant Biomaterials and Properties 6

2.6 Metal Ions: Physiological Mechanisms and Toxicity 9

2.6.1 Metals and Reactive Oxidative Species 11

2.6.2 Physiological ROS Production 11

2.6.3 Oxidative Stress 13

2.7 Physiological Impact of Metal Ions on Mechanisms of Implant Failure 15

2.7.1 Metal-Induced Innate Immune Response 16

2.7.2 Macrophage Activation by Wear Particles and Metal Ions 16

2.7.3 Macrophage Metabolism and Pro-inflammatory Stimuli 18

3 Rationale 22

3.1 Objectives and Hypothesis 22

4 Materials and Methods 23

4.1 Metal Ions 23

4.2 Murine BMDM 23

4.3 Improved Glycolytic Stress Test: Extracellular Acidification Rate (ECAR) 24

4.3.1 Buffering Factor (BF) 26

4.3.2 Proton Efflux Rate (PER) 26

4.3.3 Statistical Analysis for Glycolytic Flux Parameters 28

4.4 Cell Mortality 28

4.5 GSH and GSSG Determination 29

4.5.1 Optimization of BMDM Sample Preparation 31

5 Glycolytic Flux: Results and Discussion 33

5.1 Effects of Co^{2+}, Cr^{3+} and Ni^{2+} on Extracellular Acidification Rate (ECAR) 33

5.1.1 Effect of Co^{2+}, Cr^{3+} and Ni^{2+} on Proton Efflux Rate (PER) 37

5.2 Technical Considerations 42

5.2.1 Optimizations of the Improved Glycolytic Stress Test 42

6 Sample Preparation Improvements for Future GSH and GSSG Determination in BMDM Exposed to Metal Ions 45

6.1 Preliminary Experiments on GSH and GSSG Determination by HPLC 45

6.1.1 BMDM Dish Surface Treatment and Seeding Density 46

6.1.2 Effect of Co^{2+}, Cr^{3+} and Ni^{2+} on BMDMs Recovery 48

6.1.3 Effects of the Detachment Technique on Cell Recovery 49

7 Thesis Summary and Conclusions 52

7.1 Choice of Ions and Cell Culture Model 52

7.2 Effects of Co^{2+}, Cr^{3+} and Ni^{2+} on Glycolytic Flux in BMDMs 53

7.3 Optimization of BMDM Recovery after Exposure to Metal Ions for future GSH and GSSG Determination by HPLC 55

7.4 Conclusions of the Present Study 56

7.5 Future Studies 56

7.5.1 Hypoxia-inducible factor-1α (HIF-1α) 57

7.5.2 Quantification of PPP Flux 58

7.5.3 Measurement of Intracellular ROS and Oxidative Stress 58

References 60

Appendix 84

CO_2 Contribution Factor (CCF) 84

List of Figures

Figure 5-1 Glycolytic flux parameters in BMDMs following a 6-h exposure to 0-24 ppm Co^{2+}.. Data: means ± SEM of an N of 4. 34
Figure 5-2 Glycolytic flux parameters in BMDMs following a 6-h exposure to 0-96 ppm Ni^{2+}. Data: means ± SEM of an N of 4. 35
Figure 5-3 Glycolytic flux parameters in BMDMs following a 6-h exposure to 0-200 ppm Cr^{3+}. Data: means ± SEM of an N of 5. 36
Figure 5-4 Proton efflux rates (pmol H+/min/µg protein) in BMDMs following a 6-h exposure to Co^{2+} (0-24 ppm). Data: means ± SEM of 4. 38
Figure 5-5 Proton efflux rates (pmol H+/min/µg protein) in BMDMs following a 6-h exposure to Ni^{2+} (0-96 ppm). Data: means ± SEM of 4. 40
Figure 5-6 Proton efflux rates (pmol H+/min/µg protein) in BMDMs following a 6-h exposure to Cr^{3+} (0-200 ppm). Data: means ± SEM of 5. 41
Figure 6-1 Recovery of BMDMs (% nominal seeding density) for TC-treated plates vs. suspension plates at 85,000 cells/cm^2, 425,000 cells/cm^2, and 850,000 cells/cm^2.. 47
Figure 6-2 Recovery (% nominal seeding density) of viable (TB^-) and non-viable (TB^+) BMDM in 6-well TC-treated plates seeded at 425,000 cells/cm^2 with a 12 hour exposure to 18 ppm Co^{2+}, 150 ppm Cr^{3+} and 48 ppm Ni^{2+}(N=1). 48
Figure 6-3 Recovery of BMDMs (% nominal seeding density) that were seeded at 425,000 cells/cm^2 in 6-well and 24-well TC-treated plates and exposed to 18 ppm Co^{2+}, 150 ppm Cr^{3+} or 48 ppm Ni^{2+} for 12h (N=1). 49
Figure 6-4 Recovery (% nominal seeding density) of viable (TB^-) and non-viable (TB^+) BMDM that were seeded at 425,000 cells/cm^2 in 24-well TC-treated plates and exposed to 18 ppm Co^{2+}, 150 ppm Cr^{3+} or 48 ppm Ni^{2+} for 12h (N=1).. 50

List of Abbreviations

Abbreviation	Term
2-DG	2-Deoxyglucose
Al	Aluminum
ANOVA	Analysis of variance
As^{3+}	Trivalent arsenic
ATP	Adenosine triphosphate
BF	Buffering factor
BMDMs	Bone marrow-derived macrophage
BSA	Bovine serum albumin
CCCP	Carbonyl-cyanide m-chlorophenyl
CCF	Co_2 contribution factor
Cd^{2+}	Divalent cadmium
CGM	Complete growth medial
CJRR	Canadian Joint Replacement Registry
Co	Cobalt
CoC	Ceramic-on-ceramic
CoCrMo	Cobalt-chrome-molybdenum
Cr	Chromium
DAMPs	Danger associated molecular patterns
DMEM	Dulbecco's modified eagle Medium
DPBS	Dulbecco's phosphate-buffered saline
EA	Extracellular acidification
ECAR	Extracellular acidification rate
EDTA	Ethylenediaminetetraacetic acid
ETC	Electron transport chain
$FADH_2$	Flavin adenine dinucleotide
Fe	Iron
GP	Glutathione peroxidase
GR	Glutathione reductase
GSH	Glutathione
GSSG	Glutathione disulfide
H^+	Protons
H_2O_2	Hydrogen peroxide

HCO^{3-}	Bicarbonate
HIF-1α	Hypoxia-inducible factor-1α
HPLC	High performance liquid chromatography
HR	Hip resurfacing
IL-1/IL-6	Interleukin-1 or -6
LAL	Limulus amebocyte lysate
LPS	Lipopolysaccharide
MIM	Mitochondrial inner membrane
Mo	Molybdenum
MoM	Metal-on-metal
MoP	Metal-on-polyethylene
MPA	Meta-phosphoric acid
NADH	Nicotinamide adenine dinucleotide
NADPH	Nicotinamide adenine dinucleotide phosphate
NaOH	Sodium hydroxide
NF-κβ	Nuclear factor-κβ
Ni	Nickel
NIH	American National Institute of Health
NLRs	NOD-like receptors
NO	Nitric oxide
NOX	NADPH-oxidase
O_2^-	Superoxide anion
OCR	Oxygen consumption rate
•OH	Hydroxyl radical
ONOO	Peroxynitrite
OXPHOS	Oxidative phosphorylation
PAMPs	Pathogen-associated molecular patterns
PER	Proton efflux rate
PMF	Proton motive force
PMMA	Polymethyl methacrylate
PPP	Pentose phosphate pathway
RNS	Reactive nitrogen species
ROS	Reactive oxidative species
RPMI	Rosewell Park Memorial Institute
RT	Room temperature
SOD	Superoxide dismutase

TB	Trypan blue
TCA-cycle	Tricarboxylic acid cycle
TC-treated	Tissue culture-treated
TFA	Trifluoroacetic acid
THA	Total hip arthroplasty
Ti	Titanium
TJR	Total joint replacement
TLRs	Toll-like receptor
TNF-α	Tumor necrosis factor-α
UHMWPE	Ultra-high molecular weight polyethylene
UQ10	Ubisemiquinone
XLPE	Highly cross-linked polyethylene
Zn^{2+}	Divalent zinc

1 Introduction

1.1 Background

Over 130,000 total joint replacement surgeries were performed in Canada in 2018 [1]. These surgeries are commonly used to treat conditions such as osteoarthritis and are currently the most cost-effective method for joint restoration [2]–[4]. However, despite a high success rate and a lifespan of up to 20 years in 80% of individuals, implant failure is still a cause for concern [5]–[7]. Implant failure occurs primarily due to aseptic loosening resulting from bone loss around the implant (i.e., periprosthetic osteolysis), often caused by an inflammatory response to implant wear and corrosion products [8], [9]. Metals have been prominently used in a variety of implantable orthopaedic biomaterials due to their high mechanical reliability (e.g., fatigue strength and toughness), ability to easily meet manufacturing standards and low cost [10], [11]. However, metal ions released from implant wear and corrosion remain a major cause for concern. More specifically, cobalt and chromium ions released from cobalt-chrome-molybdenum (CoCrMo) implants have been shown to induce an innate inflammatory response and other adverse tissue reactions [12].

Previous studies have suggested that tissue damage caused by metal ions may occur due to mitochondrial dysfunction leading to increased levels of reactive oxygen species (ROS) [13]. Increased ROS production is suspected to have complex effects on cell metabolism and high levels of ROS have been reported to change the cellular ratio of reduced glutathione (GSH)/oxidized glutathione (GSSG) [14], [15]. In addition, it is well known that mitochondrial dysfunction leads to a decrease in oxidative phosphorylation, which in turn limits adenosine triphosphate (ATP) production that may be compensated by the activation of glycolysis [16]. Studies have also demonstrated that in macrophages, pro-inflammatory polarization has been associated with a metabolic switch from oxidative phosphorylation to glycolysis [16]. However, the effects of metal ions on glycolytic flux and the GSH:GSSG ratio in bone marrow-derived macrophages (BMDMs) remains largely unknown. Investigation into the potential relationship between metal ions and changes in glycolytic flux parameters may provide insight into the mechanisms involved in the macrophage-mediated response observed in periprosthetic tissues.

1.2 Objectives of the thesis

The primary objective of this thesis is to analyse the effects of Co^{2+}, Cr^{3+} and Ni^{2+} on glycolytic flux in BMDMs. Additionally, recovery of BMDMs exposed to Co^{2+}, Cr^{3+} and Ni^{2+} was improved for future determination of GSH and GSSG by HPLC.

1.3 Contributions of the thesis

This thesis demonstrates that Co^{2+} and Ni^{2+}, but not Cr^{3+}, led to an increase in glycolytic flux parameters in BMDMs. Furthermore this thesis establishes an improved method for preparing BMDMs exposed to Co^{2+}, Ni^{2+}, and Cr^{3+}. The results of the thesis suggest that in BMDMs treated with metal ions the following three improvements are necessary to achieve sample reproducibility:

a) BMDMs are seeded in 24-well tissue-culture treated dishes
b) BMDMs are seeded at a density of 425,000 cells/cm^2
c) Samples are collected using one or two treatments with an enzymatic detachment solution (Accutase).

These results may contribute to a better understanding of how macrophages respond to metal ions. These results could eventually lead to new avenues of exploration to improve implant longevity. Moreover, they may lead to the development or improvement of therapeutic approaches to treat adverse reactions, and aseptic inflammation associated with metal implantable biomaterials.

2 Literature Review

2.1 Total Joint Replacements

Total joint replacement (TJR) surgery, especially for the knee and hip, is currently the leading treatment for patients suffering from joint impairment or pain [5], [17]–[22]. It is an effective and common option to treat pain and impairment associated with degenerative joint disorders, and is also frequently used in older patients following physical trauma, such as fracture or dislocation [17], [18]. The number of TJR surgeries to be performed annually is anticipated to increase substantially in the coming decades largely due to the aging population, increased participation in sports and increased occurrence of diabetes and obesity [23]–[25]. According to Kurtz et al. [3], primary total hip arthroplasties (THA) are projected to increase by 174% between 2005 and 2030. Moreover, hip revision surgeries are expected to double by 2026 [3]. In Canada alone, approximately 59,000 hip replacements and over 70,000 knee replacements were performed in 2017-2018, as per the Canadian Joint Replacement Registry (CJRR). In the last five years, this accounts for an increase of 17.4% and 17%, respectively [4].

2.2 Medical Applications of Orthopaedic Joint Implants

TJRs are a broadly applicable treatment for many age-related degenerative joint disorders including osteoarthritis, osteoporosis, and/or avascular necrosis related to the deterioration of tissues in/on or around the joint [5], [17], [26]. Degenerative diseases lead to a loss of cartilage surrounding the joint, reduction in bone density or, in some cases, osteonecrosis (i.e., death of bone tissue). They all contribute to pain and reduced quality of life of the patients. Hip and knee pain associated with these conditions can be corrected by a joint replacement to improve quality of life and mobility [5]. Osteoarthritis is associated with aging, systemic inflammation, overuse, obesity, genetic factors and/or developmental defects leading to the deterioration of articular cartilage [27]. Reduced cartilage at the articular surface of the joint is then followed by bone degeneration or changes to the underlying bone. Osteoporosis is associated with the loss of bone density and is more common in women than men [27]. The clinical significance of osteoporosis lies in its relationship to increased incidence of fracture leading to the need for corrective orthopaedic surgeries. The aforementioned degenerative diseases and incidence of physical trauma thus lead to an increased need for implants in both younger and older patients. TJR

surgeries are safe and effective methods to treat these conditions [5], [18], [22], [28]. Hip implants are the largest weight bearing joint implant in the body, followed by knee and shoulder implants, and hence are an important area of study.

According to the British National Joint Registry, 93.2% of currently marketed hip implants will survive at least 13 years prior to requiring any revision or modification [6]. Furthermore, approximately 80% of the hip implants will have a lifespan of up to 20 years [5]–[7], [29], [30]. With elderly patients, the probability that the implant will outlive the patient is high. Unfortunately, with the growing need for implants among a younger population and medical advances that facilitate longer life expectancies, implant lifespan has become a cause for concern [31], and improving implant longevity is essential.

2.3 Implant Failure and Biocompatibility

The anticipated lifespan of a hip implant is 20 years in 80% of cases, while knee implants are only slightly less successful [5], [6], [22]. Beyond this lifespan, there are multiple reasons for implants to fail and subsequently require a more complex secondary surgery, referred to as a revision. A revision consists of a thorough debridement and replacement of worn or damaged implant components [32]. Furthermore, effective revision surgeries rely on the initial preservation of adequate healthy tissues during the primary THA. Up to 75% of hip implant failures are aseptic [5]. Aseptic failure refers to failure unrelated to infection. Most of these failures are due to aseptic loosening caused by periprosthetic osteolysis, other reasons include recurrent dislocation (6%), periprosthetic fracture (5%), or technical errors during surgery (3%) [5], [22], [33]–[37].

Studies have shown that more than 70% of hip revisions and more than 44% of knee revisions become necessary due to aseptic loosening [36], [38]–[41], which cause instability of the implant within the joint cavity [42], [43]. This instability significantly increases the risk of fracture and causes an exceptional amount of pain. Generally, aseptic loosening results from periprosthetic osteolysis, i.e., bone loss around the implant, which is often initially asymptomatic [17], [42]–[44]. Some risk factors contributing to periprosthetic osteolysis include increased weight, age, and activity level, female gender, and reduced bone quality [36], [45], [46]. Many studies have shown that metal ions and particles from implant wear and corrosion are the main cause for periprosthetic osteolysis [22], [47]. Studies have also shown that metal ions and

particles can lead to the development of adverse local tissue reactions, including type IV hypersensitivity responses and pseudotumors (i.e., destructive soft tissue masses) that can also lead to implant failure [5], [22], [47]–[51]. While the mechanisms underlying the immune response to implant wear particles and metal ions remain an active research area, wear and corrosion are tightly linked to implant design, material properties and biomechanics.

2.4 Hip Implant Design

Hip implants are composed of a multi-axial ball-and-socket joint. The ball refers to the femoral head located at the top of the femur, while the socket refers to the acetabulum of the pelvis [52]. The ball-and-socket joint composes an articulating surface that allows movement within a range of three degrees of freedom [53]. The deep set socket of the pelvis reduces the chance of dislocation despite movement through multiple planes [61], [62]. There are four classical components of a hip implant: 1) acetabular component or shell, 2) acetabular lining, 3) femoral head and, 4) femoral stem [55]. The prosthetic is composed of an acetabular component fixed into the acetabulum with a liner placed between the acetabular component and the femoral head. The femoral stem is then compacted into the femur [55]. There are two main types of hip replacement procedures available which require slightly different implant components; 1) Hip Resurfacing (HR) and, 2) stem-type devices. HR involves replacing only the articular surfaces (i.e., ball and socket) of the joint and is a bone-conserving alternative generally selected for younger patients [56]. Stem-type devices will be referred to as total hip replacements (THR) in this thesis to differentiate them from the HR. For THRs, both the articular surface and the neck of the femur are replaced, which introduces the addition of a stem component. Acetabular liners are used for both to reduce instability, friction and wear at the articular surface [55]–[57].

2.4.1 Articulating Surface and Wear

Most component designs for hip prosthetics promote stability, however the mechanical articulating surface of the joint still has contact interfaces that undergo wear [5]. Wear refers to a loss of material from the interacting surface in relative motion due to energy dissipation in the form of friction [18], [48]. Joint surfaces are subjected to a significant amount of friction resulting in multiple types of wear, such as abrasive and third-body wear [58]. Therefore, it is

essential to select materials with wear resistance and use implantation methods that reduce the wear rate in hip prosthetics.

2.5 Implant Biomaterials and Properties

The most common biomaterials used for these prosthetics are metallic alloys, ceramics, or polymeric biomaterials such as ultra-high molecular weight polyethylene (UHMWPE) [6], [59]. Two primary concerns remain when utilizing biomaterials: (1) mechanical properties, and (2) biocompatibility [60]. Biomaterials were first defined in 1987 as a nonviable material intended to interact with biological systems for a medical device [61]. The definition of a biomaterial has since evolved and is now defined by the American National Institutes of Health (NIH) as; "any substance or combination of substances, other than drugs, synthetic or natural in origin, which can be used for any period of time, and which augments or replaces partially or totally any tissue, organ, or function of the body, in order to maintain or improve the quality of life of the individual" [62]. However, it is often preferred to incorporate the need for biocompatibility into definitions of a biomaterial. A biomaterial should encompass a host outcome that is biocompatible or which alternatively elicits a desirable host response.

Polyethylene

A common material used for acetabular components is polyethylene. Polyethylene comes in two forms based on the manufacturing process, either UHMWPE or a more highly cross-linked version of UHMWPE (XLPE) [41]. UHMWPE was the first generation of polyethylene, typically used in tandem with either metal or ceramic femoral heads [6], [17]. UHMWPE wear rates for this bearing couple were shown to range from 0.01 to several millimeters per year [17], [63]. However, highly cross-linked XLPE was later developed and was shown to have lower wear rates than conventional UHMWPE [17], [64]. Generally, all metals and ceramics have higher surface hardness than polyethylene materials, making them more resistant to wear [6], [65]. Conventional UHMWPE particles have also been isolated as a main perpetrator in aseptic loosening due to the inflammatory response [34], [66]–[68].

Ceramics

Ceramic-on-ceramic (CoC) implants are used due to their low wear rates and high biotolerability [6]. However, ceramics are less ductile than metals, making them less resistant to brittle fracture, a common problem with CoC which carry a higher risk of breakage [6], [69].

Metals

Metals are a commonly used material due to their ideal mechanical characteristics, and easy workability (they can be easily fabricated into complex shapes), while simultaneously meeting manufacturing standards [78]. CoCrMo alloys have been used as implant bearing surfaces due to their hardness, toughness and overall wear resistance [71]–[73]. CoCrMo alloys are also easily workable and relatively resistant to corrosion [41]. Titanium-alloys are another common material, typically used for the femoral stem, with a high level of biocompatibility and lower elastic modulus than other metals which can be preventative against stress shielding. Titanium is also relatively corrosion resistant and has an easily modified surface [41], [74]. However, titanium is softer than most metals which makes it more susceptible to wear, and is easily scratched making it unsuitable for femoral head components [41]. Stainless steel is sometimes used for femoral implants due to its relatively high strength and low cost. However, it has a higher tendency for corrosion than other materials and a lower fatigue strength [41]. The predominant stainless steel alloy used in hip implants is stainless steel 316L. This alloy contains high concentrations of both chromium (16-18%) and nickel (10-14%), which permit a corrosion-resistant oxide layer at the implant surface [75], [76]. Therefore, despite the generally bio-inert properties of stainless steel, these implants have some associations with nickel sensitivity reactions and the release of metal ions from wear and corrosion [76].

Bearing Material Combinations

Ball-and-socket joints typically use a combination of different biomaterials for manufacturing. Some implant bearings include metal-on-polyethylene (MoP), metal-on-metal (MoM), and CoC. The most common choice has been MoP because it is a predictable and cost effective option. However, the release of sub-micron sized UHMWPE particles from conventional MoP implants made of UHMWPE was found to be a cause of periprosthetic

osteolysis, which can lead to implant loosening and consequently failure [77]. In an attempt to improve the wear properties of the conventional MoP implant, XLPE was introduced into the market in the last two decades, replacing UHMWPE components. In addition, interest in MoM hip implants re-emerged due to lower volumetric wear rate compared to conventional MoP, and a new generation of MoM implants were introduced in the 1980's [47], [48]. With the second generation of MoM implants, the wear particle-induced periprosthetic osteolysis is lower than with the conventional MoP, and the volumetric wear is lower than the first generation (1950/60s) of MoM implants [47]. However, concerns regarding the high concentration of metal ions released from implantable metals remain. Such concerns include metal ion toxicity and related adverse tissue reactions, causing investigation into MoM implants and metal implant components to re-emerge [77].[47]. Hence, one of the primary goals of this thesis is to further the understanding of the effects of metal ions from the implant wear and corrosion, or as a result of macrophage-mediated degradation of metal wear particles. Macrophages are phagocytes, which are cells of the immune-system, and participate in the response to wear particles.

Corrosion

Mechanical acceleration of corrosion in socket-joints through friction and energy dissipation is a contributor to the release of wear debris with metal implants. Complications associated with the highly corrosive behaviour exhibited by metals in the environment of the body are a cause for concern. The moisture present in human or animal tissues, combined with the warm temperature and neutral pH, cause the metal atoms to undergo an electrochemical dissolution [78]. The valence state of the metal is increased relative to its ionic form. In order for metals to achieve equilibrium in the tissue, electrons in the form of ions are released into the surrounding matter [78], [79]. Ions have been shown to accumulate in the tissues surrounding the implant, as well as disseminate to sites distant to the device causing adverse effects both locally and systemically [80], [81]. Furthermore, the ions have been shown to accumulate in relatively high concentrations near the head and along the stem as an effect of bone movement [79].

2.6 Metal Ions: Physiological Mechanisms and Toxicity

Heavy metals are naturally found in small quantities in the human body, as well as many biological systems. For example, metals such as iron or zinc in trace quantities are well-known essential metals for human health [80]. Iron is largely known for its role in oxygen carrying capacity of red blood cells, while zinc is widely accepted as an important component of wound healing [89], [90]. Metals that are also found in implants, such as Co, Cr, aluminum (Al), titanium (Ti), Ni and Mo are less frequently discussed in the context of the human system, but also feature prominent roles and need to be present to facilitate many biological functions [80]. However, in excess these metals can have largely detrimental biological effects [80].

Metal ions in the host system may arise directly from implant wear and corrosion at the implant surface, or through macrophage-mediated degradation of metal particles in the tissues surrounding the implant [84]. The degree of toxicity for these ions is linked to oxidation state, charge, concentration and time of exposure [80]. Co is an essential ion necessary for the normal biological function of vitamin B12, an important nutrient involved in the maintenance of nerve cells and other tissues [85]. Alternatively the inorganic form, as released due to corrosion, can lead to many negative cellular modifications [85], [86]. Most commonly, Co ions are found in two primary oxidation states Co^{2+} and Co^{3+} but, in physiological environments are typically found in the reduced form [87]. Therefore, Co^{2+} is the most commonly studied relative to implant corrosion [18], [66], [80], [88]. High concentrations and long exposure times to Co^{2+} can have a multitude of consequences through interactions with the host. Two ways in which Co^{2+} interacts with the host includes: (1) entering the cells through the calcium channels preventing normal calcium signalling [89], [90], and (2) binding to toll-like receptors (TLR), specifically TLR4 in human macrophages [91], [92]. Interestingly, Ni ions (specifically, Ni^{2+}) have been shown to interact with the host system through these two mechanisms as well. Ni^{2+} and Co^{2+} have very similar ionic radii (0.74 and 0.72 Å, respectively), allowing them to enter and block calcium channels (0.99 Å) in a voltage-dependant way [90]. Blocking these channels can result in the inhibition of important mitochondrial enzymes that ultimately participate in the production of ATP through mitochondrial oxidative phosphorylation [89]. Furthermore, Co^{2+} has been shown to outcompete Fe for its binding site in Fe-S clusters [93], and Ni^{2+} has been shown to decrease activity of Fe-containing enzymes [94]. Fe-S clusters are essential components of the mitochondrial electron transport chain (ETC) in the oxidative phosphorylation system [93], [94].

Cr is also important in small quantities and is implicated in the modulation of glucose metabolism through interactions involving insulin [95]. However, Cr can have detrimental physiological effects, which are also dependant on its concentration and oxidation state. Cr is typically present in +3 and +6 oxidation states but in physiological environments is rapidly reduced to the more stable form Cr^{+3} [80], [88]. The reduction of Cr^{6+} to Cr^{3+} can produce organic radicals. Cr^{6+} is freely able to cross cell membranes in its ionic form and is often reduced to Cr^{3+} after crossing the cell membrane. In the reduced form, Cr^{3+} has been shown to complex in simulated physiological fluids with organic or inorganic molecules as well as phosphates or phosphoproteins [88]. Once Cr^{3+} has formed complexes, they are able to interact with the host-system, cross the cell membrane and are often taken up by macrophages through phagocytosis [18], [88].

Studies have already established that patients with CoCrMo-based implants have highly elevated concentrations of Co^{2+} and Cr^{3+} ions [96]–[98]. The concentration of metal ions can provide insight into the post-operative health of implant patients. Reference levels of these ions measured in blood, urine and other bodily fluids derived from metal orthopaedic devices were reported in a study by Sargeant and Goswami [79]. This study incorporated data from 1375 patients and demonstrates that some ions are retained in the synovial fluid and joint capsule while some migrate in the blood or are excreted in the urine [79]. The ion levels measured in serum are frequently used measures in clinical practices. Choi *et al*. [99] reported a serum level in healthy patients of 0.13-0.80 ppb and 0.17-0.87 ppb for Co and Cr, respectively. The post-operative values increased significantly to concentrations of 0.61-115.8 ppb and 0.12-127.8 ppb for Co and Cr, respectively. Co^{2+} and Cr^{3+} are of particular interest because they are present in the joint capsule in high quantities and have the capacity to form organometallic complexes with zwitterions or negatively charged proteins [79]. These ions are positively charged (i.e., cations) which allows them to easily complex in the body's neutral pH. The formation of these organometallic complexes changes the pH of the environment which possibly contributes to the toxicity of these ions and increases their transportability and storage capacity in surrounding tissues [79].

2.6.1 Metals and Reactive Oxidative Species

Some of the metal ions released from implants are redox-active transition metal ions and participate in reduction and oxidation reactions (i.e., redox reactions). These ions contribute to the formation of ROS and reactive nitrogen species (RNS) [80], [100], which are oxidizing species in the form of radicals that can result in damage through their participation in redox reactions [101]. More specifically, radicals are a chemical species that contain one or more unpaired electrons making them highly reactive. Examples of radicals include hydroxyl radical (•OH), superoxide anion (O_2^-), nitric oxide (NO), and peroxynitrite (ONOO). ROS and RNS in the body are produced as natural by-products of metabolism.

2.6.2 Physiological ROS Production

ROS, as well as RNS, if kept at tolerable levels, are essential signalling molecules. They are involved by providing intracellular feedback information to the cell regarding metabolism from signals such as hypoxia, satiety and adipocyte differentiation [102]–[105]. ROS levels are important for redox regulation controlling physiological cellular responses, and modulating certain transcriptional events [106], as well as numerous metabolic activities [107]. In most cell types the mitochondria are the primary site of ROS production, although ROS may also be derived from organelles: such as, the endoplasmic reticulum (under stress) and in peroxisomes [107], [108]. Mitochondrial redox reactions are the largest contributors to ROS and are chiefly associated with cellular energy transduction. However, in certain cell types, cytoplasmic ROS may be derived from the nicotinamide adenine dinucleotide phosphate (NADPH) oxidase (NOX) enzyme, producing O_2^- [109]. Importantly, NOX enzymes have Fe^{2+} containing active sites which may be displaced by redox-active metal ions, such as Co^{2+} [110]. A study by Dixon *et al* [110] showed that this may contribute to an increase in iron-catalysed ROS in oxygen rich environments. Actually, 0.2-2% of oxygen consumed is converted to ROS during metabolism [102].

Metabolic Contribution to ROS

There are two main metabolic pathways associated with ATP production, which can contribute to redox and ROS homeostasis: glycolysis and oxidative phosphorylation (OXPHOS). Glycolysis produces ATP through the catabolism of glucose in the cytosol, while OXPHOS produces ATP through oxidative processes in the mitochondria. During glycolysis, glucose is broken down into pyruvate, which is then converted to acetyl-CoA in the mitochondria for entry into the tricarboxylic acid (TCA)-cycle. The latter process generates reduced forms of nicotinamide adenine dinucleotide (NADH), flavin adenine dinucleotide ($FADH_2$), and leads to substrate-level ATP production. The ETC pumps protons across the inner membrane of the mitochondria, thereby creating an electrochemical gradient that is then used by ATP synthase to generate ATP. This form of ATP generation is OXPHOS [102], [111]–[113]. The reduced NADH carries reducing equivalents to the ETC for subsequent OXPHOS production of ATP. The proton motive force (PMF) across the mitochondrial inner membrane (MIM) acts as a temporary store of Gibbs free energy which drives ATP synthase, consequently producing ATP [102]. The ETC is composed of a series of protein complexes that allow for the transfer of electrons using electron carriers such as ubisemiquinone (UQ10) and Fe-S clusters to pump protons against the gradient [111], [113], [114]. Using these electron carriers, particularly UQ10, metabolites such as NADH can transfer electrons to oxygen. Moreover, complex I and complex III of the ETC are the major sites of ROS production, and lead to the formation of ROS in the form of O_2^- [114]–[119]. O_2^- from these reactions can then be converted into hydrogen peroxide (H_2O_2) by superoxide dismutase (SOD)2 in the mitochondrial matrix, and SOD1 in the cytoplasm [117], [118]. H_2O_2 is less toxic, has a longer half-life and can traverse membranes and thus is another important signalling molecule, e.g., through reversible oxidation reactions with cysteine thiols of many proteins [102], [120].

ROS Contribution from Redox-Active Metals

The two primary forms of metabolically produced ROS are O_2^- and H_2O_2, however a more reactive species is the hydroxyl radical (•OH). •OH can be generated from H_2O_2 in the presence of metals [117]. Transition metals naturally occurring in the body such as iron (Fe), Cu, Co, Cr and Ni are able to participate in these reactions [121], [122]. As observed with Fenton

reactions [121]–[125]: $Fe^{2+} + H_2O_2 \rightarrow Fe^{3+} + \bullet OH + OH^-$, where Fe is well-known for its involvement by facilitating the reduction of hydrogen peroxide (H_2O_2) and results in the generation of •OH. The Haber-Weiss reactions take a step further, combining the Fenton equation with equations defined by Haber, Weiss, Wilstätter, and consider the involvement of metals as described by Barb *et al.* [121]–[123]. The Haber-Weiss equation describes the decomposition of H_2O_2 but defines a reaction that cannot occur in the absence of transition metals [112], [114]–[116]: $\bullet O_2^- + H_2O_2 \rightarrow O_2 + \bullet OH + OH^-$, where Fe^{2+} acts as a necessary catalyst facilitating the conversion. These equations highlight the importance of metals in redox reactions within the human system. In addition, investigations into these reactions have shown that metals can act as a catalyst for many of the redox reactions, which in turn produce excess radicals [122]. Thus, divalent metal cations can potentially contribute to increased levels of radicals and metal-mediated ROS production [111], [122]. Interestingly, Ozawa *et al.* [126] demonstrated that Cr^{6+} and Cr^{3+} have the capacity to undergo a series of Fenton-like reduction reactions that result in the generation of damaging hydroxyl radicals [79], [126], [127]. Furthermore, intracellular Co^{2+} has been shown to interact with H_2O_2 which also leads to the formation of •OH [80].

2.6.3 Oxidative Stress

At low levels, ROS are important signalling molecules interacting with many different biological pathways. However, abnormally high levels of ROS in the cell lead to oxidative stress, which refers to an imbalance between cellular levels of free radicals and antioxidant enzymes and compounds [128]–[130]. When ROS levels exceed homeostatic levels, their highly reactive nature can damage many cellular components leading to oxidative damage [108], [130]. Various studies have demonstrated that Cr^{3+} can lead to oxidative stress in a variety of cell types [80], [100], [131], and Ni^{2+} can lead to an increase in oxidative stress in BALB/3T3 and HepG2 cells [131]. Oxidative damage can include the oxidation of many important macromolecules such as lipids, proteins, and DNA which can alter many cellular functions [118], [130].

Lipid Peroxidation

Lipid damage is a critical concern stemming from oxidative damage due to the structural and functional role of lipids in membrane maintenance and formation. Lipids undergo peroxidation in the presence of ROS because the double bonds found in polyunsaturated fatty acids are vulnerable to oxidation. Polyunsaturated fatty acids are a category of biological lipids, as well as an important building blocks for many more structurally complex lipids [118], [130]. Furthermore, reactive metal ions have the potential to bind to other important biological components of the cell membrane, such as integral proteins and phospholipids. Disruption of the phospholipid bilayer can increase vulnerability to lipid peroxidation, change membrane structure and organization, and alter membrane function [128], [132], [133]. Overall, oxidative damage can lead to changes in DNA, RNA, carbohydrates, proteins, and lipids resulting in detrimental alterations to metabolic function, and potentially the induction of cell death [132].

ROS Homeostasis: Glutathione

Oxidative stress has been linked to many disease states and many mechanisms have evolved to combat it [128], [129], [132], [134]. To maintain healthy oxidant levels, there are multiple antioxidants and antioxidant enzymes in the body to neutralize oxidants. Glutathione (GSH) is the major non-enzymatic antioxidant in cells and is continuously replenished by its antioxidant enzyme counterparts (e.g., glutathione peroxidise, glutathione reductase) [117]. GSH is a thiol tripeptide that plays an important role in metabolic regulation through the reduction of H_2O_2 [102], [114], [117], [135]. In the cytosol, glutathione peroxidise (GP) enzymatically converts GSH to GSSG, as one molecule of H_2O_2 is converted to two water molecules. This prevents or decreases the opportunity for H_2O_2 to be reduced to the highly damaging and reactive •OH [117], [135], [136].

In the mitochondria, GP is necessary for regulation of H_2O_2 levels [114], [117]. Of particular interest is the involvement of GP in the intrinsic pathway where apoptosis is initiated via damage to the mitochondria due to elevated levels of ROS [79], [137]. Elevated ROS levels have been directly associated with metal ion toxicity [137]. Thus, GSH is particularly important in the detoxification of redox-active metals which have a high affinity for thiol groups.

Furthermore, GSH-S-transferases catalyse this reaction that binds the metal ions to the sulfhydryl (thiol) group of the GSH molecule.

In healthy cells, GSH concentration is highly regulated and GSSG is rapidly converted back to GSH by glutathione reductase (GR) to maintain a desirable GSH:GSSG ratio [138]. During this reduction, an NADP+ molecule is generated through the following reaction: $GSSG + NADPH + H^+ \rightarrow 2GSH + NADP^+$ [138]. NADPH is an important product of the pentose phosphate pathway (PPP) because it is required for maintaining GSH level [14], [139]. The PPP is a metabolic pathway that branches from the second step of glycolysis and plays a critical role in replenishing NADPH required for cellular redox homeostasis [14]. Since GSH is considered the most important cellular ROS scavenger, the GSH:GSSG ratio can provide vital insight into cellular metabolic health [14], [139], particularly with respect to the redox status of the cell. Therefore, despite the well-established role of GSH in scavenging ROS and mitigating metal-ion toxicity, the effect of metal ions from orthopaedic implants on the GSH:GSSG ratio in macrophages has yet to be thoroughly investigated. However, a study by Petit *et al.* [152] did investigate the role of Co and Cr ions on protein carbonyl content, a commonly used marker of oxidative damage [140]. Results showed an increase in protein carbonyl content in U937 monocytes in the presence of these metal ions [140]. *In vitro* studies have also demonstrated that Co^{2+} and Cr^{3+} ions can increase the production of ROS involved in tissue damage and apoptosis [80], [100], [141]. Moreover, a study by Balamurugan *et al.* [100] demonstrated that Cr^{3+}-induced apoptosis of lymphocytes was mediated by ROS production.

2.7 Physiological Impact of Metal Ions on Mechanisms of Implant Failure

The release of metal ions is a primary cause for concern with MoM hip implants [142], [143] because of effects such as cytotoxicity [79], [144]–[146], metal hypersensitivity [20], [147], genotoxicity and chromosomal changes [148]. Furthermore, ions are able to enter circulation, and can therefore cause these reactions both locally and remotely. Studies have demonstrated the potential of Co^{2+} and Cr^{3+} to induce tumour necrosis factor (TNF)-α release *in vitro* [149], as well as macrophage apoptosis or necrosis depending on the ion concentration and exposure duration [73]. However, the underlying mechanisms are still not well understood.

Metal ions are able to stimulate immunological responses through both specific (e.g., adaptive immune system) and non-specific immune reactions (e.g., innate immune system).

These reactions include metal hypersensitivity [37], [147] and pseudotumors [18], [49]. Studies have shown that metal ions can form organometallic complexes (e.g., haptens) [48], [150], which are capable of stimulating the adaptive immune system through a complex mechanism [37], [151]. The following review will focus on the innate-immune response (e.g., non-specific) to implant wear debris that leads to a foreign-body response.

2.7.1 Metal-Induced Innate Immune Response

As previously discussed, a principal mechanism governing implant failure is aseptic loosening, which occurs primarily as a result of periprosthetic osteolysis. The major initiating factor of periprosthetic osteolysis is the release of wear particles, primarily UHMWPE particles that induce an inflammatory response. Particle disease, a term coined in 1994 by Harris [140], encompasses the theory relating all particles released from implant surfaces with aseptic loosening and briefly relates it to chronic inflammation [152]. However, the concept was introduced in 1977 by Willert and Semlitsch, who made the initial connection between loosening tissue around the prosthesis (e.g., aseptic loosening) and wear debris [17]. The chronic inflammatory reaction to wear debris occurs as a result of a non-specific foreign-body response by the innate immune system [44], [153], [154]. Typically, the role of this inflammatory response is to eliminate foreign materials, stimulate tissue repair, and then resolve with as little collateral damage as possible [155].

2.7.2 Macrophage Activation by Wear Particles and Metal Ions

When the innate immune system is activated to protect the body against foreign materials such as wear particles, there is an influx of tissue-specific monocyte sub-populations, e.g., macrophages [17], [156], [157]. Macrophages play a vital role in the activation and maintenance of the inflammatory response to metal ions and implant wear particles [34], [68], [153], [154], [158], [159]. Macrophages are phagocytic cells that can sometimes express pro-inflammatory or anti-inflammatory characteristics depending on the stimulus for activation. The pro-inflammatory cytokines, including interleukin (IL)-1, IL-6, prostaglandins and TNF-α [154], [158], [160]–[163], lead to the recruitment of more macrophages that further augment the inflammatory response [153], [154]. The elevated levels of these cytokines have been found in

periprosthetic tissues [164], [165], and can stimulate the differentiation of cells into mature osteoclasts resulting in bone resorption around the implant [37], [166], [167]. Moreover, during an inflammatory response some studies show a decrease in osteoblast proliferation and impairment of osteoblast function [145], [166], [168]. Ultimately, this causes a local imbalance between osteoclast and osteoblast activities that can result in implant loosening.

Wear particles and by-products of implant corrosion appear to activate macrophages in multifaceted mechanisms that are not yet entirely understood and are currently an active area of research. An *in vitro* study with J774 murine macrophages demonstrated that high concentrations of Co^{2+} and Cr^{3+} can induce necrosis after prolonged exposure [73]. It has also been shown that TLRs can be activated by wear particles, as well as metal ions such as Co^{2+} and Ni^{2+} [91], [92]. Specifically, Raghavan *et al.* [91] demonstrated that Co^{2+} and Ni^{2+} are both able to stimulate an immune response by binding to TLR4s of human macrophages, possibly through receptor dimerization. Furthermore, TLRs are able to activate nuclear factor (NF)-κB [169], which is a transcription factor that plays an essential role in the inflammatory response and leads to the upregulation of many of the aforementioned pro-inflammatory cytokines [170]. Moreover, metal particles and ions have also been shown to lead to the activation of NLRP3 which is responsible for the assembly of the NLRP3 inflammasome; however, the mechanisms of activation are still not well understood [19], [171]. Notably, some literature has implicated ROS as an upstream signal leading to NLRP3 inflammasome induction [169], [172], and that mitochondrial damage can stimulate the NLRP3 inflammasome activation [173], [174].

Metal-Mediated Mitochondrial Dysfunction

As previously discussed, metal ions can induce redox-reactions and these reactions play an important role in cellular metabolism [175]. Li and Zhong [176] showed that exposure to Ni^{2+} can lead to mitochondrial ROS accumulation and induce pro-inflammatory cytokine secretion in BMDMs [176]. It has also been demonstrated that the presence of metal ions can lead to mitochondrial dysfunction and contribute to ROS accumulation in macrophages [13], [116], [176], [177]. The accumulation of redox-active metal ions can affect normal cell functioning, including the regulation of important mitochondrial and non-mitochondrial protein complexes [128]. Specifically, it was shown that cadmium (Cd^{2+}), a divalent transition metal cation known to accumulate in a number of organs, contributes to increased ROS [116]. The study

demonstrated that Cd^{2+} interacts with complexes of the ETC of the mitochondria, and that complex III was vulnerable to increased ROS-production associated with Cd^{2+} [116]. Furthermore, metal ion interference with ETC functioning can contribute to mitochondrial dysfunction. One study showed that the presence of zinc (Zn^{2+}) in high levels leads to decreased oxygen consumption and increase in the production of ROS in neuronal mitochondria [178], as well as decreased mitochondrial membrane potential, likely contributing to mitochondrial dysfunction [83], [111]. These studies demonstrate that there is a close association between elevated ROS and metal-ion associated mitochondrial dysfunction [94], [116]. The association is supported by another study, involving both Fe^{2+} and Fe^{3+}, which demonstrated that these ions cause similar effects: increasing ROS and membrane depolarization in a dose-dependent and time-dependent manner [179]. This same study showed that mitochondrial function was more severely impaired by Fe^{2+} than Fe^{3+} [179]. These studies demonstrate that metal ions are capable of increasing ROS [80], [100] and inducing mitochondrial dysfunction. Furthermore, ROS derived from the mitochondria are able to stimulate pro-inflammatory cytokine release through signal transduction pathways [180]. Mitochondrial dysfunction has been linked to the inflammatory response [181] in two important ways, such that: (1) increased ROS is capable of activating NF-kB which is a redox-sensitive transcription factor [182], and (2) activating the NLRP3 inflammasome through mitochondrial-derived DAMPs [181].

2.7.3 Macrophage Metabolism and Pro-inflammatory Stimuli

Macrophages are the major cell type involved in the inflammatory response to metal ions observed in periprosthetic tissues [63], [64]. Under conditions of high oxidative stress, macrophages are activated through the classical pro-inflammatory pathway [154], [154], [183]. In macrophages, high concentrations of ROS are able to induce the pro-inflammatory phenotype. In some cases, high levels of oxidation are utilized by macrophages as a mechanism to destroy phagocytised pathogens [183]. Studies have shown that in macrophages, pro-inflammatory polarization leads to a metabolic switch from OXPHOS to glycolysis for ATP production [14], [16], [183]. The metabolic phenomenon is closely linked to the Warburg effect where cells, in this case pro-inflammatory macrophages, rely primarily on aerobic glycolysis for ATP even in the presence of oxygen rather than mitochondrial OXPHOS [16], [183], [184]. Mitochondrial dysfunction compromises OXPHOS [185], and thereby may also disrupt energy-dependent

mechanisms such as apoptosis [186]. Energy depletion (i.e., low intracellular ATP levels) results in necrotic cell death and correspondingly, increased tissue damage [186].

Glycolysis

The Warburg effect was first described by Otto Warburg in the 1920's and was originally discovered in cancer cells [184], [187], [188]. Most cancer cells rely on glycolysis for ATP production, a counterintuitive metabolic adaptation since glycolysis is generally less efficient at ATP production than OXPHOS [187]. Glycolysis only produces 2 molecules of ATP per molecule of glucose, compared to the roughly 32 molecules generated through OXPHOS in the mitochondria [187], [188]. There are several hypotheses for why glycolytic activity and glucose uptake are increased in proliferative cells, even in the presence of oxygen [187], [188]. In 1956, Warburg proposed that the increase in glycolysis may be due to mitochondrial dysfunction [184]. However, another theory suggested that the Warburg effect may be to accommodate the tumour microenvironment, based on the principle that the acidification of the microenvironment may be necessary for tumor cross-signalling behaviours [188]. Glycolysis rapidly generates 2 molecules of ATP, during which glucose is broken down resulting in the production of protons (H^+) and lactate. It has been demonstrated that Co^{2+} increases glucose uptake in liver cells, fibroblasts, and myoblasts [189], and Ni^{2+} increases lactate production in human fibroblasts [190]. The elevated level of glucose consumption consequently leads to a decrease in pH (i.e., acidification) of the microenvironment [188], [191]. The TCA cycle in the mitochondria may also contribute to the pH of the microenvironment. The TCA cycle can contribute to acidification through respiration as CO_2 is converted into bicarbonate (HCO^{3-}) and H^+ in the mitochondria [192]. The metabolic adaptation seen in both tumor cells and pro-inflammatory stimulated macrophages is clear, yet the precise ontology of the phenomenon is still not fully understood [85], [87].

Interestingly, it has been demonstrated that ROS may also interfere with glycolysis by inhibiting glycolytic enzymes, and this consequently increases glycolytic flux through the oxidative branch of PPP responsible for the generation of NADPH [193]. Higher concentrations of NADPH allow more GSH production to combat elevated levels of oxidative stress [14], [193]. Recent studies with RAW 264.7 macrophages have found an important relationship between metal ions and cell metabolism [194]. Salloum *et al.* [107] showed that Co^{2+}, but not Cr^{3+}, leads to 1) a significant increase in ROS and protein carbonyl content (two markers of oxidative stress); 2) induced mitochondrial dysfunction; and 3) lead to a decrease in mitochondrial respiration. Correspondingly, a decrease in mitochondrial respiration means that the energy demands of the cell must be met through alternative ATP generating pathways.

To summarize, a review of the literature demonstrates that transition metal ions can disrupt cellular redox-status, increase the concentration of intracellular ROS, and induce oxidative stress. Prior research also demonstrated that some metal ions increase glucose uptake, impair mitochondrial function (e.g., decrease mitochondrial respiration), and activate important pro-inflammatory mediators. Furthermore, pro-inflammatory macrophages undergo metabolic adaptations by meeting energy demands primarily through glycolysis. Increased flux through glycolytic pathways can help combat oxidative stress; such that in the first step of glycolysis, glucose is converted to glucose-6-phosphate (G6P) which branches to the oxidative PPP, and generates NADPH necessary for the reduction of GSSG to GSH. However, the effect of metal ions released from orthopaedic devices during wear and corrosion, such as Co^{2+}, Cr^{3+} and sometimes Ni^{2+} on macrophage metabolism, specifically glycolytic flux, and glutathione ratio, remains largely unknown.

3 Rationale

3.1 Objectives and Hypothesis

The overall objective of this research is to analyze the effects of metal ions on energy metabolism in macrophages. This research will improve our understanding of the mechanisms underlying implant failure, and potentially facilitate the development of therapeutic approaches to increase implant longevity. The primary objective of this thesis is to analyze the effects of Co^{2+}, Cr^{3+} and Ni^{2+} on glycolytic flux parameters in murine BMDMs. The hypothesis for this objective was that macrophage exposure to Co^{2+}, Cr^{3+} or Ni^{2+} will result in an increase in glycolytic flux. Additionally, to evaluate the effects of metal ions on reduced glutathione (GSH)/oxidized glutathione (GSSG) ratio in BMDMs exposed to Co^{2+}, Cr^{3+} and Ni^{2+} using high performance liquid chromatography (HPLC) sample preparation parameters will be improved.

4 Materials and Methods

4.1 Metal Ions

Stock solutions of metal ions were prepared fresh under aseptic conditions as previously described [87]. Solutions of Co^{2+}, Cr^{3+} and Ni^{2+} were prepared from the following salts: $CoCl_2 \cdot 6H_2O$ (≥99.5% purity; Fisher Scientific, Waltham, MA), $CrCl_3 \cdot 6H_2O$ (≥99.2% purity; Sigma-Aldrich, St Louis, MO), and $NiCl_2 \cdot 6H_2O$ (≥99.999% purity; Sigma-Aldrich). The salts were dissolved in culture-grade water (Lonza, Walkersville, MD) and the solution sterile filtered through 0.2-μm pore size cellulose acetate syringe filters (VWR, Mississauga, ON).

Solutions of Co^{2+}, Cr^{3+} and Ni^{2+} were tested for endotoxin. Duplicates of each sample were prepared and the concentrations of metal ions tested were 50 ppm and 300 ppm Cr^{3+}, 48 ppm Co^{2+}, and 96 ppm Ni^{2+}. A commercial limulus amebocyte lysate (LAL)-based endotoxin assay was used (Genscript Toxin Sensor Chromogenic LAL Endotoxin Assay kit; Genscript, Piscataway, USA) as per the manufacturer's instructions [195]. Absorbance was measured at 545nm using a hybrid microplate reader (SynergyTM 4; BioTek, Winooski, VT).

4.2 Murine BMDM

This research was approved by the University of Ottawa Animal Care Committee (Protocol ME-2350). Bone marrow cells were harvested from the tibia, femur and pelvic bones of 4 to 16 week-old female C57BL/6NCrl mice (Charles River Laboratory, Montréal, QC). Cells were harvested and differentiated as previously described [196], except that the medium used was Dulbecco's modified Eagle medium (DMEM)-based (Wisent, St-Bruno, QC). The BMDMs were harvested after a 6-day differentiation period, collected by centrifugation (300 *g* for 10 min) and re-suspended to 1 x 10^6 cells/mL in complete growth medium (CGM made of DMEM [Wisent, St-Bruno, QC] supplemented with 8% (v/v) heat-inactivated ultra-low endotoxin [0.05 EU/mL] fetal bovine serum [FBS; NorthBio, Toronto, ON, catalog no. NBSF-701], and 100 U/mL of penicillin and streptomycin [Thermo Fisher Scientific, Waltham, MA]).

4.3 Improved Glycolytic Stress Test: Extracellular Acidification Rate (ECAR)

Extracellular acidification rates (ECAR) were measured with an extracellular flux analyzer (Seahorse XFe96 Analyzer; Agilent Technologies, Santa Clara, CA) using an improved glycolytic stress test adapted from Mookerjee *et al.* [192]. The probes of the cartridge (XFe96 Extracellular Flux Assay Kit Cartridge; Agilent Technologies,) were hydrated 24 hr before each experiment by submerging the probes in calibrant (XF calibrant, pH7.4, Agilent Technologies) and placing the cartridge at 37°C without CO_2 until the time of loading, as per the manufacturer's instructions.

BMDMs were seeded in tissue culture-treated polystyrene 96-well microplates (Seahorse XFe96 V3 PS Cell Culture Microplates; Agilent Technologies) at 90,000 cells/well in CGM and incubated 3h to allow attachment at 37°C under a humidified atmosphere of 95% air and 5% CO_2 (cell culture conditions). At the end of the incubation, the culture medium was replaced with CGM containing no metal ions (negative control; cell culture-grade water; Lonza, Walkersville, MD), 6-24 ppm Co^{2+}, 50-200 ppm Cr^{3+}, 12-96 ppm Ni^{2+} or 1 μg/mL lipopolysacchrides (LPS) (Sigma-Aldrich) for an additional 6h under cell culture conditions. Each condition was prepared in sextuplicate.

The assay medium was freshly prepared using modified DMEM without glucose, L-glutamine, phenol red, sodium pyruvate and sodium bicarbonate (Sigma-Aldrich). The assay medium was supplemented with 2 mM glutamine (Wisent), either 5 mM (for assays with BMDM exposed to Co^{2+} or Ni^{2+}) or 2 mM (for the assay with BDMD exposed to Cr^{3+}) HEPES (Sigma-Aldrich) and 500 U/mL carbonic anhydrase (Sigma-Aldrich). The carbonic anhydrase was added to the assay medium to ensure quantitative conversion of CO_2 to HCO^{3-} and H^+ [197]. The carbonic anhydrase was prepared for supplementation by reconstituting in cell culture-grade water and was filtered through a 0.2-μm pore cellulose acetate filter (VWR, Mississauga, ON) for sterilization. The pH of the assay medium was adjusted to a final pH of 7.3-7.4 immediately before use. After the 6h incubation with no ions, metal ions, or LPS the cells were washed twice with the assay medium (without carbonic anhydrase) and incubated under cell culture conditions with complete assay medium (with carbonic anhydrase) 45-60 min.

Drugs were prepared and loaded into a hydrated XFe96 Extracellular Flux Assay Kit Cartridge (Agilent Technologies) with four injection ports A, B, C and D. Sequential injections from each port were programmed throughout the assay. Between three and six measurements

were taken after each sequential injection while mixing occurs. Before any injections occur, 3 consecutive ECAR measurements were taken corresponding to the basal acidification (i.e., basal ECAR). Basal ECAR was measured with glucose-deprived cells to determine the acidification rate present in the absence of glucose. Prior to the glucose injection, ECAR measurements for the cells are at their basal level and are corresponding to contributions to extracellular acidification (EA) from mitochondrial CO_2 production [192], [198]. The basal ECAR measurements were followed by 3-6 measurements for each of the following parameters: glycolysis, glycolytic capacity, and maximal glycolytic capacity. These parameters were measured after sequential injections of glucose (10 mM final concentration in the microplate: Sigma-Aldrich), and rotenone and antimycin A (0.5 μM each; Sigma-Aldrich), monensin (10 μM; Sigma-Aldrich) with carbonyl cyanide m-chlorophenyl hydrazone (CCCP; 2 μM; Sigma-Aldrich). Glycolysis was measured after the first injection (glucose), which provided a substrate for glycolysis to occur (1 glucose $\rightarrow$ 2 lactate$^-$ + 2 H^+) [192]. The second injection, rotenone and antimycin A, prevents oxidative phosphorylation by inhibiting complex I and complex III of the ETC, respectively [192], [198]. Consequently, the energy demands of the cell are met primarily through glycolysis, ultimately establishing the glycolytic capacity of the cell. The third injection (monensin and CCCP) aims to increase the energy demands of the cell. Monensin works as an ionophore and increases the influx of Na^+ into the mitochondrial matrix. This consequently increases the activity of the Na^+/K^+-ATPase of the plasma membrane to export Na^+, while simultaneously hydrolysing ATP [192]. CCCP dissipates the proton gradient subsequently decreasing the electrochemical potential across the MIM [199]. Therefore, when combined, injections of the ionophore monensin and mitochondrial uncoupler CCCP cause the cell to reach its maximal glycolytic capacity [192], [199]. An injection of 2-DG (a glucose analog) was performed at the end of the experiment to confirm that glucose was the substrate responsible for the observed acidification. 2-DG competitively inhibits the conversion of glucose-6-phosphate to fructose-6-phosphate at the phosphoglucoisomerase step of glycolysis [200].

Following these measurements, the samples were removed from the extracellular flux analyzer and the cells were washed with 180 μL of cold Dulbecco's phosphate-buffered saline (DPBS) and lysed in 40 μL of 1N sodium hydroxide (NaOH). ECAR data were normalized to protein quantity using the Bradford protein determination (Thermo Fisher Scientific), and bovine serum albumin (BSA) standards (Thermo Fisher Scientific) as per the manufacturer's

instructions [201]. Absorbance was measured at 595 nm using a hybrid microplate reader. Agilent Wave Inc (version 2.6.0) software was used to normalize the ECAR data with the results of the Bradford protein determination and exported into Excel for manual analysis. The 3 consecutive measurements for the basal ECAR were averaged for analysis. The most stable value reached for each of the other three parameters (glycolysis, glycolytic capacity and, maximal glycolytic capacity) was selected for analysis.

4.3.1 Buffering Factor (BF)

In order to determine the EA coming from glycolysis through the production of lactate and H^+, contributions to EA from mitochondrial CO_2 production should be corrected for. Agilent Technologies, has previously measured CO_2 contribution factor (CCF) values for a number of cell lines. Agilent Technologies established that a CCF ratio of 0.61 was suitable for most cell lines. In addition, Salloum et al. [194] recently demonstrated that treatment with ions does not significantly influence the CCF value. Therefore the CCF value of 0.61 provided by Agilent Technologies was applied to controls and samples for future calculations.

The buffering factor (BF; mmol/L/pH) refers to the buffering capacity of the system which accounts for both the buffering capacity of the assay medium and the conditions of the assay [202]. The medium used for Co^{2+} and Ni^{2+} samples had a lower concentration of HEPES (2 mM) than the Cr^{3+} samples (5 mM), and therefore each had a different BF which was determined experimentally [203].

4.3.2 Proton Efflux Rate (PER)

The PER were calculated for each dataset. The PER (i.e., $_{total}$PER) is an improved metric that is calculated from the ECAR measurements. The PER accounts for the effect of CCF on the pH of the medium, as well as the BF of the medium, and plate geometry [191]. The PER contribution from glycolysis (i.e., $_{glycolytic}$PER) was calculated by taking the $_{total}$PER (calculated by the Wave Software) measurements and subtracting the contribution to EA from mitochondrial-derived CO_2 (i.e$._{, mitochondrial}$PER). PER values were calculated for basal [without glucose] levels in glucose-deprived cells to provide information into the PER contribution that is

dependent on mitochondrial ATP production. PER values were also calculated with values after glucose was injected, to isolate the PER contribution from glycolysis (i.e., [with glucose]) [202].

In order to determine the PER values, normalized OCR data was analyzed from measurements taken during each of the ECAR experiments. The basal OCR measurements (e.g., before glucose was injected) were averaged to obtain $_{without\text{-}glucose}OCR$ values. OCR measurements were also analysed for the parameters following injections of glucose and R/AA ($_{with\text{-}glucose}OCR$ and $_{r/aa}OCR$, respectively). From these measurements $_{mitochondrial}OCR$, both [with glucose] (equation 4.1) and [without glucose] (Eq. 4.2) was calculated:

$$[\text{without glucose}]\ {}_{mitochondrial}OCR = {}_{basal}OCR - {}_{r/aa}OCR \qquad \text{(Eq. 4.1)}$$

Or

$$[\text{with glucose}]\ {}_{mitochondrial}OCR = {}_{with\text{-}glucose}OCR - {}_{r/aa}OCR \qquad \text{(Eq. 4.2)}$$

The $_{total}PER$ (Eq. 4.3) was calculated as well for values [with glucose] and [without glucose] [202].

$$ {}_{total}PER\ (\text{pmol } H^{+}/\text{min}) = \frac{\text{ECAR (mpH/min)} \times \text{BF (mmol/L/pH)} \times \text{Vol measurement chamber } (\mu L) \times \text{kvol}}{} \qquad \text{(Eq. 4.3)}$$

Calculations were performed with the ECAR data either [without glucose] or [with glucose], the BF of the medium (1.1 or 2.4 mmol/L/pH), the volume of the micro-chamber (2.28 µL) and the correction for the pseudo-volume of the micro-chamber (1.6 kvol). Once the $_{total}PER$ was calculated, the $_{mitochondrial}PER$ and $_{glycolytic}PER$ were isolated. The $_{mitochondrial}PER$ was determined using: CCF = $_{mitochondrial}PER/_{mitochondrial}OCR$ [202], which is calculated using the pre-established CCF ratio (0.61) provided by Agilent Technologies, and the $_{mitochondrial}OCR$ which was calculated as described above. The $_{mitochondrial}PER$ was calculated for both parameters, either [with glucose] or [without glucose].

Finally, the $_{glycolytic}PER$ was isolated using: $_{Total}PER - {}_{mitochondrial}PER = {}_{glycolytic}PER$, and was calculated for values [with glucose] and [without glucose], as well [202]. $_{mitochondrial}PER$ and

$_{glycolytic}$PER were calculated for each condition in sextuplicate and the average for each condition was calculated after removing any outliers. Finally, the above steps were repeated for all datasets and the average $_{glycolytic}$PER and $_{mitochondrial}$PER were calculated for all the experiments for either the basal or glycolysis parameters for Co^{2+} (n=4), Ni^{2+} (n=4) and Cr^{3+} (n=5).

4.3.3 Statistical Analysis for Glycolytic Flux Parameters

A Tietjen-Moore test was ran between the sextuplicate wells of each condition and for each parameter to remove outliers. This Grubbs-type statistical test was used for each experiment individually, as well as to isolate outliers between experiments. Statistical analyses were performed using a one-way analysis of variance (ANOVA) followed by Tukey-Kramer post-hoc tests if the assumption of homogeneity of variance was met, as per Levene's test. Otherwise, a Welch ANOVA was performed followed by Games-Howell post-hoc tests. Statistical analyses were performed using commercial software (IBM SPSS; Statistics 25 software).

4.4 Cell Mortality

Cell mortality was measured at 6 and 12 hr to verify that cell death was not amplified by an increased exposure time to ions. BMDMs were seeded at 6 million cells in 100x15 mm petri dishes (Grenier, Bio-One) and allowed to adhere for 3 hrs, to allow attachment under cell culture conditions. At the end of the attachment period, BMDMs were exposed to CGM prepared with either no metal ions, 18 ppm Co^{2+} or 1 μg/mL LPS (Sigma-Aldrich) in duplicate for either 6 hrs or 12 hrs under cell culture conditions. At the end of the 6 or 12 h incubations, the BMDMs were detached by pipetting using CGM, transferred to 50 mL tubes and centrifuged at 300g for 10 min. The cell pellets were re-suspended in 1 mL of CGM. Trypan blue (TB) exclusion assay was used to count the number of viable (TB^-) and non-viable (TB^+) cells. Trypan blue (Sigma, 0.04% [w/v] final concentration) dye and an improved Neubauer hemocytometer (Hausser Scientific, Horsham, PA) were used to count the number of stained and unstained cells in each sample. The percentage of non-viable cells after the 12h exposure was compared to that at 6h.

4.5 GSH and GSSG Determination

The BMDMs were rinsed with 5 mL of CGM and detached by pipetting using a 10-mL Class-A volumetric pipette (SIBATA Scientific Technology, Saitama, Japan) as previously described [196] with CGM. Twelve million cells were seeded in 145x20 mm tissue-culture (TC)-treated plates (Grenier, Bio-One); or, 6 million cells in 100x15mm petri dishes (Grenier, Bio-One). The BMDMs were incubated in CGM for 3 hrs to allow attachment under cell culture conditions. At the end of the incubation, BMDMs were exposed to 18 ppm Co^{2+}, 150 ppm Cr^{3+}, 48 ppm Ni^{2+} or 1 μg/mL LPS for 12h as above.

HPLC assay for GSH and GSSG

The HPLC assay for GSH and GSSG was based the procedure used in Dr. Mary-Ellen Harper's laboratory (University of Ottawa) and was originally published by Mailloux *et al.* [204]–[206]. The mobile phase consisted of 0.1% trifluoroacetic acid (TFA; Sigma-Aldrich) prepared in HPLC-grade methanol (Fisher Scientific) and was filtered through a 0.2 μm filter via vacuum filtration. The homogenization buffer containing TRIS (Sigma-Aldrich), ethylenediaminetetraacetic acid (EDTA; Sigma-Aldrich) and sucrose (BioShop Canada, Burlington, ON) was dissolved in the mobile phase and kept on ice. The 1:1 HPLC buffer was always prepared fresh, by combining a 1:1 solution of mobile phase and homogenization buffer with 33.5-36.5% meta-phosphoric acid (MPA; Sigma-Aldrich) and 0.11% TFA, final concentration. All the buffers were kept on ice during the experiment.

Lyophilized GSH and GSSG (Sigma-Aldrich) were used to prepare 100 mM stock solutions. Standard stock solutions were prepared carefully in a volumetric flask in the 1:1 HPLC buffer. Acidic solutions minimize oxidation of GSH to GSSG in the stock solutions during storage [207]–[209]. Finally, the standards were stored under Argon to minimize oxidation during storage, and frozen/stored at -80°C. Freshly thawed GSH and GSSG standards were diluted from the stock solutions on the day of the experiment in 1:1 HPLC buffer, to a concentration of 1 mM, 0.1 mM, 0.01 mM and 0.001 mM.

HPLC Standard Curve

The GSH and GSSG contents of the standards were measured using HPLC by loading 210 µL of each standard into a 96-well plate (Agilent Technologies, U shape, polypropylene) with the compatible sealing mat (Agilent Technologies). The HPLC was performed using an Agilent Technologies Binary Pump 1100 series HPLC system with a Pursuit C18 column (150 × 4.6 mm, 5-µm pore size; Agilent Technologies, Santa Clara) with Agilent ChemStation software for the HPLC analysis. The flow rate was of 1 mL/min with a detection wavelength of 215 nm for both GSH and GSSG [102], [210], [211].

BMDM Sample Preparation for HPLC Assay

Following incubation (12h), cells were detached by pipetting (as previously described), and transferred to a pre-chilled (ice-cold) 50 mL tube. The cells were centrifuged at 300 g for 10 min at 4°C and the cell pellet was re-suspended in 5 mL of ice-cold DPBS (Sigma-Aldrich). Samples were then transferred into 15 mL tubes (Fisher Scientific) and 100 µL from each sample was aliquoted for cell counting using dye-exclusion hemocytometry under phase contrast microscopy. The 15 mL tubes containing the samples were centrifuged again (1,000 g for 10 min at 4°C) and the pellets were lysed on ice in 210 µL of 1:1 HPLC buffer for 20 minutes. The lysates were centrifuged at 14,000 g for 20 min at 4°C to remove any insoluble material and the supernatant was collected (on ice). The supernatant was injected into the HPLC column immediately with injection volumes of either 40/80 µL or 50/100 µL to gather preliminary data.

Verification of Standards

The standards were prepared as described above in 1:1 HPLC buffer and volumes of 40 µL and 80 µL were immediately injected into the HPLC column. The GSH and GSSG concentrations were measured again after 6-9 hrs at room temperature (in the HPLC auto-sampler) to verify the stability of GSH and GSSG during the experiment.

4.5.1 Optimization of BMDM Sample Preparation

Optimizing BMDM Plating and Recovery

To determine optimal cell recovery, cell recovery was assessed for the following cell densities; 85,000 cells/cm^2, 425,000 cells/cm^2 and 850,000 cells/cm^2 in either TC-treated or untreated (100 x 15 mm) plates or 24-well plates (without metal ions). BMDMs were seeded as described and allowed to adhere for 3h under cell culture conditions. After the incubation period, the medium was replaced with CGM (without metal ions or LPS). The BMDMs were then incubated for an additional 12h, rinsed gently with 900 µL of cold DPBS, and 900 µL of enzymatic cell detachment solution (Accutase, Innovative Cell Technologies) was added to each well. The microplates were incubated at RT for 15 min. The contents of each well were collected into individual tubes and the wells were washed twice using a micropipette with cold DPBS, the wash was also collected. The samples were centrifuged at 300 g for 10 min (4°C) and re-suspended in 1 mL of cold DPBS. The samples were immediately counted by dye-exclusion hemocytometry using phase contrast microscopy. The same process was repeated with the 100x15mm dishes without the enzymatic cell detachment solution. The cells were detached by pipetting, as described above and the cells were collected by centrifugation and re-suspended in 1 mL of cold DPBS for counting. Cell recovery was measured by dye-exclusion hemocytometry using phase contrast microscopy, as previously described.

Optimizing Recovery of BMDMs Exposed to Co^{2+}, Cr^{3+} and Ni^{2+}

BMDMs were seeded at a cell density of 425,000 cells/cm^2 in 6-well TC-treated microplates and incubated for 3h to allow attachment under cell culture conditions. After the incubation, the medium was replaced with CGM containing no metal ions, 18 ppm Co^{2+}, 150 ppm Cr^{3+} or 48 ppm Ni^{2+} and the cells were incubated for 12h under cell culture conditions. The medium was removed and 1500 µL of enzymatic cell-detachment solution (Accutase, Sigma-Aldrich) was added to each well and the cells were incubated at room temperature for 15 min. The contents of each well were collected and processed as previously described, centrifuged at 300g for 10 min (4°C) and re-suspended in 1 mL of cold (4°C) DPBS. The samples were immediately assessed for cell recovery.

Optimizing BMDM Detachment Technique: 6-well vs 12-well TC-treated plates

In order to establish differences in detachment efficiency between 6-well and 24-well TC-treated plates a final experiment was done. BMDMs were prepared (20 plates of $15x10^6$ BMDMs per plate) and were collected by detachment with pipette in pre-warmed CGM. Collected cells were seeded by a fellow lab member (experimenter 1), with several years of cell culture experience, who counted and seeded the BMDMs at cell density of 425,000 cells/cm^2. The cells were seeded in 6-well and 24-well TC-treated microplates and the procedure was performed independently by two experimenters. The samples were left to adhere for 3h to allow attachment at 37°C under cell culture conditions. At the end of the attachment period, the CGM was replaced with CGM containing no metal ions, 18 ppm Co^{2+}, 150 ppm Cr^{3+} or 48 ppm Ni^{2+}, in duplicates and incubated for 12h under cell culture conditions. At the end of the incubation, both experimenters independently detached the cells by removing the medium and rinsing the cells with cold DPBS. The rinse for each sample was collected in 15-mL centrifuge tubes. Cells were then treated twice with an enzymatic detachment solution (Accutase) for 15 min at room temperature and both were collected with the rinse. The samples were centrifuged at 300g for 10 min and re-suspended in 1 mL of D-PBS and cell mortality was determined (as previously described).

5 Glycolytic Flux: Results and Discussion

ECAR may be used as an indicator of glycolytic flux, as glycolysis directly contributes to the acidification of the microenvironment. As glycolysis rapidly generates 2 moles of ATP per mole of glucose broken down and 2 moles of protons (H^+)are produced [188]. Therefore, when glycolytic activity increases to meet new energy demands, there is a corresponding decrease in pH (i.e., acidification) of the extracellular environment when the buffering capacity is insufficient [188], [191]. Using an extracellular flux analyzer allows real-time measurements of ECAR, as well as oxygen consumption rates (OCR) in live cells using real-time injections of various substrates, stimulators and/or inhibitors (i.e., drugs). ECAR provides insight into glycolytic activity by measuring changes in the rate of glycolytic proton production in the medium using pH sensors (or probes). The measured parameters (i.e., glycolysis, glycolytic capacity and, maximal glycolytic capacity) all provide insight into the upregulation of glycolysis, as seen in pro-inflammatory activated macrophages to meet energy demands. Alternatively, metrics such as PER, improve our understanding of the contribution to EA derived from sources other than glycolysis such as from CO_2-dependant acidification [202]. Small contributions to the acidification of the microenvironment are derived from the TCA-cycle during mitochondrial respiration [192]. During this process CO_2 is converted to HCO^{3-} and H^+, further decreasing extracellular pH when buffering capacity is insufficient [192]. PER is also able to account for buffering capacity of the medium and from the plate geometry. Therefore, both measurements of ECAR and PER are important for accurate assessment of the glycolytic behaviour of the BMDMs.

5.1 Effects of Co^{2+}, Cr^{3+} and Ni^{2+} on Extracellular Acidification Rate (ECAR)

ECAR results showed that Co^{2+} and Ni^{2+} stimulated an increase in all glycolytic parameters (glycolysis, glycolytic capacity, and maximal glycolytic capacity), relative to the negative control. Results demonstrated that Co^{2+} increased glycolysis by up to approximately 78% (p=0.008*)*, glycolytic capacity by up to 185% (p<0.001), and maximal glycolytic capacity by up to 222% (p<0.001), relative to the negative control as depicted in Figure 5-1.

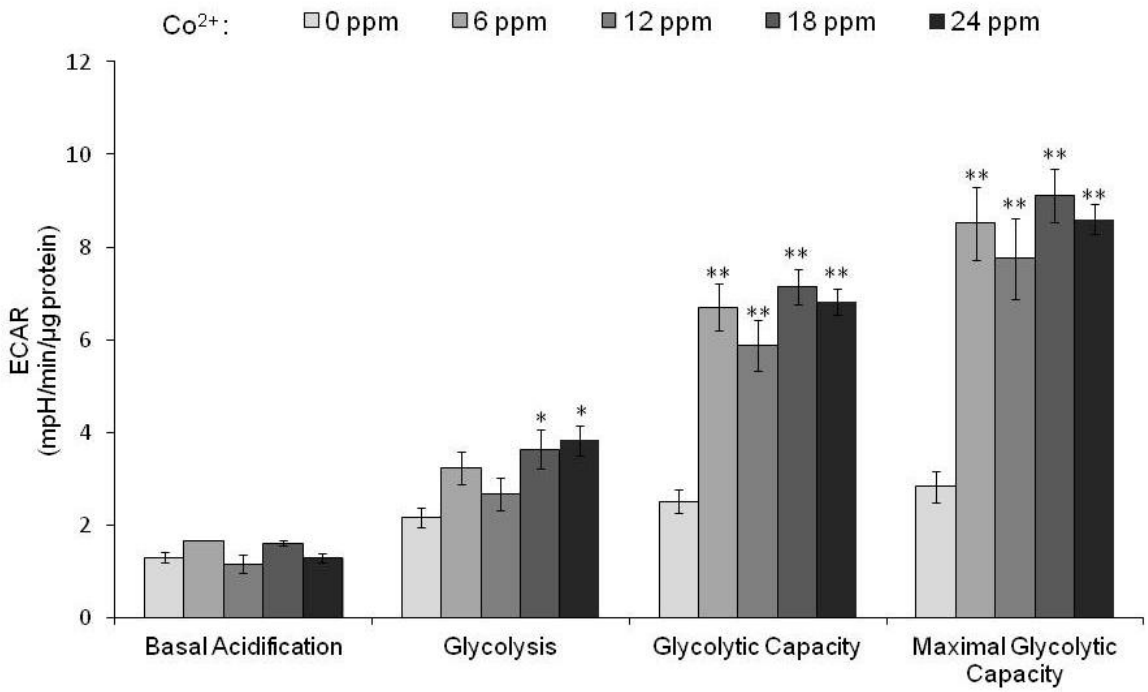

Figure 5-1 Glycolytic flux parameters in BMDMs following a 6-h exposure to 0-24 ppm Co^{2+}. ECAR were measured with an extracellular flux analyzer using an improved glycolytic stress test. ECAR was measured after the sequential injection of glucose, rotenone/antimycin A, and monensin/CCCP, as described in materials and methods. ECAR was normalized to protein concentration using a Bradford protein determination assay. * and ** indicate a significant difference between a given condition and the negative control (no ions) with $p<0.05$ and $p<0.001$, respectively. Data: means ± SEM of an N of 4.

Similarly, Ni^{2+} treatment led to an increase in glycolysis by up to approximately 144%, glycolytic capacity by up to 240%, and maximal glycolytic capacity by up to 245%, relative to the negative control ($p<0.001$ in all cases; Figure 5-2). ECAR values demonstrated a significant increase ($p<0.001$, Figure 5-2) with all concentrations of Ni^{2+} for glycolytic capacity and maximal glycolytic capacity.

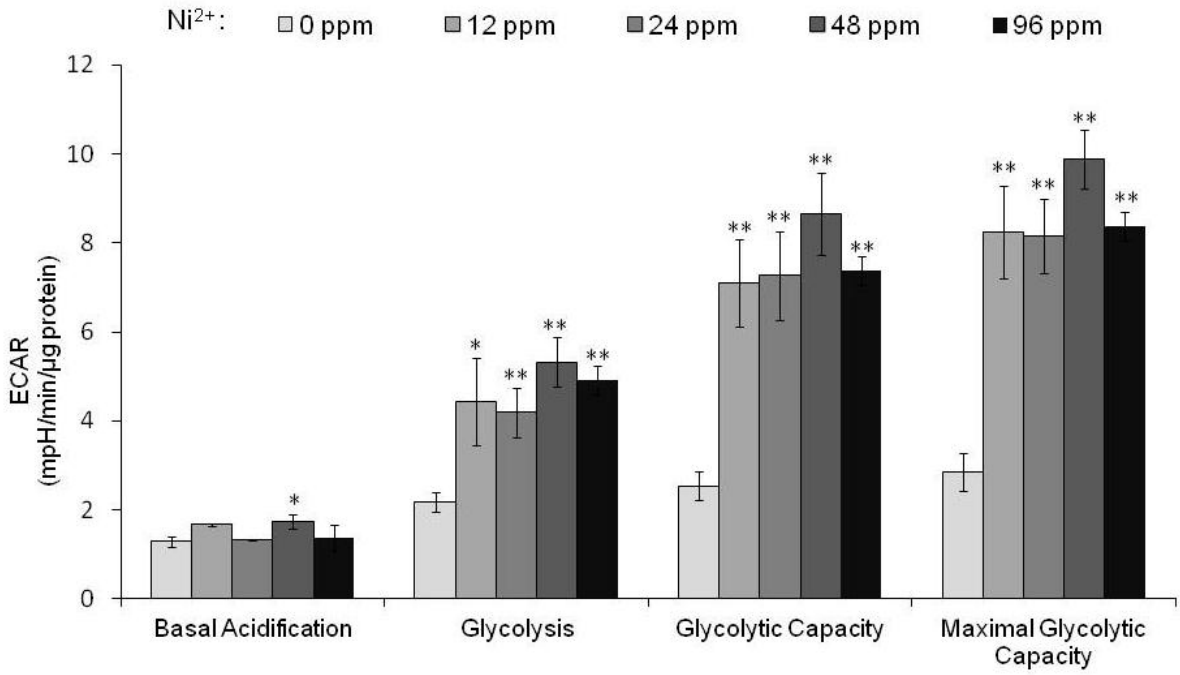

Figure 5-2 Glycolytic flux parameters in BMDMs following a 6-h exposure to 0-96 ppm Ni^{2+}. ECAR were measured with an extracellular flux analyzer using an improved glycolytic stress test. ECAR was measured after the sequential injection of glucose, rotenone/antimycin A, and monensin/CCCP, as described in materials and methods. ECAR was normalized to protein concentration using a Bradford protein determination assay. * and ** indicate a significant difference between a given condition and the negative control (no ions) with $p<0.05$ and $p<0.001$, respectively. Data: means ± SEM of an N of 4.

These results demonstrated that both Co^{2+} and Ni^{2+} lead to significant increases in all glycolytic parameters (glycolysis, glycolytic capacity, and maximal glycolytic capacity), demonstrating that there was a metabolic change due to the presence of these ions. A significant increase in maximal glycolytic capacity of up to 245% was observed with 48 ppm Ni^{2+} ($p<0.001$, Figure 5-2), and an increase of up to 222% with 18 ppm Co^{2+} ($p<0.001$, Figure 5-1), both relative to the negative control. For both ions, the highest concentrations of 24 ppm Co^{2+} and 96 ppm Ni^{2+} did not yield the highest change in glycolytic parameters, likely due to the increase cytotoxicity at these concentrations.

The basal parameters were used to provide insight into EA before glucose injection. A small significant increase in the basal parameter was seen with 48 ppm Ni^{2+} ($p=0.01$, Figure 5-2), which overall stimulated the largest glycolytic response based on measurements of all other parameters. Nevertheless, there were no significant increases in the basal parameters for any other concentrations tested for either Co^{2+}, or Ni^{2+}. The PER results, to be discussed below,

provide more insight into the relative contribution of glycolytic flux and mitochondrial respiration.

In contrast to the Co^{2+} and Ni^{2+} results, BMDMs treated with 200 ppm Cr^{3+} demonstrated a decrease in glycolysis by as much as 25% ($p=0.01$), glycolytic capacity by as much as 44% ($p<0.001$), and maximal glycolytic capacity by as much as 42% ($p<0.001$), relative to the negative control, as represented in Figure 5-3. Significant decreases in ECAR results for 200 ppm Cr^{3+} may be due to increased cytotoxicity at the highest concentration, which is paralleled by the decreases in ECAR parameters observed for the highest concentrations of Co^{2+} and Ni^{2+} as well. No changes were observed with all concentrations tested at and below 150 ppm Cr^{3+} for glycolysis, glycolytic capacity, and maximal glycolytic capacity.

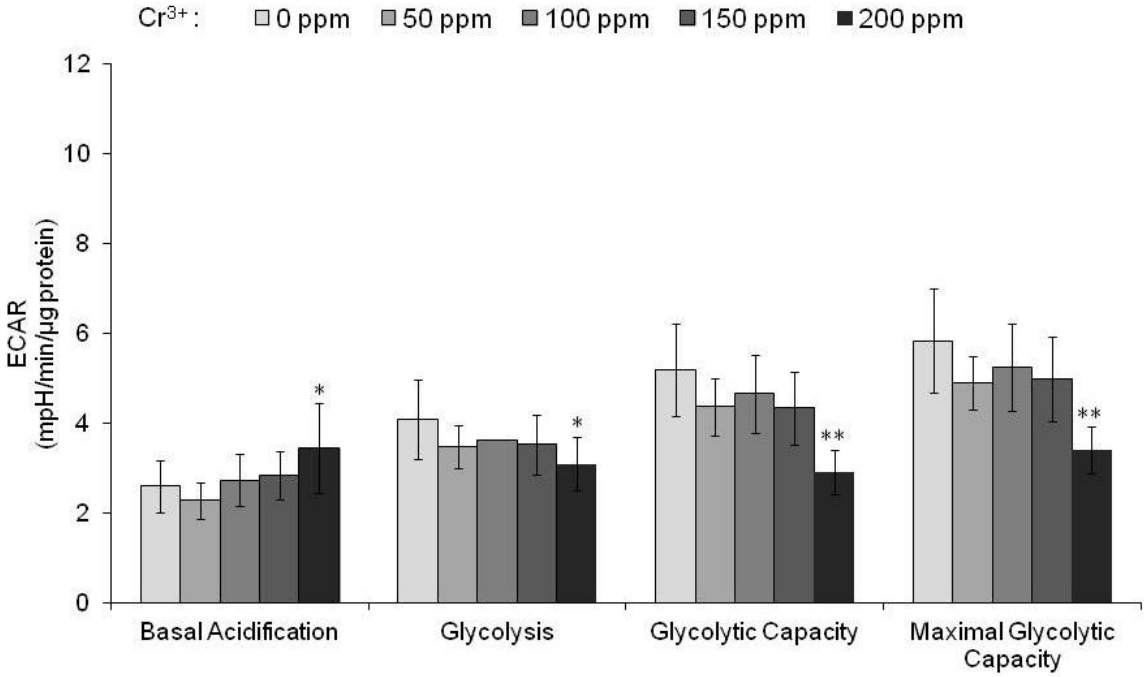

Figure 5-3 Glycolytic flux parameters in BMDMs following a 6-h exposure to 0-200 ppm Cr^{3+}. ECAR were measured with an extracellular flux analyzer using an improved glycolytic stress test. ECAR was measured after the sequential injection of glucose, rotenone/antimycin A, and monensin/CCCP, as described in materials and methods. ECAR was normalized to protein concentration using a Bradford protein determination assay. * and ** indicate a significant difference between a given condition and the negative control (no ions) with $p<0.05$ and $p<0.001$, respectively. Data: means ± SEM of an N of 5.

Overall, the ECAR results indicated that Co^{2+} and Ni^{2+}, but not Cr^{3+}, lead to an increase in glycolytic flux parameters, except basal acidification. Moreover, Cr^{3+} actually caused a decrease in glycolytic parameters, relative to the negative control.

5.1.1 Effect of Co^{2+}, Cr^{3+} and Ni^{2+} on Proton Efflux Rate (PER)

Unlike ECAR results, the PER results are not dependent on the buffering capacity of the system, because the buffering capacity was mathematically taken into account. The results present the PER in two forms: (A) PER [based on measurements without glucose], and (B) PER [based on measurements with glucose]. Calculations for PER [without glucose] (A) are under basal conditions before glucose has been injected into the system. Calculations for PER [with glucose] (B) are under glycolytic conditions after 10 mM of glucose (final concentration) has been injected into the system. The total PER was calculated, from which the relative contributions of mitochondria and glycolysis to the total PER were calculated. The mitochondrial contribution to total PER (i.e., PER mitochondrial) corresponds to the contribution to PER from mitochondrial CO_2 production and CO_2 hydration, which ultimately leads to the release of protons. The contribution from the generation of protons through glycolysis to total PER is presented as glycolytic PER (i.e., PER glycolytic).

The results for PER [based on measurements without glucose] (A) and PER [based on measurements with glucose] (B) are presented for Co^{2+} (Figure 5-4), Ni^{2+} (Figure 5-5) and Cr^{3+} (Figure 5-6). Results for BMDMs treated with Co^{2+} showed a significant decrease in the mitochondrial PER results [without glucose] of up to 66% ($p<0.05$, Figure 5-4A). For the results [with glucose], a decrease of 30% for 12 ppm, 32% for 18 ppm and 35% for 24 ppm ($p<0.001$ for all values, Figure 5-4B) was observed. Furthermore, Co^{2+} also stimulated a significant increase ($p<0.001$) in glycolytic PER of up to 647% (Figure 5-4A) in results [without glucose], and up to 266% (Figure 5-4B) in PER results [with glucose].

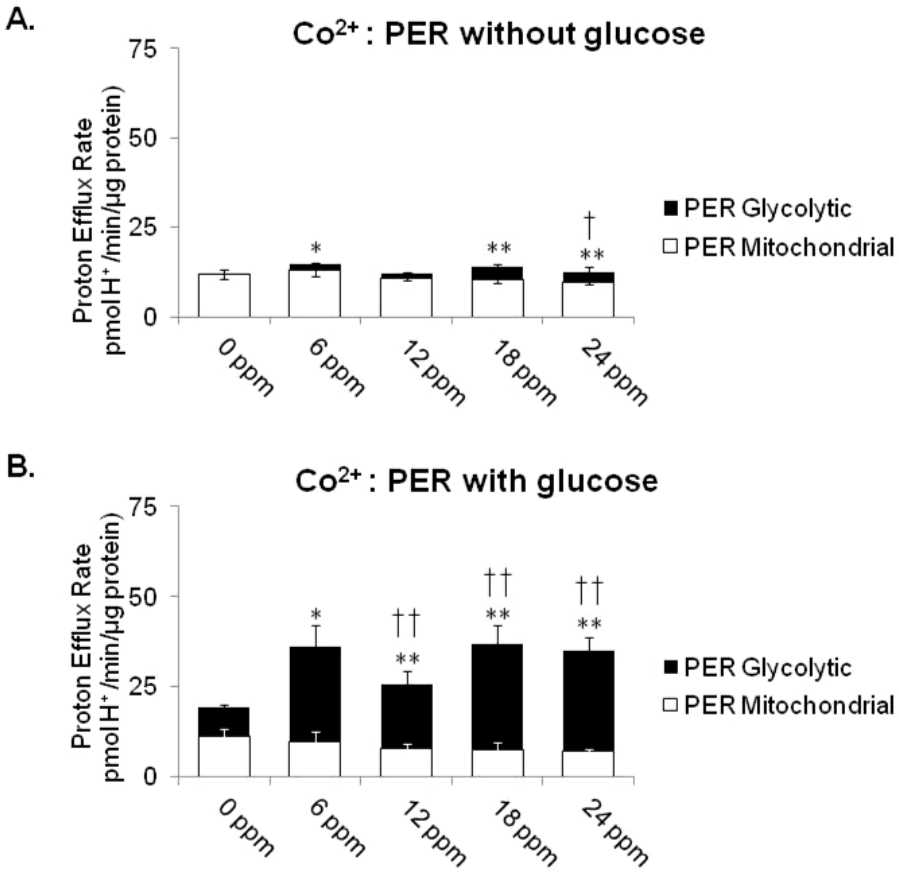

Figure 5-4 Proton efflux rates (pmol H+/min/µg protein) in BMDMs following a 6-h exposure to Co^{2+} (0-24 ppm). * and ** indicate a significant difference between a given condition and the negative control with $p<0.05$ and $p<0.001$, respectively for PER glycolytic. † and †† indicate a significant difference between a given condition and the negative control (no ions) with $p<0.05$ and $p<0.001$, respectively for PER mitochondrial. The PER values are normalized to protein content using a Bradford protein determination assay. PER were calculated as described under Materials and Methods. Data: means ± SEM of 4.

Overall, the results of Co^{2+} indicate that the increase in PER was primarily due to glycolysis (Figure 5-4 B), and therefore glycolytic flux was quantifiably increased in the presence of Co^{2+}. Furthermore, the significant decreases in mitochondrial PER (Figure 5-4 B) in the presence of Co^{2+} relative to the negative control, demonstrate that mitochondrial PER production may be impaired.

Accordingly, results for Ni^{2+} showed a significant decrease in mitochondrial PER in the results [based on measurements without glucose] of 26% ($p<0.001$, Figure 5-5A) with 96 ppm Ni^{2+}. For the results [based on measurements with glucose], a decrease in mitochondrial PER of up to 69% ($p<0.001$, Figure 5-5B) was observed, again with the highest concentration of 96 ppm

Ni^{2+} (all relative to the negative control). This result is comparable to the PER results for Co^{2+}, and indicates that mitochondrial PER contribution is also decreased in the presence of Ni^{2+}. Furthermore, the results also showed a significant increase in glycolytic PER as high as 2334% with 96 ppm Ni^{2+} [based on measurements without glucose] ($p<0.001$, Figure 5-5A), and up to 348% with 48 ppm Ni^{2+} ($p<0.001$, Figure 5-5B) in the PER results [with glucose], again relative to the negative control. These results indicate that in the presence of glucose, Ni^{2+} also causes an increase in glycolytic flux. Moreover, significant increases ($p<0.001$, relative to the negative control) were seen in glycolytic PER values with Ni^{2+} in a concentration-dependent manner, by up to 156% with 6 ppm, 228% with 12 ppm, and 345% with 96 ppm (Figure 5-5B, with glucose).

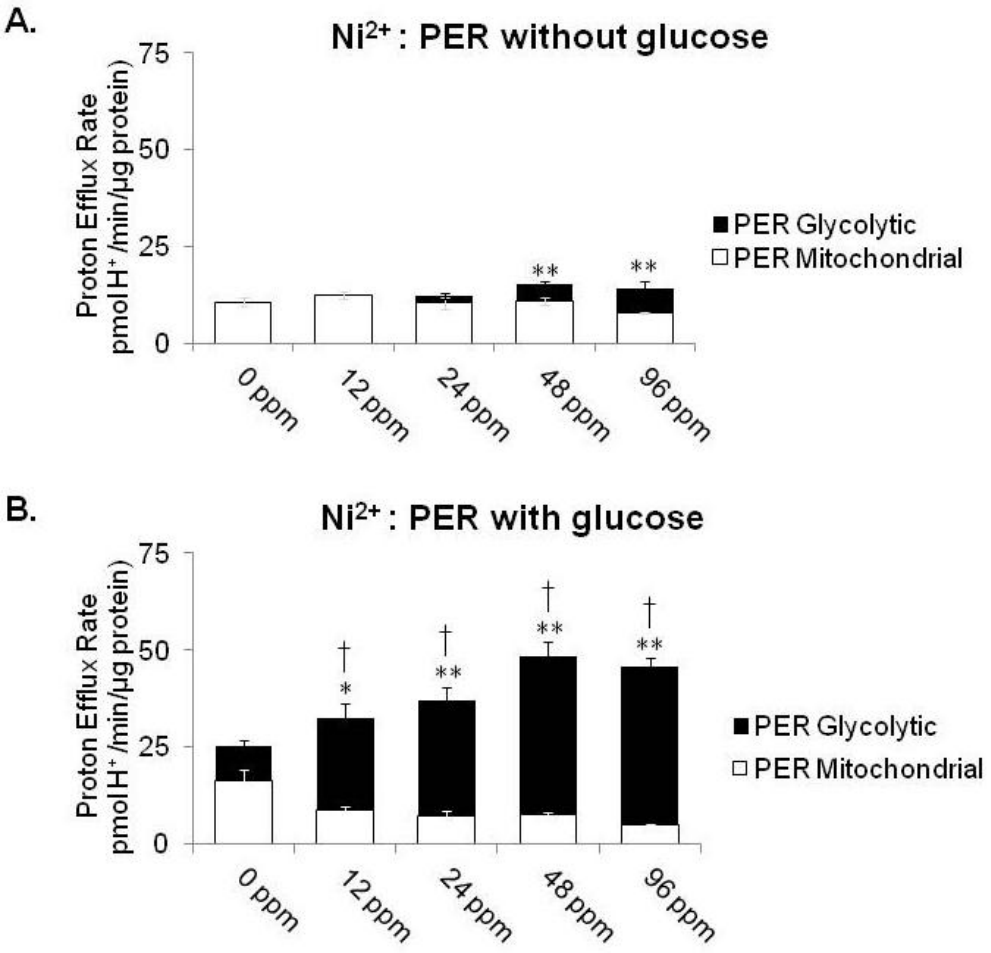

Figure 5-5 Proton efflux rates (pmol H+/min/µg protein) in BMDMs following a 6-h exposure to Ni^{2+} (0-96 ppm). * and ** indicate a significant difference between a given condition and the negative control with $p<0.05$ and $p<0.001$, respectively for PER glycolytic. † and †† indicate a significant difference between a given condition and the negative control (no ions) with $p<0.05$ and $p<0.001$, respectively for PER mitochondrial. The PER values are normalized to protein content using a Bradford protein determination assay. PER were calculated as described under Materials and Methods. Data: means ± SEM of 4.

Interestingly, results demonstrated a significant increase in glycolytic PER of 114% with 200 ppm Cr^{3+} ($p<0.001$, in Figure 5-6A) [based on measurements without glucose], and small increases in all other test conditions, relative to the negative control. However, in the results [with glucose], Cr^{3+} caused a decrease in PER glycolytic with all concentrations except 100 ppm Cr^{3+}, with a significant decrease of as much as 50% with 200 ppm Cr^{3+} ($p<0.001$, Figure 5-6B), relative to the negative control. The mitochondrial PER values were consistently similar to the

negative control for both basal and glycolytic results, indicating that Cr^{3+} likely does not affect mitochondrial PER.

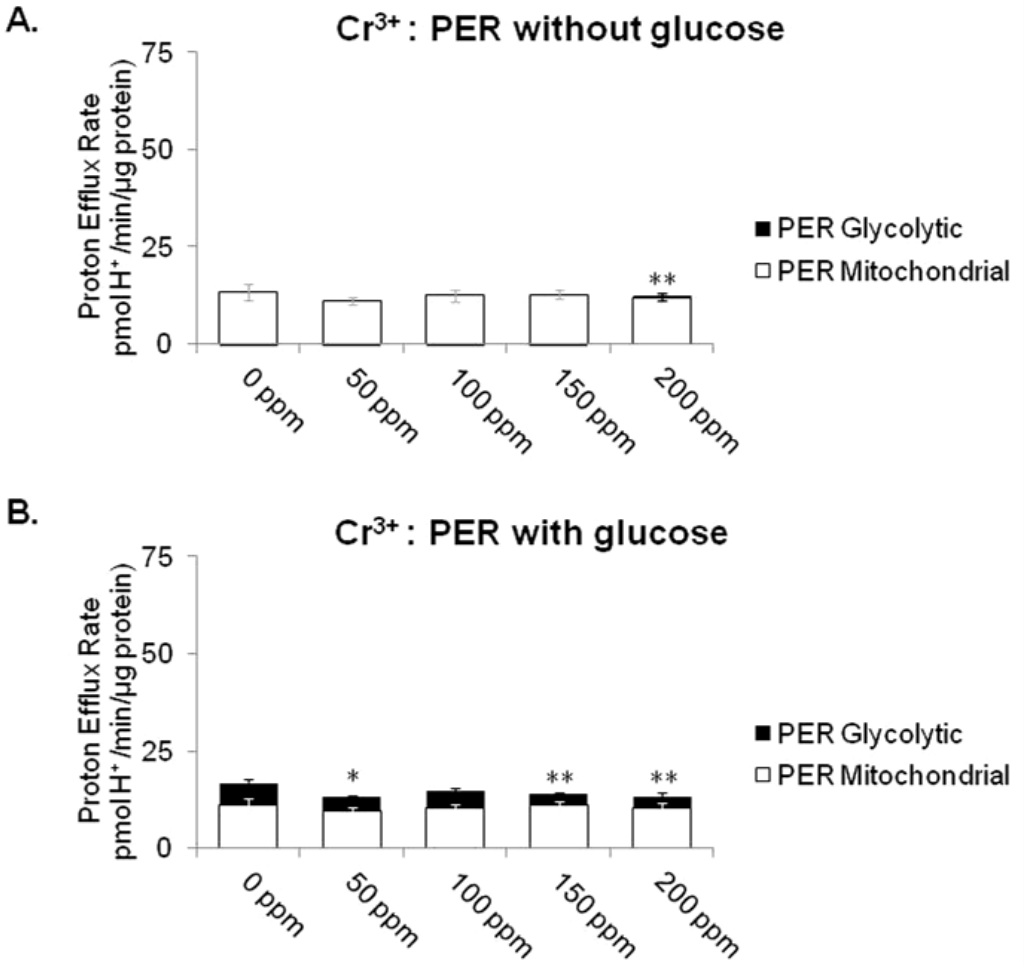

Figure 5-6 Proton efflux rates (pmol H+/min/µg protein) in BMDMs following a 6-h exposure to Cr^{3+} (0-200 ppm). * and ** indicate a significant difference between a given condition and the negative control with $p<0.05$ and $p<0.001$, respectively for PER glycolytic. † and †† indicate a significant difference between a given condition and the negative control (no ions) with $p<0.05$ and $p<0.001$, respectively for PER mitochondrial. The PER values are normalized to protein content using a Bradford protein determination assay. PER were calculated as described under Materials and Methods. Data: means ± SEM of 5.

Overall, the results for Co^{2+} and Ni^{2+} are very similar for all tested PER and ECAR parameters, while the results for Cr^{3+} demonstrate a drastically different metabolic response in BMDMs. Co^{2+} and Ni^{2+} generally led to a significant and substantial increase in glycolytic PER and other glycolytic test parameters, and accordingly a small but significant decrease in mitochondrial PER, relative to the negative control. Alternatively, Cr^{3+} generally led to a small

but significant decrease in glycolytic PER (relative to the negative control), and had no significant impact on the mitochondrial PER results.

5.2 Technical Considerations

In order to adapt glycolytic stress test protocol, which had been established for RAW 264.7 macrophages, for use with BMDMs some technical modifications were necessary. Moreover, exposure to Co^{2+} and Ni^{2+} demonstrated differences in metabolic response compared to Cr^{3+} that also required some improvement. These technical considerations for the protocol are described below.

5.2.1 Optimizations of the Improved Glycolytic Stress Test

The present study used an improved glycolytic stress test for measuring ECAR parameters, and was adapted in this thesis for use in an *in vitro* BMDMs model. The improved glycolytic stress test used in this thesis was adapted from the method for RAW 264.7 macrophages [212]. The improved glycolytic stress test was based on a paper originally published by Mookerjee *et al.*[192]. The method described in [107] was for RAW 264.7 macrophages, which is a highly proliferative and more metabolically active immortalized cell line [107]. Therefore, the method was optimized in this thesis for BMDMs. The improved glycolytic stress test protocol for BMDMs was finalized after optimizing the following parameters for Co^{2+} and Ni^{2+}, as well as Cr^{3+}: the medium composition, the injection drugs, and cell seeding density.

Optimization of Medium, Drugs and Cell Density for BMDMs

The protocol for the improved glycolytic stress test was adapted for BMDMs with optimization of the medium composition (e.g., concentrations of glutamine, HEPES and carbonic anhydrase), the concentration of monensin, and the cell seeding density. A concentration of 2 mM glutamine was used based on previous articles using BMDMs [213]–[215]. The concentrations tested for monensin were based on a paper by Mookerjee *et al.* [216], which recommended 20 μM, and considering the concentrations previously used in Dr. Catelas' lab. It was also recommended by Mookerjee *et al.* [216] to use the lowest effective concentration of

monensin, and therefore testing a range was essential due to the potential toxicity of the drug. The seeding densities were empirically selected based on: 1) the seeding density used for BMDMs measurements of OCR [217]; and 2) the recommended values by Agilent Technologies for BMDMs and from previously published articles [218], [219], [220], [221]. The HEPES concentrations were selected to ensure that acidification will not cause retroinhibition of glycolysis while remaining large enough to be detectable with reasonable accuracy and precision.

Notably, the medium used for preliminary experiments (data not shown) was RPMI-1640 containing 1 mM HEPES without bicarbonate, phenol red, glutamine or glucose as previously used for assays with BMDMs [196], and was the medium recommended by Agilent Technologies for BMDMs [219]. However, research done by peers in the laboratory revealed that Cr^{3+} ions may precipitate in RMPI-1640 media, and it has been previously shown that in simulated physiological fluids, Cr^{3+} is able to form complexes that may elicit a different immune response [88]. Ultimately, a DMEM-based medium without glucose, L-glutamine, phenol red, sodium pyruvate and sodium bicarbonate was used and the aforementioned parameters were optimized in this medium.

Preliminary experiments (data not shown) analysed seeding densities of $9x10^4$, $12x10^4$, $16x10^4$ and $18x10^4$ cells/well in the DMEM-based medium. HEPES, carbonic anhydrase and monensin concentrations were also optimized by testing 0 mM, 1 mM, 2 mM, 3.5 mM, and 5 mM of HEPES (Sigma), 10 μM, 20 μM and 30 μM of monensin, and conditions with and without carbonic anhydrase (500 U/mL, final concentration in the medium). Based on these preliminary experiments, it was empirically determined that a seeding density of $9x10^4$ cells/well would be used with carbonic anhydrase, and a concentration of 10 μM of monensin. These conditions were selected because they minimized monensin-related cytotoxicity, provided an ideal pH range ($\Delta pH \leq$ ca. 0.2 pH units per min) for detection at all injection points, and reduced variability between measurements. However, a preliminary experiment with metal ions revealed that a higher concentration of 5 mM HEPES was required to obtain an adequate buffering capacity to accommodate the highly glycolytic metabolic response observed with Co^{2+} and Ni^{2+}. Interestingly, the metabolic response observed with Cr^{3+} was significantly different and required additional optimizations.

Optimization for Experiments with Chromium

Preliminary experiments with Cr^{3+} revealed that the glycolytic response, and consequently level of acidification observed, were much lower with Cr^{3+} than with Co^{2+} or Ni^{2+}. Therefore, either the number of cells or level of buffering needed to be further optimized. Optimization experiments were performed testing 1 mM, 2 mM, and 3 mM of HEPES with either no ions, 50 ppm Cr^{3+} , 100 ppm Cr^{3+} or LPS (in triplicates), following the same protocol as used with Co^{2+} or Ni^{2+}. The optimizations were repeated until there was adequate reproducibility between experiments. Finally, it was empirically determined that with 0-200 ppm Cr^{3+}, the medium required a lower buffering capacity (2 mM HEPES) than with Co^{2+} or Ni^{2+} (5 mM HEPES) to detect the significantly reduced effect on the extracellular acidification. The cell seeding density was not changed to retain consistency with results for Co^{2+} and Ni^{2+}.

6 Sample Preparation Improvements for Future GSH and GSSG Determination in BMDM Exposed to Metal Ions

This chapter presents a series of preliminary experiments (n=1), aiming to optimize BMDM recovery after exposure to metal ions for future GSH and GSSG determination by HPLC. This optimization was undertaken after preliminary experiments to determine GSH and GSSG by HPLC were found to be irreproducible due to insufficient recovery of BMDMs after exposure to metal ions. Additional experiments will be required to strengthen the conclusions, in particular with regards to the potential use of an enzymatic detachment solution (Accutase).

6.1 Preliminary Experiments on GSH and GSSG Determination by HPLC

In order to investigate the glutathione redox status of BMDMs exposed to Co^{2+}, Cr^{3+} and Ni^{2+} an HPLC method was selected to quantify GSH and GSSG. Different methods for GSH and GSSG quantification have been previously described, such as commercial glutathione assay kits and separation by HPLC with fluorescence [222], [223] or UV detection [229], [231], [232]. However, some HPLC methods (e.g., HPLC with fluorescence) rely on a derivatization step which does not allow GSH and GSSG to be determined simultaneously, and can sometimes require two analyses to be done in parallel [226]. Alternatively, glutathione assay kits often use an enzymatic recycling method which also requires derivatization, and uses measurements of total glutathione and GSH to quantify GSSG rather than measuring it directly [227]. As a result, an HPLC method that quantifies both GSH and GSSG simultaneously, without a derivatization step was utilized as previously described [204]–[206]. However, the method needed to be adapted for BMDMs treated with metal ions, such as Co^{2+}, Ni^{2+}, and Cr^{3+}. BMDMs are highly adherent [196], and treatment with metal ions can interfere with the cell membrane [128], [132], which may affect the cell detachment and recovery. As a result, a high cell number (12 million cells per sample) was empirically determined based on preliminary data (not shown) which suggested that the HPLC assay required a large number of BMDMs in order to detect glutathione. Difficulty in detecting GSH, despite a large number of plated cells, is likely due to a low cell recovery, in addition to the fact, the sample must be very concentrated in the lysis buffer to obtain measurable concentrations of GSH and GSSG (based on preliminary data not shown).

Overall, a lack of reproducibility in the results, after several preliminary experiments, lead to improvements of cell recovery by testing: 1) dish surface treatment and size, 2) seeding density, and 3) detachment technique.

It should be noted that injection volumes of 40 and 80 µL, or 50 and 100 µL were also tested during preliminary HPLC experiments (data not shown). It was determined that injection volumes of 40 and 80 µL would be appropriate for future experiments. Finally,, the stability of the GSH and GSSG standards, freshly prepared in 0.11% TFA, were also verified by measuring the GSH and GSSG content at 0h after preparation and again, after ~9h at RT. The slopes of the standard curves generated for the measured GSH and GSSG standard solutions (at 0h and 9h) were similar (data not shown), and therefore the GSH standard is likely not being oxidized to GSSG throughout the duration of the experiment, when prepared in an acidic buffer.

6.1.1 BMDM Dish Surface Treatment and Seeding Density

Dish surface is an important parameter for BMDMs adhesion, and detachment. Due to the adhesive nature of BMDMs, the detachment process from TC-treated plates can impose shear stress on the cells that could potentially influence results if the cells are too highly adherent, and reduce the number of viable cells successfully detached. Alternatively, the untreated surface of suspension plates may lead to inadequate BMDMs adhesion, resulting in a net loss in overall cell yield during the initial medium change. TC-treated plates have a treated surface to promote adhesion. In aims to improve cell recovery, BMDMs were plated in either TC-treated or suspension plates, and at seeding densities of 85,000 cells/cm^2, 425,000 cells/cm^2, and 850,000 cells/cm^2 (Figure 6-1). These seeding densities were selected based on the seeding density used for the improved glycolytic stress test, and to keep culture conditions as consistent as possible.

Overall, the results presented in Figure 6-1, revealed that TC-treated plates yielded a higher recovery (up to 99% higher) than suspension plates with all tested seeding densities, with or without, enzymatic detachment solution (Accutase, Figure 6-1). A seeding density of 425,000 cells/cm^2 led to a BMDM recovery of 72% and was comparable to 71% for the cells seeded at 85,000 cells/cm^2, when using TC-treated plates (Figure 6-1). The recovery appeared to be higher than with a cell density of 850,000 cells/cm^2.

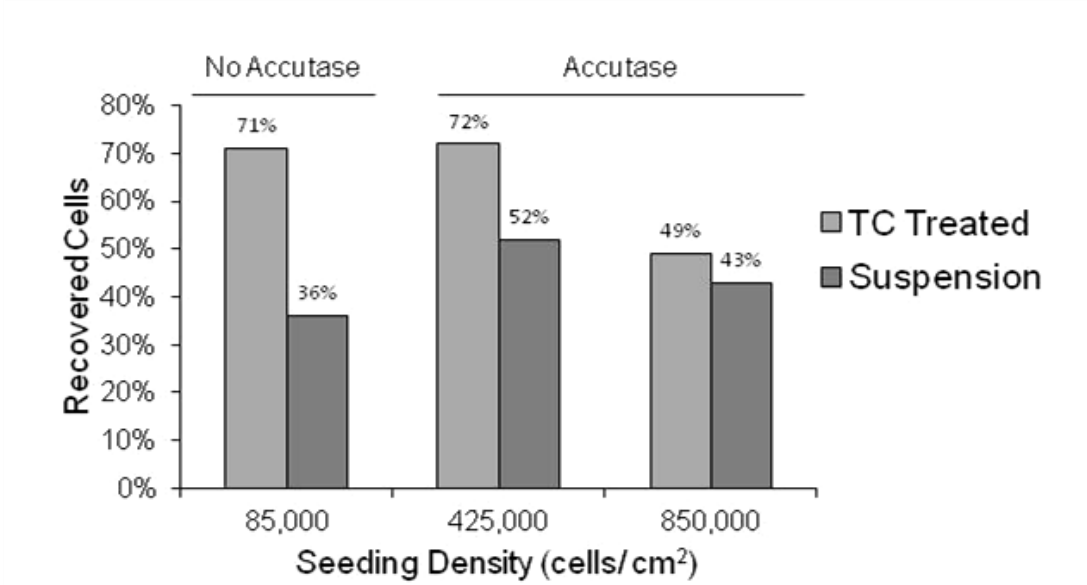

Figure 6-1 Recovery of BMDM (% nominal seeding density) for TC-treated plates vs. suspension plates at 85,000 cells/cm^2, 425,000 cells/cm^2, and 850,000 cells/cm^2. BMDMs were seeded and allowed to adhere for 3 hrs. The medium was replaced with CGM and cells were incubated for an additional 12 hrs at 37°C/5% CO_2. Cells were detached by pipette detachment with or without Accutase and counted by dye exclusion hemocytometry (N=1).

Overall, the results of this experiment indicated that without metal ions, TC-treated plates a seeding density of 425,000 cells/cm^2 and use of an enzymatic detachment solution for detachment yielded optimal BMDMs recovery. Notably, a seeding density of 85,000 cells/cm^2 without Accutase also yielded similar cell recovery. However, the option to use the higher seeding density, which can increase the speed of sample preparation, may be more beneficial for future HPLC procedures. Moreover, to reduce the shear stress imposed on BMDMs during detachment, it is suggested to use an enzymatic detachment solution (Accutase). Therefore, the use of 425,000 cells/cm^2 and the enzymatic detachment solution may be preferable. Nevertheless, considering that the ultimate goal is to measure GSH and GSSG by HPLC, the effect of Accutase on these metabolites would need to be determined.

6.1.2 Effect of Co^{2+}, Cr^{3+} and Ni^{2+} on BMDMs Recovery

The effects of Co^{2+}, Cr^{3+} and Ni^{2+} on cell recovery were then tested. Indeed, preliminary experiments demonstrated that BMDMs treated with metal ions resulted in high variability in protein quantity between samples based on the protein determination assays (data not shown), despite visually consistent cell plating and similar cell distribution (microscopically analysed). Therefore, the effects of 18 ppm Co^{2+}, 150 ppm Cr^{3+} and 48 ppm Ni^{2+} on BMDMs recovery were analysed using dye exclusion hemocytometry to count the number of live cells (e.g., viable, TB^-) and dead cells (e.g., non-viable cells, TB^+) recovered using pipette detachment, and with or without the enzymatic detachment solution (Accutase) as presented in Figure 6-2. The results suggest that all three ions resulted in a decrease in overall cell recovery relative to the negative control (Figure 6-2). Overall the recovery of viable cells for BMDMs treated with 150 ppm Cr^{3+} was only around 33%, which appears to be lower than with the other two metal ions tested (Figure 6-2).

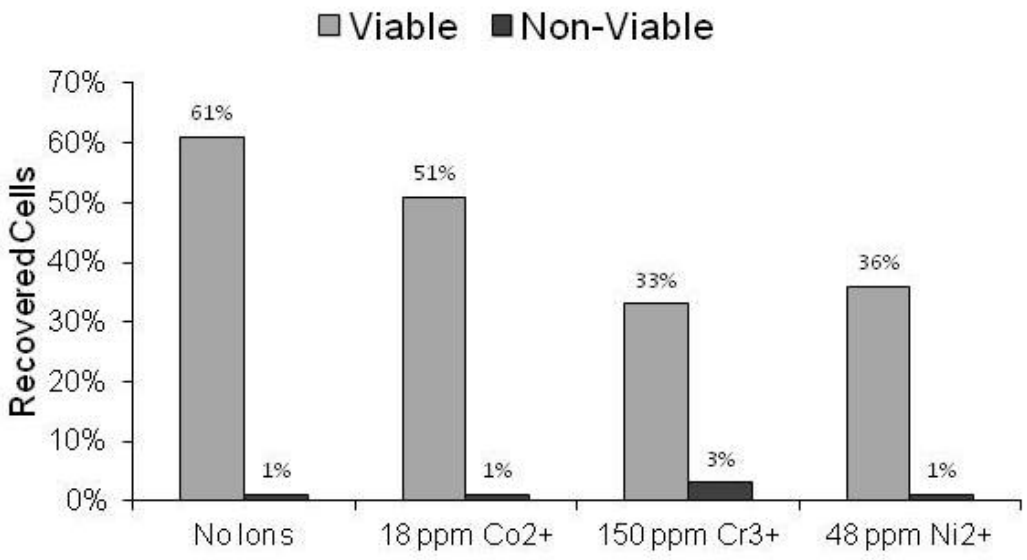

Figure 6-2 Recovery (% nominal seeding density) of viable (TB^-) and non-viable (TB^+) BMDM in 6-well TC-treated plates seeded at 425,000 cells/cm^2 with a 12 hour exposure to 18 ppm Co^{2+}, 150 ppm Cr^{3+} and 48 ppm Ni^{2+}(N=1).

Moreover, the results for the negative control (Figure 6-1, no ions) with 6-well plates compared to those with 24-well plates (Figure 6-2) when using a seeding density of 425,000

cells/cm^2, suggest a lower cell recovery when using larger wells. The well size may affect detachment due to a difference in the level of difficulty detaching at the edge of the wells, compared to the centre where BMDMs tend to have a stronger adherence. Moreover, difficulty in the detachment may be reduced by performing two treatments with the enzymatic detachment solution, by decreasing the well size or by using a more gentle detachment technique, and therefore these parameters were tested.

6.1.3 Effects of the Detachment Technique on Cell Recovery

In order to assess the effects of the detachment technique on the recovery of cells in presence of metal ions, two different experimenters counted the number of viable and non-viable cells plated in 6-well and 24-well plates with metal ions, following two consecutive treatments with an enzymatic detachment solution. The results presented in Figure 6-3 suggest that the use of 24-well plates yielded a better overall BMDM recovery than the use of 6-well plates (up to around 100 to 130% for both experiments; Figure 6-3, A & B) in agreement with the previous results.

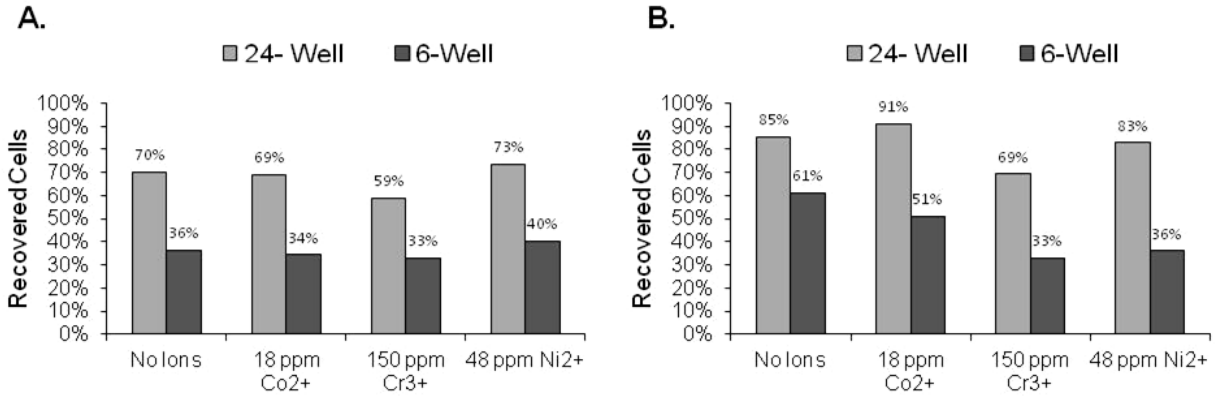

Figure 6-3 Recovery of BMDMs (% nominal seeding density) that were seeded at 425,000 cells/cm^2 in 6-well and 24-well TC-treated plates and exposed to 18 ppm Co^{2+}, 150 ppm Cr^{3+} or 48 ppm Ni^{2+} for 12h (N=1). After the 12 hour incubation with ions, BMDMs were detached by rinsing with pre-warmed D-PBS (collected) and two 15 minute treatments with enzymatic detachment solution (Accutase). Cells were collected by pipette detachment; supernatants from all steps were collected and pooled for centrifugation and analyzed by dye exclusion hemocytometry. (A) Experimenter 1; (B) Experimenter 2.

Overall, both experimenters (Figure 6-4 A & B, N=1) appeared to have very similar cell recoveries. However, the percentage of dead cells appeared to be much higher for experimenter 1

who likely used a more aggressive detachment approach. Experimenter 2 had very few non-viable cells in all samples (Figure 6-4, B, N=1). The apparent differences in cell recovery between experimenters may be due to different experience with detaching BMDMs, as well as the nature of the technique which is subject to inter-individual variation. Indeed, experimenter 1 is more familiar with RAW 264.7 macrophages and may use a rougher technique than experimenter 2, more familiar with BMDMs.

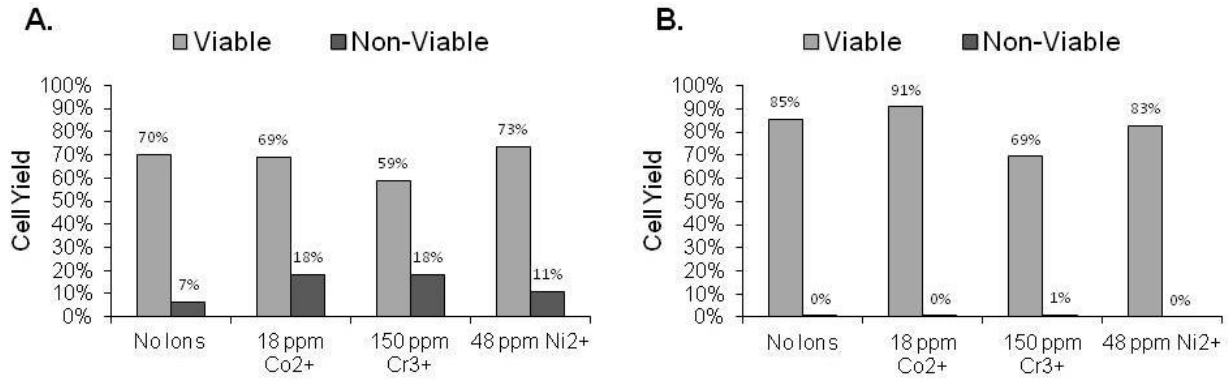

Figure 6-4 Recovery (% nominal seeding density) of viable (TB^-) and non-viable (TB^+) BMDM that were seeded at 425,000 cells/cm^2 in 24-well TC-treated plates and exposed to 18 ppm Co^{2+}, 150 ppm Cr^{3+} or 48 ppm Ni^{2+} for 12h (N=1). After the 12 hour incubation with ions, BMDMs were detached by rinsing with pre-warmed D-PBS (collected) and two 15 minute incubations with an enzymatic detachment solution (Accutase) in which cells were collected by pipette detachment; supernatants from all steps were collected for centrifugation and analyzed by dye exclusion hemocytometry. (A) Experimenter 1; (B) Experimenter 2.

Results presented in Figure 6-4 indicates that the addition of the second treatment of enzymatic detachment solution (Accutase) may lead to a higher overall cell recovery of 85% (Figure 6-4), as compared to one treatment which yielded only 72% (Figure 6-1). However, during HPLC quantification experiments a rapid harvesting of the cells is important to ensure measurement accuracy. Therefore, due to the time requirement for an additional treatment of enzymatic detachment solution and the modest increase in recovery associated with the second treatment, the use of one to two treatments should be determined based on the detachment efficiency of the experimenter. Moreover, small differences are possible between experimenters depending on their individual techniques. Therefore, it would be beneficial for new experimenters to perform practice experiments to help gauge how rough or gentle to be when performing pipette detachment. Based on these results, it is concluded that recovery may be improved with the following parameters: a) 24-well, TC-treated plates for sample preparation, b)

seeding density of 425,000 cells/cm^2, and c) one to two treatments of enzymatic detachment solution.

7 Thesis Summary and Conclusions

7.1 Choice of Ions and Cell Culture Model

The present research analyzed the effects of Co^{2+}, Cr^{3+} and Ni^{2+} on glycolytic flux in BMDMs. Additionally, the study improved a protocol for the sample preparation of BMDMs exposed tometal ions for future quantification of glutathione by HPLC. Co^{2+}, Cr^{3+} and Ni^{2+} ions were emphasized due to the prevalence of metals containing these ions in orthopaedic implants and subsequent ion release into the periprosthetic tissues [48], [59], [72]. In particular, these ions are released from common metal implant alloys such as stainless steel and CoCrMo, and are associated with many potential adverse tissue reactions, including aseptic inflammation [41], [59], [71]–[73], [75], [76], [109], [228]. The ion concentrations tested were 6-24 ppm Co^{2+}, 50-200 ppm Cr^{3+} and 12-96 ppm Ni^{2+}, which are notably higher than those observed *in vivo* (ppb) in bodily fluids (such as blood, serum, synovial fluid and urine) [79], [97], [229], [230]. Due to the *in vitro* nature of the study, higher concentrations were selected based on the hypothesis that *in vitro* pro-inflammatory macrophage activation would require a higher concentration than *in vivo*, where a multitude of stimulating factors are likely up-regulating the effect of the ions [196]. Furthermore, it can be speculated that these ions are present in periprosthetic tissues at concentrations likely exceeding those in body fluid [73], [107], [196]. These metal ion concentrations were also based on past *in vitro* studies analysing the effects of these metal ions on varying aspects of pro-inflammatory macrophage activation, cytotoxicity and bioenergetics [73], [87], [107], [196], [218].

Macrophages are well established as the predominant cell type present in periprosthetic tissues, and are found in notably higher concentrations at the tissue-implant interface [34], [51], [73], [158], [231]. BMDMs were specifically selected as the model of choice due to their accessibility, high achievable cell yield per mouse and morphological similarities to macrophages found in the periprosthetic tissues [196], [213], [232], [233]. However, the cell model presents a limitation for this work due to the murine origin of the primary cells being used, as well as inter-donor variability. The presence of Co^{2+}, Cr^{3+} and Ni^{2+} have been previously linked to IL-1β release, a pro-inflammatory cytokine secreted by macrophages [19], [176]. Furthermore, a recent study by Ferko *et al.* [196] demonstrated that IL-1β release was highest

with Cr^{3+} and present with Ni^{2+}, but not with Co^{2+} indicating that Cr^{3+} may be acting through different mechanisms [196].

7.2 Effects of Co^{2+}, Cr^{3+} and Ni^{2+} on Glycolytic Flux in BMDMs

It has been established that Co^{2+}, Cr^{3+} and Ni^{2+} are associated with high levels of oxidative stress, capable of contributing to these adverse tissue reactions and consequently, implant failure [80], [140], [166], [176], [177]. Interestingly, macrophages undergo a pro-inflammatory phenotypic change associated with a metabolic shift from oxidative phosphorylation to glycolysis, and that glucose uptake is a critical component in the pro-inflammatory phenotype [16], [234]–[238]. Furthermore, oxidative stress is mediated by increased glucose uptake, and is also a known driver of the pro-inflammatory phenotype [237]. However, the effects of Co^{2+}, Cr^{3+} and Ni^{2+} on glycolytic flux in primary macrophages remained largely unknown.

In fulfilment of the primary objective of this thesis, the effects of Co^{2+}, Cr^{3+} and Ni^{2+} on glycolytic flux in murine BMDMs were analysed through measurements of glycolytic flux parameters. The ECAR results revealed an overall increase in all glycolytic parameters; glycolysis, glycolytic capacity and maximal glycolytic capacity, with both Co^{2+} and Ni^{2+}. This increase suggests that in the presence of these metal ions, there is a resultant metabolic change increasing glycolysis to meet metabolic and energy demands. Furthermore, the increase in maximal glycolytic capacity with Co^{2+} and Ni^{2+} suggests that these ions may potentially increase the activity of rate-limiting glycolytic enzymes, allowing the cell to achieve a higher maximal glycolytic rate compared to cells that were not exposed to these metal ions. A previous study has shown that Co^{2+} is able to increase glycolytic enzyme activity resulting in an increase in glucose uptake in 3T3-L1 fibroblasts [189]. Other studies have also demonstrated that in astrocytes, Cu^{2+} increases the activity of glycolytic enzymes [239], [240]. Therefore, some evidence exists to support the observation that Co^{2+} and transition metal ions may increase maximal glycolytic capacity by increasing the activity of rate-limiting glycolytic enzymes. These results were supported by the PER results for both Co^{2+} and Ni^{2+} which also demonstrated an increase in glycolytic PER relative to the negative control. Moreover, a subsequent decrease in mitochondrial PER was also observed, as ATP demands are likely being met primarily through glycolytic activity.

Alternatively, exposure to Cr^{3+} resulted in a decrease in all glycolytic flux parameters which was reflected in both ECAR and PER results. These results demonstrate that Cr^{3+} likely does not contribute to the aforementioned metabolic changes observed with Co^{2+} and Ni^{2+}, and is likely acting through alternative mechanisms to induce an inflammatory response.

It is suspected that a decrease in mitochondrial respiration (often associated with mitochondrial dysfunction) would result in an increase in glycolytic flux in order to meet the ATP demands of the cell. Salloum *et al.* [107] have recently demonstrated that in RAW 264.7 macrophages, Co^{2+}, but not Cr^{3+} [107]. Moreover, previous results demonstrated that Co^{2+} and Ni^{2+}, but not Cr^{3+}, contribute to a decrease in mitochondrial respiration parameters in BMDMs [217]. Therefore, these results for mitochondrial respiration combined with the results from this thesis on glycolytic flux indicate that Co^{2+} and Ni^{2+}, but not Cr^{3+}, can induce a metabolic shift from oxidative phosphorylation to glycolysis in BMDMs. This metabolic shift is likely similar to that associated with the metabolic pro-inflammatory reprogramming of macrophages [16], and may therefore contribute to the inflammatory response observed in periprosthetic tissues.

A recent study demonstrated that exposure to Cr^{3+} in RAW 264.7 macrophages led to an increase in glycolytic flux, although to a lesser extent than observed for cells exposed to Co^{2+} [194]. This result with Cr^{3+} in RAW 264.7 macrophages is not in alignment with the results presented in this thesis using BMDMs, in which exposure to Cr^{3+} lead to a decrease in glycolytic flux parameters. The results with RAW 264.7 macrophages also indicate that the Cr^{3+}-induced increase in glycolytic metabolism did not occur in compensation for a decrease in mitochondrial function, since it was previously published that the latter was unaffected by Cr^{3+} does not induce mitochondrial dysfunction in RAW 264.7 macrophages [107]. It can be noted that RAW 264.7 macrophages have a higher metabolic rate than primary macrophages (such as BMDMs) which may explain some differences in the glycolytic response [107], [214]. Ultimately, the mechanisms governing the Cr^{3+}-induced decreased in glycolytic flux parameters observed with BMDMs remain unclear. It is possible that some of the observed decreases in glycolytic flux are associated with cytotoxicity of Cr^{3+} in BMDMs at the highest concentration (e.g., 200 ppm Cr^{3+}). It may be also be speculated that Cr^{3+} could have an inhibitory effect on glycolytic enzymes [80], [241], which could ultimately contribute to the observed decrease in glycolytic parameters. Future studies may be able to explain the differences in the metabolic response observed with Cr^{3+}, as compared to Co^{2+} and Ni^{2+}. Moreover, a limitation of the glycolytic flux analysis

includes the 6h incubation time during which the BMDMs were exposed to the metal ions. This incubation time was based on previous studies of ECAR with RAW 264.7 macrophages[212] and OCR with BMDMs [217]. Measuring ROS levels at different time points in BMDMs exposed to Co^{2+}, Cr^{3+} and Ni^{2+}could shed more light into the differences in the metabolic response observed between the metal ions.

Previous studies have demonstrated that oxidative stress increases in a variety of cell types exposed to metal ions, such as Co^{2+}[80], [107], Cr^{3+} [80], [100], [107], [131], [242] and Ni^{2+} [131], [242]. Moreover, metal ions can contribute to the generation of ROS and oxidative stress in a multifaceted approach. Co^{2+} and Cr^{3+} have been shown to increase ROS production by participating in Fenton-like reactions [79], [126], [127]. Ni^{2+}, Co^{2+} and Cd^{2+} have been shown to increase ROS by inducing mitochondrial dysfunction that consequently augments ROS production [13], [116], [176], [177]. This increase in ROS production has the potential to cause oxidative stress. Changes in redox-status, such as an increase in oxidative stress, provides important intracellular feedback governing the metabolic behaviour of cells. Since glutathione is the major non-enzymatic ROS scavenger, and a fundamental determinant of redox-status, measuring the GSH:GSSG ratio in BMDMs exposed to Co^{2+}, Cr^{3+} and Ni^{2+}, provides important information regarding cellular redox-status in the presence of these metal ions. Moreover, findings could potentially provide insight into the role of redox-status in governing the metabolic adaptations observed in response to these metal ions, and the inflammatory reactions.

7.3 Optimization of BMDM Recovery after Exposure to Metal Ions for future GSH and GSSG Determination by HPLC

A better recovery of BMDMs treated with Co^{2+}, Cr^{3+} and Ni^{2+} may be achieved with three important changes to sample preparation based on the results presented in this thesis. These improvements are the use of: a) 24-well, TC-treated plates; b) a seeding density of 425,000 cells/cm^2; and c) one or two treatments of enzymatic detachment solution (Accutase). With these improvements to the seeding and detachment procedure, BMDM recovery should be improved to allow the optimization of HPLC parameters for the determination of GSH and GSSG in BMDMs treated with Co^{2+}, Cr^{3+} and Ni^{2+} in the future. Indeed, preliminary HPLC measurements of GSH

and GSSG in BMDMs treated with these ions were not reproducible; suggesting that cell recovery after exposure to metal ions would need optimized.

7.4 Conclusions of the Present Study

In conclusion, in fulfilment of the primary objective of this thesis, it was demonstrated that Co^{2+} and Ni^{2+}, but not Cr^{3+}, lead to an increase in glycolytic flux in BMDMs. Moreover, Co^{2+} and Ni^{2+} caused an increase in maximal glycolytic capacity in BMDMs, which suggests that there may be a subsequent increase in rate-limiting glycolytic enzymes in the presence of these metal ions. This finding presents a potential avenue for future studies through the implication that Co^{2+} and Ni^{2+} -induced metabolic changes may contribute to the pro-inflammatory response observed in the tissues surrounding metal implants. Future investigations into the rate-limiting glycolytic enzymes that may be involved in this response could shed more light into the mechanisms through which this increase in glycolytic flux occurs. Moreover, these findings demonstrate that Cr^{3+} may be acting through different mechanisms altogether.

Additionally, this study contributed to improving BMDM recovery after exposure toCo^{2+}, Cr^{3+} and Ni^{2+}. Improvement or cell recovery achieved by using: a) 24-well, TC-treated plates, b) seeding density of 425,000 cells/cm^2, and c) one or two consecutive treatments of enzymatic detachment solution (specifically, Accutase) for each sample. Improving cell recovery as presented in this thesis in preparation of future HPLC experiments for the quantification of GSH and GSSG metabolites.

Overall, this study will contribute to a better understanding of the underlying mechanisms of the biological response to metal ions derived from implant wear and corrosion. These results and the results of future studies may help the development of potential therapeutic approaches, particularly those aiming to modulate the inflammatory response to these metal ions, in order to increase implant longevity.

7.5 Future Studies

The present study established cell culture parameters to improve BMDM recovery after exposure to metal ions for future experiments aiming to quantify GSH and GSSG in BMDMs treated with Co^{2+}, Ni^{2+} and Cr^{3+} using HPLC. Future studies should aim to quantify the

concentration of GSH and GSSG using the adaptations to the protocol for sample preparation presented in this thesis. Quantification of GSH and GSSG may provide information into the impact of metal ions on the redox-status of the cell.

This research, combined with future studies, could ultimately elucidate differences between the effects of Co^{2+}, Cr^{3+} and Ni^{2+}on possible mechanisms of macrophage activation, changes in redox-status and metal-mediated increases in oxidative stress. To this aim, other studies could potentially improve the understanding of the signalling pathways possibly involved in this response, such as the stabilization of hypoxia-inducible factor-1α (HIF-1α), changes in PPP flux and levels of ROS production in BMDMs exposed to Co^{2+}, Cr^{3+} and Ni^{2+}.

7.5.1 Hypoxia-inducible factor-1α (HIF-1α)

Stabilization of HIF-1α in BMDMs exposed to Co^{2+}, Cr^{3+} and Ni^{2+} should be evaluated, since it could provide insight into the underlying mechanisms leading to an increase in glycolytic metabolism in BMDMs exposed to Co^{2+} and Ni^{2+}, but not to Cr^{3+}, as presented in this thesis. HIF-1α is an inducible transcription factor that is known to up-regulate glycolysis by increasing glycolytic enzymes and glucose transporters [243]. Moreover, HIF-1α is expressed in macrophages, and under inflammatory conditions is tightly linked to metabolic reprogramming [244]. Interestingly, recent results indicated that Co^{2+}, but not Cr^{3+}, lead to the stabilization of HIF-1α in RAW 264.7 macrophages [194]. In other studies, HIF-1α was shown to be stabilized by Ni^{2+}, and led to an increase in HIF-1α gene encoding for glycolytic enzymes in rat liver cells [107], [242]. However, the effect of Ni^{2+} on the stabilization of HIF-1α in BMDMs has not been evaluated. Furthermore, the results presented in this thesis demonstrated an up-regulation of glycolytic flux with Co^{2+} and Ni^{2+}, but not with Cr^{3+}, in BMDMs. Finally, results with BMDMs exposed to Cr^{3+} differed from those previously reported with RAW 264.7 macrophages [194]. Therefore, future studies evaluating the stabilization of HIF-1α in BMDMs exposed to Co^{2+}, $Cr^{3+}$and Ni^{2+}, may shed light into the differences observed in glycolytic flux between the RAW 264.7 macrophages and BMDMs. Moreover, HIF-1α is known to be involved in the up-regulation of glycolytic enzyme transcription [242], and suspected to be a rate-limiting factor determining the maximal glycolytic capacity for macrophages[244]. Therefore, measuring HIF-

1α stabilization may lead to a better understanding of the increase in glycolytic flux, and maximal glycolytic capacity, observed with Co^{2+} and Ni^{2+}, but not Cr^{3+} in this study.

7.5.2 Quantification of PPP Flux

It is well known that a decrease in oxidative phosphorylation lowers the cytosolic ATP/ADP and ATP/AMP ratios, which activates glycolysis to meet ATP demands [14], [245]. Furthermore, when levels of mitochondrial ROS increase, there may be a temporary change in GSH:GSSG ratio and consequently NADPH/NADP ratio. This change activates the pentose phosphate pathway (PPP) to regenerate NADPH [14], and ultimately GSH to maintain normal physiological conditions [193]. Therefore, it is suspected that if Co^{2+}, Ni^{2+}, but not Cr^{3+}, led to a decrease in mitochondrial ATP production due to a decrease in OXPHOS there would be a metabolic shift increasing the need for NADPH resulting in an increase in PPP flux, and an increase in glycolytic flux to meet energy demands.. Finally, when combined with data for the quantification of GSH and GSSG, it could advance our understanding of the effects of these metal ions on redox-status and macrophage activation.

7.5.3 Measurement of Intracellular ROS and Oxidative Stress

The results of this thesis contributed to our understanding of the relationship between metal ions and aspects of cellular energy, specifically glycolytic flux. It is known that a decrease in OXPHOS associated with mitochondrial dysfunction typically leads to the activation of glycolysis to meet ATP demands [14], [245]. Moreover, mitochondrial dysfunction is known to be associated with high levels of mitochondrial ROS and ultimately oxidative stress. ROS is suspected to be capable of inducing inflammasome activation [169], [172, 201], [174], [246]. While the importance of mitochondria as cellular ATP generators has long been established, the relationship between cellular energy and oxidative stress due to metal ions has not yet been thoroughly explored. Therefore, to evaluate the connection between the metabolic changes of BMDMs to Co^{2+}, Ni^{2+}, and Cr^{3+} with increased production of ROS and oxidative stress, both ROS production and oxidative damage should be quantified. Based on the present study, it appears that Ni^{2+} and Co^{2+} may function through similar mechanisms and that these metal ions function differently than Cr^{3+}, although more investigation is necessary. The difference between

these metal ions on macrophage-activation was also observed by Ferko *et al.* [196], who reported that Co^{2+} and Ni^{2+} likely contribute to aseptic inflammation through different mechanisms than Cr^{3+}. Therefore, further investigation into the different mechanisms by which Co^{2+}, Ni^{2+}, and Cr^{3+} contribute to the aseptic inflammatory response is necessary.

References

[1] Canadian Institute for Health Information, “Hip and knee replacements in Canada: CJRR report | CIHI,” Jun. 20, 2019. https://www.cihi.ca/en/hip-and-knee-replacements-in-canada-cjrr-report-0 (accessed Jun. 26, 2019).

[2] R. W. Crawford and D. W. Murray, “Total hip replacement: indications for surgery and risk factors for failure,” *Ann. Rheum. Dis.*, vol. 56, no. 8, pp. 455–457, Aug. 1997, doi: 10.1136/ard.56.8.455.

[3] S. Kurtz, K. Ong, E. Lau, F. Mowat, and M. Halpern, “Projections of primary and revision hip and knee arthroplasty in the United States from 2005 to 2030,” *J. Bone Joint Surg. Am.*, vol. 89, no. 4, pp. 780–785, Apr. 2007, doi: 10.2106/JBJS.F.00222.

[4] M. E. Daigle, A. M. Weinstein, J. N. Katz, and E. Losina, “The cost-effectiveness of total joint arthroplasty: a systematic review of published literature,” *Best Pract. Res. Clin. Rheumatol.*, vol. 26, no. 5, pp. 649–658, Oct. 2012, doi: 10.1016/j.berh.2012.07.013.

[5] G. Holt, C. Murnaghan, J. Reilly, and R. M. D. Meek, “The biology of aseptic osteolysis,” *Clin. Orthop.*, vol. 460, pp. 240–252, Jul. 2007, doi: 10.1097/BLO.0b013e31804b4147.

[6] L. Zagra and E. Gallazzi, “Bearing surfaces in primary total hip arthroplasty,” *EFORT Open Rev.*, vol. 3, no. 5, pp. 217–224, May 2018, doi: 10.1302/2058-5241.3.180300.

[7] J. J. Callaghan, J. C. Albright, D. D. Goetz, J. P. Olejniczak, and R. C. Johnston, “Charnley Total Hip Arthroplasty with Cement : Minimum Twenty-five-Year Follow-up*,” *JBJS*, vol. 82, no. 4, p. 487, Apr. 2000.

[8] M. Spector, S. Shortkroff, H. P. Hsu, N. Lane, C. B. Sledge, and T. S. Thornhill, “Tissue changes around loose prostheses. A canine model to investigate the effects of an antiinflammatory agent,” *Clin. Orthop.*, no. 261, pp. 140–152, Dec. 1990.

[9] M. T. Manley and P. Serekian, “Wear debris. An environmental issue in total joint replacement,” *Clin. Orthop.*, no. 298, pp. 137–146, Jan. 1994.

[10] M. A. Hussein, A. S. Mohammed, and N. Al-Aqeeli, “Wear Characteristics of Metallic Biomaterials: A Review,” *Materials*, vol. 8, no. 5, pp. 2749–2768, May 2015, doi: 10.3390/ma8052749.

[11] M. Abdel-Hady Gepreel and M. Niinomi, “Biocompatibility of Ti-alloys for long-term implantation,” *J. Mech. Behav. Biomed. Mater.*, vol. 20, pp. 407–415, Apr. 2013, doi: 10.1016/j.jmbbm.2012.11.014.

[12] K. Merritt and S. A. D. E. Brown, “Effects of Metal Particles and Ions on the Biological System,” *Tech. Orthop. Winter 1993*, vol. 8, no. 4, pp. 228–236, 1993.

[13] W. Chen *et al.*, “Wear Particles Promote Reactive Oxygen Species-Mediated Inflammation via the Nicotinamide Adenine Dinucleotide Phosphate Oxidase Pathway in Macrophages Surrounding Loosened Implants,” *Cell. Physiol. Biochem.*, vol. 35, no. 5, pp. 1857–1867, 2015, doi: 10.1159/000373996.

[14] K. C. Patra and N. Hay, “The pentose phosphate pathway and cancer,” *Trends Biochem. Sci.*, vol. 39, no. 8, pp. 347–354, Aug. 2014, doi: 10.1016/j.tibs.2014.06.005.

[15] P. Korge, G. Calmettes, and J. N. Weiss, “Increased Reactive Oxygen Species Production During Reductive Stress: The Roles of Mitochondrial Glutathione and Thioredoxin Reductases,” *Biochim. Biophys. Acta*, vol. 1847, no. 0, pp. 514–525, 2015, doi: 10.1016/j.bbabio.2015.02.012.

[16] B. Kelly and L. A. J. O’Neill, “Metabolic reprogramming in macrophages and dendritic cells in innate immunity,” *Cell Res.*, vol. 25, no. 7, pp. 771–784, Jul. 2015, doi: 10.1038/cr.2015.68.

[17] J. Gallo, S. B. Goodman, Y. T. Konttinen, and M. Raska, “Particle disease: Biologic mechanisms of periprosthetic osteolysis in total hip arthroplasty,” *Innate Immun.*, vol. 19, no. 2, pp. 213–224, 2013, doi: 10.1177/1753425912451779.

[18] H. S. Gill, G. Grammatopoulos, S. Adshead, E. Tsialogiannis, and E. Tsiridis, “Molecular and immune toxicity of CoCr nanoparticles in MoM hip arthroplasty,” *Trends Mol. Med.*, vol. 18, no. 3, pp. 145–155, Mar. 2012, doi: 10.1016/j.molmed.2011.12.002.

[19] M. S. Caicedo, R. Desai, K. McAllister, A. Reddy, J. J. Jacobs, and N. J. Hallab, “Soluble and particulate Co-Cr-Mo alloy implant metals activate the inflammasome danger signaling pathway in human macrophages: A novel mechanism for implant debris reactivity,” *J. Orthop. Res.*, vol. 27, no. 7, pp. 847–854, 2009, doi: 10.1002/jor.20826.

[20] N. Hallab, K. Merritt, and J. J. Jacobs, “Metal Sensitivity in Patients with Orthopaedic Implants,” *JBJS*, vol. 83, no. 3, p. 428, Mar. 2001.

[21] D. T. Felson, “Osteoarthritis: New Insights. Part 1: The Disease and Its Risk Factors,” *Ann. Intern. Med.*, vol. 133, no. 8, p. 635, Oct. 2000, doi: 10.7326/0003-4819-133-8-200010170-00016.

[22] P. A. Revell, “The combined role of wear particles, macrophages and lymphocytes in the loosening of total joint prostheses,” *J. R. Soc. Interface*, vol. 5, no. 28, pp. 1263–1278, Nov. 2008, doi: 10.1098/rsif.2008.0142.

[23] R. Iorio, B. Puskas, W. L. Healy, J. F. Tilzey, L. M. Specht, and M. S. Thompson, “Cementless Acetabular Fixation With and Without Screws: Analysis of Stability and Migration,” *J. Arthroplasty*, vol. 25, no. 2, pp. 309–313, Feb. 2010, doi: 10.1016/j.arth.2009.01.023.

[24] S. R. Cummings, J. L. Kelsey, M. C. Nevitt, and K. J. O’dowd, “EPIDEMIOLOGY OF OSTEOPOROSIS AND OSTEOPOROTIC FRACTURES,” *Epidemiol. Rev.*, vol. 7, no. 1, pp. 178–208, Jan. 1985, doi: 10.1093/oxfordjournals.epirev.a036281.

[25] D. T. Felson, “Epidemiology of hip and knee osteoarthritis.,” *Epidemiol. Rev.*, vol. 10, pp. 1–28, 1988, doi: 10.1093/oxfordjournals.epirev.a036019.

[26] J. J. Jacobs, K. A. Roebuck, M. Archibeck, N. J. Hallab, and T. T. Glant, “Osteolysis: basic science.,” *Clin. Orthop.*, no. 393, pp. 71–77, 2001.

[27] R. Altman *et al.*, “Development of criteria for the classification and reporting of osteoarthritis: Classification of osteoarthritis of the knee,” *Arthritis Rheum.*, vol. 29, no. 8, pp. 1039–1049, 1986, doi: 10.1002/art.1780290816.

[28] I. D. Learmonth, “Biocompatibility: a biomechanical and biological concept in total hip replacement,” *The Surgeon*, vol. 1, no. 1, pp. 1–8, Feb. 2003, doi: 10.1016/S1479-666X(03)80002-1.

[29] B. F. Kavanagh *et al.*, “Charnley low-friction arthroplasty of the hip. Twenty-year results with cement,” *J. Arthroplasty*, vol. 9, no. 3, pp. 229–234, Jun. 1994.

[30] D. J. Berry, W. S. Harmsen, M. E. Cabanela, and B. F. Morrey, “Twenty-five-year survivorship of two thousand consecutive primary Charnley total hip replacements: factors affecting survivorship of acetabular and femoral components,” *J. Bone Joint Surg. Am.*, vol. 84, no. 2, pp. 171–177, Feb. 2002, doi: 10.2106/00004623-200202000-00002.

[31] R. Iorio *et al.*, “Orthopaedic Surgeon Workforce and Volume Assessment for Total Hip and Knee Replacement in the United States: Preparing for an Epidemic:,” *J. Bone Jt. Surg.-Am. Vol.*, vol. 90, no. 7, pp. 1598–1605, Jul. 2008, doi: 10.2106/JBJS.H.00067.

[32] S. B. Goodman, M. Trindade, T. Ma, M. Genovese, and R. L. Smith, “Pharmacologic modulation of periprosthetic osteolysis,” *Clin. Orthop.*, no. 430, pp. 39–45, Jan. 2005, doi: 10.1097/01.blo.0000149998.88218.05.

[33] M. Dobzyniak, T. K. Fehring, and S. Odum, “Early Failure in Total Hip Arthroplasty:,” *Clin. Orthop.*, vol. 447, pp. 76–78, Jun. 2006, doi: 10.1097/01.blo.0000203484.90711.52.

[34] P. Campbell, S. Ma, B. Yeom, H. McKellop, T. P. Schmalzried, and H. C. Amstutz, “Isolation of predominantly submicron-sized UHMWPE wear particles from periprosthetic tissues,” *J. Biomed. Mater. Res.*, vol. 29, no. 1, pp. 127–131, 1995, doi: 10.1002/jbm.820290118.

[35] W. J. Maloney, R. L. Smith, T. P. Schmalzried, J. Chiba, D. Huene, and H. Rubash, “Isolation and characterization of wear particles generated in patients who have had failure of a hip arthroplasty without cement,” *J. Bone*, vol. 77, no. 9, pp. 1301–1310, Sep. 1995.

[36] K. Magone, D. Luckenbill, and T. Goswami, “Metal ions as inflammatory initiators of osteolysis,” *Arch. Orthop. Trauma Surg.*, vol. 135, no. 5, pp. 683–695, May 2015, doi: 10.1007/s00402-015-2196-8.

[37] N. J. Hallab and J. J. Jacobs, “Biologic effects of implant debris,” *Bull. NYU Hosp. Jt. Dis.*, vol. 67, no. 2, pp. 182–188, 2009.

[38] S. Landgraeber, M. Jäger, J. J. Jacobs, and N. J. Hallab, “The Pathology of Orthopedic Implant Failure Is Mediated by Innate Immune System Cytokines,” *Mediators of Inflammation*, 2014. https://www.hindawi.com/journals/mi/2014/185150/ (accessed Aug. 29, 2019).

[39] P. Herberts and H. Malchau, “Long-term registration has improved the quality of hip replacement: A review of the Swedish THR Register comparing 160,000 cases,” *Acta Orthop. Scand.*, vol. 71, no. 2, pp. 111–121, Jan. 2000, doi: 10.1080/000164700317413067.

[40] O. Robertsson, K. Knutson, S. Lewold, and L. Lidgren, “The Swedish Knee Arthroplasty Register 1975-1997: An update with special emphasis on 41,223 knees operated on in 1988-1997,” *Acta Orthop. Scand.*, vol. 72, no. 5, pp. 503–513, Jan. 2001, doi: 10.1080/000164701753532853.

[41] S. B. Mirza, D. G. Dunlop, S. S. Panesar, S. G. Naqvi, S. Gangoo, and S. Salih, “Basic Science Considerations in Primary Total Hip Replacement Arthroplasty,” *Open Orthop. J.*, vol. 4, pp. 169–180, May 2010, doi: 10.2174/1874325001004010169.

[42] Y. Abu-Amer, I. Darwech, and J. C. Clohisy, “Aseptic loosening of total joint replacements: mechanisms underlying osteolysis and potential therapies,” *Arthritis Res. Ther.*, vol. 9, no. Suppl 1, p. S6, 2007, doi: 10.1186/ar2170.

[43] J. Drummond, P. Tran, and C. Fary, “Metal-on-Metal Hip Arthroplasty: A Review of Adverse Reactions and Patient Management,” *J. Funct. Biomater.*, vol. 6, no. 3, pp. 486–499, Jun. 2015, doi: 10.3390/jfb6030486.

[44] S. B. Goodman, “Wear Particles, Periprosthetic Osteolysis and the Immune System,” *Biomaterials*, vol. 28, no. 34, pp. 5044–5048, Dec. 2007, doi: 10.1016/j.biomaterials.2007.06.035.

[45] B. Ollivere, J. A. Wimhurst, I. M. Clark, and S. T. Donell, “Current concepts in osteolysis,” *J. Bone Joint Surg. Br.*, vol. 94, no. 1, pp. 10–15, Jan. 2012, doi: 10.1302/0301-620X.94B1.28047.

[46] R. T. Beck, K. D. Illingworth, and K. J. Saleh, “Review of periprosthetic osteolysis in total joint arthroplasty: an emphasis on host factors and future directions,” *J. Orthop. Res. Off. Publ. Orthop. Res. Soc.*, vol. 30, no. 4, pp. 541–546, Apr. 2012, doi: 10.1002/jor.21554.

[47] R. VanOs, L. L. Lildhar, E. A. Lehoux, P. E. Beaulé, and I. Catelas, “In vitro macrophage response to nanometer-size chromium oxide particles,” *J. Biomed. Mater. Res. B Appl. Biomater.*, vol. 102, no. 1, pp. 149–159, Jan. 2014, doi: 10.1002/jbm.b.32991.

[48] I. Catelas and M. A. Wimmer, “New insights into wear and biological effects of metal-on-metal bearings.,” *J. Bone Joint Surg. Am.*, vol. 93 Suppl 2, no. Suppl 2, pp. 76–83, May 2011, doi: 10.2106/JBJS.J.01877.

[49] H. Pandit *et al.*, “Pseudotumours associated with metal-on-metal hip resurfacings,” *J. Bone Joint Surg. Br.*, vol. 90, no. 7, pp. 847–851, Jul. 2008, doi: 10.1302/0301-620X.90B7.20213.

[50] S. Glyn-Jones, H. Pandit, Y.-M. Kwon, H. Doll, H. S. Gill, and D. W. Murray, “Risk factors for inflammatory pseudotumour formation following hip resurfacing,” *J. Bone Joint Surg. Br.*, vol. 91, no. 12, pp. 1566–1574, Dec. 2009, doi: 10.1302/0301-620X.91B12.22287.

[51] P. Campbell, E. Ebramzadeh, S. Nelson, K. Takamura, K. De Smet, and H. C. Amstutz, “Histological features of pseudotumor-like tissues from metal-on-metal hips,” *Clin. Orthop.*, vol. 468, no. 9, pp. 2321–2327, Sep. 2010, doi: 10.1007/s11999-010-1372-y.

[52] K. F. Bowman, J. Fox, and J. K. Sekiya, “A Clinically Relevant Review of Hip Biomechanics,” *Arthroscopy*, vol. 26, no. 8, pp. 1118–1129, Aug. 2010, doi: 10.1016/j.arthro.2010.01.027.

[53] G. Johnson, “1 - Biomechanics of joints,” in *Joint Replacement Technology*, P. A. Revell, Ed. Woodhead Publishing, 2008, pp. 3–30.

[54] D. P. Byrne, K. J. Mulhall, and J. F. Baker, “Anatomy & Biomechanics of the Hip,” *Open Sports Med. J.*, vol. 4, no. 1, pp. 51–57, Jan. 2010, doi: 10.2174/1874387001004010051.

[55] L. L. Hench, *New Materials and Technologies for Healthcare*. World Scientific, 2012.

[56] “Metal-on-Metal Total Hip Resurfacing Arthroplasty,” *Ont. Health Technol. Assess. Ser.*, vol. 6, no. 4, pp. 1–57, Feb. 2006.

[57] D. g. Lewallen, “Acetabular cup and liner options,” *Orthop. Proc.*, vol. 99-B, no. SUPP_7, pp. 12–12, Apr. 2017, doi: 10.1302/1358-992X.99BSUPP_7.CCJR2016-012.

[58] T. P. Schmalzried and J. J. Callaghan, “Current Concepts Review - Wear in Total Hip and Knee Replacements*,” *JBJS*, vol. 81, no. 1, p. 115, Jan. 1999.

[59] J. O. Galante, J. Lemons, M. Spector, P. D. Wilson, and T. M. Wright, “The biologic effects of implant materials,” *J. Orthop. Res.*, vol. 9, no. 5, pp. 760–775, Sep. 1991, doi: 10.1002/jor.1100090516.

[60] D. F. Williams and European Society for Biomaterials, Eds., *Definitions in biomaterials: proceedings of a consensus conference of the European Society for Biomaterials, Chester, England, March 3-5, 1986*. Amsterdam; New York: Elsevier, 1987.

[61] K. S. Katti, “Biomaterials in total joint replacement,” *Colloids Surf. B Biointerfaces*, vol. 39, no. 3, pp. 133–142, Dec. 2004, doi: 10.1016/j.colsurfb.2003.12.002.

[62] C. P. Bergmann and A. Stumpf, *Dental Ceramics: Microstructure, Properties and Degradation*. Berlin Heidelberg: Springer-Verlag, 2013.

[63] J. H. Dumbleton, M. T. Manley, and A. A. Edidin, “A literature review of the association between wear rate and osteolysis in total hip arthroplasty,” *J. Arthroplasty*, vol. 17, no. 5, pp. 649–661, Aug. 2002, doi: 10.1054/arth.2002.33664.

[64] S. M. Kurtz, H. A. Gawel, and J. D. Patel, “History and Systematic Review of Wear and Osteolysis Outcomes for First-generation Highly Crosslinked Polyethylene,” *Clin. Orthop.*, vol. 469, no. 8, pp. 2262–2277, Aug. 2011, doi: 10.1007/s11999-011-1872-4.

[65] D. C. Hansen, “Metal Corrosion in the Human Body: The Ultimate Bio-Corrosion Scenario,” *Electrochem. Soc. Interface*, p. 4, 2008.

[66] I. Catelas, A. Petit, R. Marchand, D. J. Zukor, L. Yahia, and O. L. Huk, “Cytotoxicity and macrophage cytokine release induced by ceramic and polyethylene particles in vitro,” *J. Bone Joint Surg. Br.*, vol. 81, no. 3, pp. 516–521, May 1999.

[67] Hernandez, E. Keating, P. Faris, J. Meding, and M. Ritter, “Polyethylene wear in uncemented acetabular components,” *J. Bone Joint Surg. Br.*, vol. 76-B, no. 2, pp. 263–266, Mar. 1994, doi: 10.1302/0301-620X.76B2.8113288.

[68] S. Santavirta, D. Nordström, K. Metsärinne, and Y. T. Konttinen, “Biocompatibility of polyethylene and host response to loosening of cementless total hip replacement.,” *Clin. Orthop.*, no. 297, pp. 100–110, Dec. 1993.

[69] M. Geetha, A. K. Singh, R. Asokamani, and A. K. Gogia, “Ti based biomaterials, the ultimate choice for orthopaedic implants – A review,” *Prog. Mater. Sci.*, vol. 54, no. 3, pp. 397–425, May 2009, doi: 10.1016/j.pmatsci.2008.06.004.

[70] G. M. Raghavendra, K. Varaprasad, and T. Jayaramudu, “Chapter 2 - Biomaterials: Design, Development and Biomedical Applications,” in *Nanotechnology Applications for Tissue Engineering*, S. Thomas, Y. Grohens, and N. Ninan, Eds. Oxford: William Andrew Publishing, 2015, pp. 21–44.

[71] H. McKellop *et al.*, “In vivo wear of three types of metal on metal hip prostheses during two decades of use,” *Clin. Orthop.*, no. 329 Suppl, pp. S128-140, Aug. 1996, doi: 10.1097/00003086-199608001-00013.

[72] C. B. Rieker, P. Köttig, R. Schön, M. Windler, and U. P. Wyss, “Clinical Wear Performance of Metal-on-Metal Hip Arthroplasties,” *Altern. Bear. Surf. Total Jt. Replace.*, Jan. 1998, doi: 10.1520/STP12836S.

[73] I. Catelas *et al.*, “Quantitative analysis of macrophage apoptosis vs. necrosis induced by cobalt and chromium ions in vitro,” *Biomaterials*, vol. 26, no. 15, pp. 2441–2453, May 2005, doi: 10.1016/j.biomaterials.2004.08.004.

[74] O. E. Pohler, “Unalloyed titanium for implants in bone surgery,” *Injury*, vol. 31 Suppl 4, pp. 7–13, Dec. 2000, doi: 10.1016/s0020-1383(00)80016-9.

[75] D. Cadosch, E. Chan, O. P. Gautschi, and L. Filgueira, “Metal is not inert: Role of metal ions released by biocorrosion in aseptic loosening—Current concepts,” *J. Biomed. Mater. Res. A*, vol. 91A, no. 4, pp. 1252–1262, 2009, doi: 10.1002/jbm.a.32625.

[76] J. A. Disegi and H. Wyss, “Implant Materials for Fracture Fixation: A Clinical Perspective,” *Orthop. Thorofare*, vol. 12, no. 1, pp. 75–79, Jan. 1989.

[77] C. Y. Hu and T.-R. Yoon, “Recent updates for biomaterials used in total hip arthroplasty,” *Biomater. Res.*, vol. 22, no. 1, p. 33, Dec. 2018, doi: 10.1186/s40824-018-0144-8.

[78] T. M. Sridhar, S. P. Vinodhini, U. K. Mudali, B. Venkatachalapathy, and K. Ravichandran, “Load-bearing metallic implants: electrochemical characterisation of corrosion phenomena,” *Mater. Technol.*, vol. 31, no. 12, pp. 705–718, Oct. 2016, doi: 10.1080/10667857.2016.1220752.

[79] A. Sargeant and T. Goswami, “Hip implants – Paper VI – Ion concentrations,” *Mater. Des.*, vol. 28, no. 1, pp. 155–171, Jan. 2007, doi: 10.1016/j.matdes.2005.05.018.

[80] B. Scharf *et al.*, “Molecular analysis of chromium and cobalt-related toxicity,” *Sci. Rep.*, vol. 4, Jul. 2014, doi: 10.1038/srep05729.

[81] G. M. Keegan, I. D. Learmonth, and C. P. Case, “A systematic comparison of the actual, potential, and theoretical health effects of cobalt and chromium exposures from industry and surgical implants,” *Crit. Rev. Toxicol.*, vol. 38, no. 8, pp. 645–674, 2008, doi: 10.1080/10408440701845534.

[82] N. Abbaspour, R. Hurrell, and R. Kelishadi, “Review on iron and its importance for human health,” *J. Res. Med. Sci. Off. J. Isfahan Univ. Med. Sci.*, vol. 19, no. 2, pp. 164–174, Feb. 2014.

[83] K. E. Dineley, L. L. Richards, T. V. Votyakova, and I. J. Reynolds, “Zinc causes loss of membrane potential and elevates reactive oxygen species in rat brain mitochondria,” *Mitochondrion*, vol. 5, no. 1, pp. 55–65, Feb. 2005.

[84] Y. Mu, T. Kobayashi, M. Sumita, A. Yamamoto, and T. Hanawa, “Metal ion release from titanium with active oxygen species generated by rat macrophages in vitro,” *J. Biomed. Mater. Res.*, vol. 49, no. 2, pp. 238–243, Feb. 2000, doi: 10.1002/(sici)1097-4636(200002)49:2<238::aid-jbm12>3.0.co;2-j.

[85] K. Czarnek, S. Terpiłowska, and A. K. Siwicki, “Selected aspects of the action of cobalt ions in the human body,” *Cent.-Eur. J. Immunol.*, vol. 40, no. 2, pp. 236–242, 2015, doi: 10.5114/ceji.2015.52837.

[86] O. Karovic *et al.*, “Toxic effects of cobalt in primary cultures of mouse astrocytes. Similarities with hypoxia and role of HIF-1alpha,” *Biochem. Pharmacol.*, vol. 73, no. 5, pp. 694–708, Mar. 2007, doi: 10.1016/j.bcp.2006.11.008.

[87] S. J. Baskey, E. A. Lehoux, and I. Catelas, “Effects of cobalt and chromium ions on lymphocyte migration,” *J. Orthop. Res. Off. Publ. Orthop. Res. Soc.*, vol. 35, no. 4, pp. 916–924, 2017, doi: 10.1002/jor.23336.

[88] C. Tkaczyk *et al.*, “The molecular structure of complexes formed by chromium or cobalt ions in simulated physiological fluids,” *Biomaterials*, vol. 30, no. 4, pp. 460–467, Feb. 2009, doi: 10.1016/j.biomaterials.2008.09.055.

[89] T. E. Gunter, D. I. Yule, K. K. Gunter, R. A. Eliseev, and J. D. Salter, “Calcium and mitochondria,” *FEBS Lett.*, vol. 567, no. 1, pp. 96–102, Jun. 2004, doi: 10.1016/j.febslet.2004.03.071.

[90] D. Díaz, R. Bartolo, D. M. Delgadillo, F. Higueldo, and J. C. Gomora, “Contrasting effects of Cd2+ and Co2+ on the blocking/unblocking of human Cav3 channels,” *J. Membr. Biol.*, vol. 207, no. 2, pp. 91–105, Sep. 2005, doi: 10.1007/s00232-005-0804-1.

[91] B. Raghavan, S. F. Martin, P. R. Esser, M. Goebeler, and M. Schmidt, “Metal allergens nickel and cobalt facilitate TLR4 homodimerization independently of MD2,” *EMBO Rep.*, vol. 13, no. 12, pp. 1109–1115, Dec. 2012, doi: 10.1038/embor.2012.155.

[92] M. Schmidt *et al.*, “Crucial role for human Toll-like receptor 4 in the development of contact allergy to nickel,” *Nat. Immunol.*, vol. 11, no. 9, pp. 814–819, Sep. 2010, doi: 10.1038/ni.1919.

[93] A. W. Foster, D. Osman, and N. J. Robinson, “Metal Preferences and Metallation,” *J. Biol. Chem.*, vol. 289, no. 41, pp. 28095–28103, Oct. 2014, doi: 10.1074/jbc.R114.588145.

[94] H. Chen and M. Costa, “Effect of soluble nickel on cellular energy metabolism in A549 cells,” *Exp. Biol. Med. Maywood NJ*, vol. 231, no. 9, pp. 1474–1480, Oct. 2006.

[95] T. H. Lim, T. Sargent, and N. Kusubov, “Kinetics of trace element chromium(III) in the human body,” *Am. J. Physiol.*, vol. 244, no. 4, pp. R445-454, Apr. 1983, doi: 10.1152/ajpregu.1983.244.4.R445.

[96] J. J. Jacobs *et al.*, “Metal Release in Patients Who Have Had a Primary Total Hip Arthroplasty. A Prospective, Controlled, Longitudinal Study*,” *JBJS*, vol. 80, no. 10, p. 1447, Oct. 1998.

[97] A. K. Skipor, P. A. Campbell, L. M. Patterson, H. C. Anstutz, T. P. Schmalzried, and J. J. Jacobs, “Serum and urine metal levels in patients with metal-on-metal surface arthroplasty,” *J. Mater. Sci. Mater. Med.*, vol. 13, no. 12, pp. 1227–1234, Dec. 2002, doi: 10.1023/a:1021179029640.

[98] J. A. Geller, H. Malchau, C. Bragdon, M. Greene, W. H. Harris, and A. A. Freiberg, “Large Diameter Femoral Heads on Highly Cross-linked Polyethylene: Minimum 3-year Results.,” *Clin. Orthop. Relat. Res. 1976-2007*, vol. 447, pp. 53–59, Jun. 2006, doi: 10.1097/01.blo.0000218742.61624.80.

[99] H.-J. Choi, S.-J. Lim, Y.-S. Park, and S.-Y. Lee, “Simple and robust ICP-MS method for simultaneous determination of serum Co and Cr in routine clinical practice,” *Clin. Chim. Acta*, vol. 439, pp. 91–96, Jan. 2015, doi: 10.1016/j.cca.2014.09.019.

[100] K. Balamurugan, R. Rajaram, T. Ramasami, and S. Narayanan, “Chromium(III)-induced apoptosis of lymphocytes: death decision by ROS and Src-family tyrosine kinases,” *Free Radic. Biol. Med.*, vol. 33, no. 12, pp. 1622–1640, Dec. 2002, doi: 10.1016/s0891-5849(02)01115-2.

[101] D. Río and L. A, “ROS and RNS in plant physiology: an overview,” *J. Exp. Bot.*, vol. 66, no. 10, pp. 2827–2837, May 2015, doi: 10.1093/jxb/erv099.

[102] R. J. Mailloux, S. L. McBride, and M.-E. Harper, “Unearthing the secrets of mitochondrial ROS and glutathione in bioenergetics,” *Trends Biochem. Sci.*, vol. 38, no. 12, pp. 592–602, Dec. 2013, doi: 10.1016/j.tibs.2013.09.001.

[103] K. V. Tormos *et al.*, “Mitochondrial complex III ROS regulate adipocyte differentiation,” *Cell Metab.*, vol. 14, no. 4, pp. 537–544, Oct. 2011, doi: 10.1016/j.cmet.2011.08.007.

[104] A.-B. Al-Mehdi *et al.*, “Perinuclear Mitochondrial Clustering Creates an Oxidant-Rich Nuclear Domain Required for Hypoxia-Induced Transcription,” *Sci. Signal.*, vol. 5, no. 231, p. ra47, Jul. 2012, doi: 10.1126/scisignal.2002712.

[105] K. Loh *et al.*, “Reactive oxygen species enhance insulin sensitivity,” *Cell Metab.*, vol. 10, no. 4, pp. 260–272, Oct. 2009, doi: 10.1016/j.cmet.2009.08.009.

[106] B. Brüne *et al.*, “Redox Control of Inflammation in Macrophages,” *Antioxid. Redox Signal.*, vol. 19, no. 6, pp. 595–637, Aug. 2013, doi: 10.1089/ars.2012.4785.

[107] Z. Salloum, E. A. Lehoux, M.-E. Harper, and I. Catelas, "Effects of cobalt and chromium ions on oxidative stress and energy metabolism in macrophages in vitro,” *J. Orthop. Res.* 2018 Dec; 36(12):3178–3187. doi: 10.1002/jor.24130. Epub 2018 Oct 9.

[108] K. M. Holmström and T. Finkel, “Cellular mechanisms and physiological consequences of redox-dependent signalling,” *Nat. Rev. Mol. Cell Biol.*, vol. 15, no. 6, p. 411, 2014.

[109] T. Davidson, Q. Ke, and M. Costa, “Chapter 9 - Selected Molecular Mechanisms of Metal Toxicity and Carcinogenicity,” in *Handbook on the Toxicology of Metals (Fourth Edition)*, G. F. Nordberg, B. A. Fowler, and M. Nordberg, Eds. San Diego: Academic Press, 2015, pp. 173–196.

[110] S. J. Dixon and B. R. Stockwell, “The role of iron and reactive oxygen species in cell death,” *Nat. Chem. Biol.*, vol. 10, no. 1, pp. 9–17, Jan. 2014, doi: 10.1038/nchembio.1416.

[111] E. Nam, J. Han, J.-M. Suh, Y. Yi, and M. H. Lim, “Link of impaired metal ion homeostasis to mitochondrial dysfunction in neurons,” *Curr. Opin. Chem. Biol.*, vol. 43, pp. 8–14, Apr. 2018, doi: 10.1016/j.cbpa.2017.09.009.

[112] G. Meisenberg, *Principles of medical biochemistry*, 3rd ed. Philadelphia: Elsevier/Saunders, 2012.

[113] W. Kühlbrandt, “Structure and function of mitochondrial membrane protein complexes,” *BMC Biol.*, vol. 13, Oct. 2015, doi: 10.1186/s12915-015-0201-x.

[114] J. F. Turrens, “Superoxide Production by the Mitochondrial Respiratory Chain,” *Biosci. Rep.*, vol. 17, no. 1, pp. 3–8, Feb. 1997, doi: 10.1023/A:1027374931887.

[115] B. Alberts, A. Johnson, J. Lewis, M. Raff, K. Roberts, and P. Walter, “Electron-Transport Chains and Their Proton Pumps,” *Mol. Biol. Cell 4th Ed.*, 2002, Accessed: Sep. 19, 2019. [Online]. Available: https://www.ncbi.nlm.nih.gov/books/NBK26904/.

[116] Y. Wang, J. Fang, S. S. Leonard, and K. M. Krishna Rao, “Cadmium inhibits the electron transfer chain and induces Reactive Oxygen Species,” *Free Radic. Biol. Med.*, vol. 36, no. 11, pp. 1434–1443, Jun. 2004, doi: 10.1016/j.freeradbiomed.2004.03.010.

[117] S. Raha and B. H. Robinson, “Mitochondria, oxygen free radicals, disease and ageing,” *Trends Biochem. Sci.*, vol. 25, no. 10, pp. 502–508, Oct. 2000, doi: 10.1016/S0968-0004(00)01674-1.

[118] J. P. Kehrer, “The Haber–Weiss reaction and mechanisms of toxicity,” *Toxicology*, vol. 149, no. 1, pp. 43–50, Aug. 2000, doi: 10.1016/S0300-483X(00)00231-6.

[119] J. St-Pierre, J. A. Buckingham, S. J. Roebuck, and M. D. Brand, “Topology of Superoxide Production from Different Sites in the Mitochondrial Electron Transport Chain,” *J. Biol. Chem.*, vol. 277, no. 47, pp. 44784–44790, Nov. 2002, doi: 10.1074/jbc.M207217200.

[120] T. Finkel, “Signal transduction by reactive oxygen species,” *J. Cell Biol.*, vol. 194, no. 1, pp. 7–15, Jul. 2011, doi: 10.1083/jcb.201102095.

[121] S. I. Liochev and I. Fridovich, “The Haber-Weiss cycle—70 years later: an alternative view,” *Redox Rep.*, vol. 7, no. 1, pp. 55–57, Feb. 2002, doi: 10.1179/135100002125000190.

[122] W. G. Barb, J. H. Baxendale, P. George, and K. R. Hargrave, “Reactions of ferrous and ferric ions with hydrogen peroxide. Part I.—The ferrous ion reaction,” *Trans. Faraday Soc.*, vol. 47, no. 0, pp. 462–500, Jan. 1951, doi: 10.1039/TF9514700462.

[123] F. Haber, J. Weiss, and W. J. Pope, “The catalytic decomposition of hydrogen peroxide by iron salts,” *Proc. R. Soc. Lond. Ser. - Math. Phys. Sci.*, vol. 147, no. 861, pp. 332–351, Nov. 1934, doi: 10.1098/rspa.1934.0221.

[124] H. J. H. Fenton, “LXXIII.—Oxidation of tartaric acid in presence of iron,” *J. Chem. Soc. Trans.*, vol. 65, pp. 899–910, 1894, doi: 10.1039/CT8946500899.

[125] P. Wardman and L. P. Candeias, “Fenton Chemistry: An Introduction,” *Radiat. Res.*, vol. 145, no. 5, pp. 523–531, 1996, doi: 10.2307/3579270.

[126] T. Ozawa and A. Hanaki, “Spin-trapping studies on the reactions of Cr(III) with hydrogen peroxide in the presence of biological reductants: is Cr(III) non-toxic?,” *Biochem. Int.*, vol. 22, no. 2, pp. 343–352, Oct. 1990.

[127] S. J. Stohs and D. Bagchi, “Oxidative mechanisms in the toxicity of metal ions,” *Free Radic. Biol. Med.*, vol. 18, no. 2, pp. 321–336, Feb. 1995, doi: 10.1016/0891-5849(94)00159-H.

[128] M. Valko, K. Jomova, C. Rhodes, K. Kuča, and K. Musílek, “Redox- and non-redox-metal-induced formation of free radicals and their role in human disease,” *Arch. Toxicol.*, vol. 90, no. 1, pp. 1–37, 2016, doi: 10.1007/s00204-015-1579-5.

[129] H. Sies, “Oxidative stress: a concept in redox biology and medicine,” *Redox Biol.*, vol. 4, pp. 180–183, Apr. 2015, doi: 10.1016/j.redox.2015.01.002.

[130] Klaunig J E *et al.*, “The role of oxidative stress in chemical carcinogenesis.,” *Environ. Health Perspect.*, vol. 106, no. suppl 1, pp. 289–295, Feb. 1998, doi: 10.1289/ehp.98106s1289.

[131] S. Terpilowska and A. K. Siwicki, “Cell cycle and transmembrane mitochondrial potential analysis after treatment with chromium(III), iron(III), molybdenum(III) or nickel(II) and their mixtures,” *Toxicol. Res.*, vol. 8, no. 2, pp. 188–195, Mar. 2019, doi: 10.1039/C8TX00233A.

[132] B. I. Frohnert and D. A. Bernlohr, “Protein Carbonylation, Mitochondrial Dysfunction, and Insulin Resistance123,” *Adv. Nutr.*, vol. 4, no. 2, pp. 157–163, Mar. 2013, doi: 10.3945/an.112.003319.

[133] R. F. Jacob and R. P. Mason, “Lipid Peroxidation Induces Cholesterol Domain Formation in Model Membranes,” *J. Biol. Chem.*, vol. 280, no. 47, pp. 39380–39387, Nov. 2005, doi: 10.1074/jbc.M507587200.

[134] M. Valko, D. Leibfritz, J. Moncol, M. T. D. Cronin, M. Mazur, and J. Telser, “Free radicals and antioxidants in normal physiological functions and human disease,” *Int. J. Biochem. Cell Biol.*, vol. 39, no. 1, pp. 44–84, Jan. 2007, doi: 10.1016/j.biocel.2006.07.001.

[135] R. N. Appala, S. Chigurupati, R. V. V. S. S. Appala, K. Krishnan Selvarajan, and J. Islam Mohammad, “A Simple HPLC-UV Method for the Determination of Glutathione in PC-12 Cells,” *Scientifica*, vol. 2016, 2016, doi: 10.1155/2016/6897890.

[136] M. C. Reed, R. L. Thomas, J. Pavisic, S. J. James, C. M. Ulrich, and H. F. Nijhout, “A mathematical model of glutathione metabolism,” *Theor. Biol. Med. Model.*, vol. 5, p. 8, Apr. 2008, doi: 10.1186/1742-4682-5-8.

[137] M. D. Pulido and A. R. Parrish, “Metal-induced apoptosis: mechanisms,” *Mutat. Res. Mol. Mech. Mutagen.*, vol. 533, no. 1, pp. 227–241, Dec. 2003, doi: 10.1016/j.mrfmmm.2003.07.015.

[138] V. I. Lushchak, “Glutathione Homeostasis and Functions: Potential Targets for Medical Interventions,” *Journal of Amino Acids*, 2012. https://www.hindawi.com/journals/jaa/2012/736837/ (accessed Oct. 02, 2019).

[139] O. ZITKA *et al.*, “Redox status expressed as GSH:GSSG ratio as a marker for oxidative stress in paediatric tumour patients,” *Oncol. Lett.*, vol. 4, no. 6, pp. 1247–1253, Dec. 2012, doi: 10.3892/ol.2012.931.

[140] A. Petit, F. Mwale, C. Tkaczyk, J. Antoniou, D. J. Zukor, and O. L. Huk, "Induction of protein oxidation by cobalt and chromium ions in human U937 macrophages," *Biomaterials*, vol. 26, no. 21, pp. 4416–4422, Jul. 2005, doi: 10.1016/j.biomaterials.2004.11.019.

[141] R. J. Mailloux and M.-E. Harper, "Uncoupling proteins and the control of mitochondrial reactive oxygen species production," *Free Radic. Biol. Med.*, vol. 51, no. 6, pp. 1106–1115, Sep. 2011, doi: 10.1016/j.freeradbiomed.2011.06.022.

[142] P. Paavolainen, E. Pukkala, P. Pulkkinen, and T. Visuri, "Cancer incidence in Finnish hip replacement patients from 1980 to 1995: a nationwide cohort study involving 31,651 patients," *J. Arthroplasty*, vol. 14, no. 3, pp. 272–280, Apr. 1999, doi: 10.1016/s0883-5403(99)90051-7.

[143] S. J. MacDonald *et al.*, "Metal-on-metal versus polyethylene in hip arthroplasty: a randomized clinical trial," *Clin. Orthop.*, no. 406, pp. 282–296, Jan. 2003, doi: 10.1097/01.blo.0000043066.62337.9d.

[144] T. Rae, "A study on the effects of particulate metals of orthopaedic interest on murine macrophages in vitro," *J. Bone Joint Surg. Br.*, vol. 57, no. 4, pp. 444–450, Nov. 1975.

[145] D. R. Haynes, S. D. Rogers, S. Hay, M. J. Pearcy, and D. W. Howie, "The differences in toxicity and release of bone-resorbing mediators induced by titanium and cobalt-chromium-alloy wear particles," *J. Bone Joint Surg. Am.*, vol. 75, no. 6, pp. 825–834, Jun. 1993, doi: 10.2106/00004623-199306000-00004.

[146] A. G. Cobb and T. P. Schmalzreid, "The clinical significance of metal ion release from cobalt-chromium metal-on-metal hip joint arthroplasty," *Proc. Inst. Mech. Eng. [H]*, vol. 220, no. 2, pp. 385–398, Feb. 2006, doi: 10.1243/09544119JEIM78.

[147] D. J. Gawkrodger, "Metal sensitivities and orthopaedic implants revisited: the potential for metal allergy with the new metal-on-metal joint prostheses," *Br. J. Dermatol.*, vol. 148, no. 6, pp. 1089–1093, Jun. 2003, doi: 10.1046/j.1365-2133.2003.05404.x.

[148] C. P. Case, "Chromosomal changes after surgery for joint replacement," *J. Bone Joint Surg. Br.*, vol. 83, no. 8, pp. 1093–1095, Nov. 2001, doi: 10.1302/0301-620x.83b8.12755.

[149] I. Catelas, A. Petit, D. J. Zukor, J. Antoniou, and O. L. Huk, "TNF-α secretion and macrophage mortality induced by cobalt and chromium ions in vitro-Qualitative analysis of apoptosis," *Biomaterials*, vol. 24, no. 3, pp. 383–391, Feb. 2003, doi: 10.1016/S0142-9612(02)00351-4.

[150] Y. Wang and S. Dai, “Structural basis of metal hypersensitivity,” *Immunol. Res.*, vol. 55, no. 0, pp. 83–90, Mar. 2013, doi: 10.1007/s12026-012-8351-1.

[151] J. Aaseth, L. Gerhardsson, M. A. Skaug, and J. Alexander, “Chapter 1 - General Chemistry of Metal Toxicity and Basis for Metal Complexation,” in *Chelation Therapy in the Treatment of Metal Intoxication*, J. Aaseth, G. Crisponi, and O. Andersen, Eds. Boston: Academic Press, 2016, pp. 1–33.

[152] W. H. Harris, “Osteolysis and particle disease in hip replacement: A review,” *Acta Orthop. Scand.*, vol. 65, no. 1, pp. 113–123, Jan. 1994, doi: 10.3109/17453679408993734.

[153] C. Nich *et al.*, “Macrophages – Key Cells in the Response to Wear Debris from Joint Replacements,” *J. Biomed. Mater. Res. A*, vol. 101, no. 10, pp. 3033–3045, Oct. 2013, doi: 10.1002/jbm.a.34599.

[154] C. Nich and S. B. Goodman, “The role of macrophages in the biological reaction to wear debris from joint replacements,” *J. Long. Term Eff. Med. Implants*, vol. 24, no. 4, pp. 259–265, 2014.

[155] J. Gallo, M. Raska, E. Kriegova, and S. B. Goodman, “Inflammation and its resolution and the musculoskeletal system,” *J. Orthop. Transl.*, vol. 10, pp. 52–67, Jul. 2017, doi: 10.1016/j.jot.2017.05.007.

[156] S. B. Goodman and T. Ma, “Cellular chemotaxis induced by wear particles from joint replacements,” *Biomaterials*, vol. 31, no. 19, pp. 5045–5050, Jul. 2010, doi: 10.1016/j.biomaterials.2010.03.046.

[157] J. M. Anderson, A. Rodriguez, and D. T. Chang, “FOREIGN BODY REACTION TO BIOMATERIALS,” *Semin. Immunol.*, vol. 20, no. 2, pp. 86–100, Apr. 2008, doi: 10.1016/j.smim.2007.11.004.

[158] E. Ingham and J. Fisher, “The role of macrophages in osteolysis of total joint replacement,” *Biomaterials*, vol. 26, no. 11, pp. 1271–1286, Apr. 2005, doi: 10.1016/j.biomaterials.2004.04.035.

[159] P. M. Kou and J. E. Babensee, “Macrophage and dendritic cell phenotypic diversity in the context of biomaterials,” *J. Biomed. Mater. Res. A*, vol. 96A, no. 1, pp. 239–260, 2011, doi: 10.1002/jbm.a.32971.

[160] J. Chiba, H. E. Rubash, K. J. Kim, and Y. Iwaki, “The characterization of cytokines in the interface tissue obtained from failed cementless total hip arthroplasty with and without

femoral osteolysis.," *Clin. Orthop.*, vol. 300, pp. 304–312, 1994, doi: 10.1097/00003086-199403000-00043.

[161] A. Sabokbar and N. Rushton, "Role of inflammatory mediators and adhesion molecules in the pathogenesis of aseptic loosening in total hip arthroplasties," *J. Arthroplasty*, vol. 10, no. 6, pp. 810–816, Dec. 1995, doi: 10.1016/S0883-5403(05)80080-4.

[162] J. W. Xu *et al.*, "Tumor necrosis factor-alpha (TNF-alpha) in loosening of total hip replacement (THR).," *Clin. Exp. Rheumatol.*, vol. 14, no. 6, pp. 643–648, 1996.

[163] J-W. Xu T. F. Li1, G. Partsch, A. C. eponis, S. Santavirta and Y.T. Konttinen, "Interleukin-11 (IL-11) in Aseptic Loosening of Total Hip Replacement (THR)," *Scand. J. Rheumatol.*, vol. 27, no. 5, pp. 363–367, Jan. 1998, doi: 10.1080/03009749850154393.

[164] S. A. Clarke, R. A. Brooks, J. L. Hobby, J. A. Wimhurst, B. J. Myer, and N. Rushton, "Correlation of synovial fluid cytokine levels with histological and clinical parameters of primary and revision total hip and total knee replacements," *Acta Orthop. Scand.*, vol. 72, no. 5, pp. 491–498, Oct. 2001, doi: 10.1080/000164701753532835.

[165] A. P. Davies, H. G. Willert, P. A. Campbell, I. D. Learmonth, and C. P. Case, "An unusual lymphocytic perivascular infiltration in tissues around contemporary metal-on-metal joint replacements," *J. Bone Joint Surg. Am.*, vol. 87, no. 1, pp. 18–27, Jan. 2005, doi: 10.2106/JBJS.C.00949.

[166] V. Sansone, D. Pagani, and M. Melato, "The effects on bone cells of metal ions released from orthopaedic implants. A review," *Clin. Cases Miner. Bone Metab.*, vol. 10, no. 1, pp. 34–40, 2013, doi: 10.11138/ccmbm/2013.10.1.034.

[167] C.-T. Wang, Y.-T. Lin, B.-L. Chiang, S.-S. Lee, and S.-M. Hou, "Over-expression of receptor activator of nuclear factor-kappaB ligand (RANKL), inflammatory cytokines, and chemokines in periprosthetic osteolysis of loosened total hip arthroplasty," *Biomaterials*, vol. 31, no. 1, pp. 77–82, Jan. 2010, doi: 10.1016/j.biomaterials.2009.09.017.

[168] W. P. Zijlstra, S. K. Bulstra, J. J. A. M. van Raay, B. M. van Leeuwen, and R. Kuijer, "Cobalt and chromium ions reduce human osteoblast-like cell activity in vitro, reduce the OPG to RANKL ratio, and induce oxidative stress," *J. Orthop. Res. Off. Publ. Orthop. Res. Soc.*, vol. 30, no. 5, pp. 740–747, May 2012, doi: 10.1002/jor.21581.

[169] F. G. Bauernfeind *et al.*, "Cutting edge: NF-kappaB activating pattern recognition and cytokine receptors license NLRP3 inflammasome activation by regulating NLRP3

expression," *J. Immunol. Baltim. Md 1950*, vol. 183, no. 2, pp. 787–791, Jul. 2009, doi: 10.4049/jimmunol.0901363.

[170] B. Hoesel and J. A. Schmid, "The complexity of NF-κB signaling in inflammation and cancer," *Mol. Cancer*, vol. 12, p. 86, Aug. 2013, doi: 10.1186/1476-4598-12-86.

[171] L. Samelko, S. Landgraeber, K. McAllister, J. Jacobs, and N. J. Hallab, "Cobalt Alloy Implant Debris Induces Inflammation and Bone Loss Primarily through Danger Signaling, Not TLR4 Activation: Implications for DAMP-ening Implant Related Inflammation," *PloS One*, vol. 11, no. 7, p. e0160141, 2016, doi: 10.1371/journal.pone.0160141.

[172] H.-Y. Tan, N. Wang, S. Li, M. Hong, X. Wang, and Y. Feng, "The Reactive Oxygen Species in Macrophage Polarization: Reflecting Its Dual Role in Progression and Treatment of Human Diseases," *Oxidative Medicine and Cellular Longevity*, 2016. https://www.hindawi.com/journals/omcl/2016/2795090/ (accessed Dec. 08, 2019).

[173] R. Zhou, A. S. Yazdi, P. Menu, and J. Tschopp, "A role for mitochondria in NLRP3 inflammasome activation," *Nature*, vol. 469, no. 7329, pp. 221–225, Jan. 2011, doi: 10.1038/nature09663.

[174] R. Allam *et al.*, "Mitochondrial apoptosis is dispensable for NLRP3 inflammasome activation but non-apoptotic caspase-8 is required for inflammasome priming," *EMBO Rep.*, vol. 15, no. 9, pp. 982–990, Sep. 2014, doi: 10.15252/embr.201438463.

[175] C. Strydom, C. Robinson, E. Pretorius, J. M. Whitcutt, J. Marx, and M. S. (Riana) Bornman, "The effect of selected metals on the central metabolic pathways in biology : a review," Oct. 2006, Accessed: Sep. 09, 2019. [Online]. Available: https://repository.up.ac.za/handle/2263/5006.

[176] X. Li and F. Zhong, "Nickel induces interleukin-1β secretion via the NLRP3-ASC-caspase-1 pathway," *Inflammation*, vol. 37, no. 2, pp. 457–466, Apr. 2014, doi: 10.1007/s10753-013-9759-z.

[177] E. PH Chan, A. Mhawi, P. Clode, M. Saunders, and L. Filgueira, "Effects of titanium(iv) ions on human monocyte -derived dendritic cells," *Metallomics*, vol. 1, no. 2, pp. 166–174, 2009, doi: 10.1039/B820871A.

[178] S. L. Sensi *et al.*, "Modulation of mitochondrial function by endogenous Zn2+ pools," *Proc. Natl. Acad. Sci. U. S. A.*, vol. 100, no. 10, pp. 6157–6162, May 2003, doi: 10.1073/pnas.1031598100.

[179] J. Sripetchwandee, J. Sanit, N. Chattipakorn, and S. C. Chattipakorn, "Mitochondrial calcium uniporter blocker effectively prevents brain mitochondrial dysfunction caused by iron overload," *Life Sci.*, vol. 92, no. 4–5, pp. 298–304, 2013, doi: 10.1016/j.lfs.2013.01.004.

[180] E. Naik and V. M. Dixit, "Mitochondrial reactive oxygen species drive proinflammatory cytokine production," *J. Exp. Med.*, vol. 208, no. 3, pp. 417–420, Mar. 2011, doi: 10.1084/jem.20110367.

[181] M. J. López-Armada, R. R. Riveiro-Naveira, C. Vaamonde-García, and M. N. Valcárcel-Ares, "Mitochondrial dysfunction and the inflammatory response," *Mitochondrion*, vol. 13, no. 2, pp. 106–118, Mar. 2013, doi: 10.1016/j.mito.2013.01.003.

[182] Y. Kabe, K. Ando, S. Hirao, M. Yoshida, and H. Handa, "Redox regulation of NF-kappaB activation: distinct redox regulation between the cytoplasm and the nucleus," *Antioxid. Redox Signal.*, vol. 7, no. 3–4, pp. 395–403, Apr. 2005, doi: 10.1089/ars.2005.7.395.

[183] Y. Nonnenmacher and K. Hiller, "Biochemistry of proinflammatory macrophage activation," *Cell. Mol. Life Sci. CMLS*, vol. 75, no. 12, pp. 2093–2109, 2018, doi: 10.1007/s00018-018-2784-1.

[184] O. Warburg, "On the Origin of Cancer Cells," *Science*, vol. 123, no. 3191, pp. 309–314, Feb. 1956, doi: 10.1126/science.123.3191.309.

[185] G. P. Eckert *et al.*, "Mitochondrial Dysfunction—A Pharmacological Target in Alzheimer's Disease," *Mol. Neurobiol.*, vol. 46, no. 1, pp. 136–150, Aug. 2012, doi: 10.1007/s12035-012-8271-z.

[186] Y. Eguchi, S. Shimizu, and Y. Tsujimoto, "Intracellular ATP levels determine cell death fate by apoptosis or necrosis," *Cancer Res.*, vol. 57, no. 10, pp. 1835–1840, May 1997.

[187] A. Vazquez, J. Liu, Y. Zhou, and Z. N. Oltvai, "Catabolic efficiency of aerobic glycolysis: The Warburg effect revisited," *BMC Syst. Biol.*, vol. 4, no. 1, p. 58, May 2010, doi: 10.1186/1752-0509-4-58.

[188] M. V. Liberti and J. W. Locasale, "The Warburg Effect: How Does it Benefit Cancer Cells?," *Trends Biochem. Sci.*, vol. 41, no. 3, pp. 211–218, Mar. 2016, doi: 10.1016/j.tibs.2015.12.001.

[189] D.-Y. Hwang and F. Ismail-Beigi, “Glucose uptake and lactate production in cells exposed to CoCl(2) and in cells overexpressing the Glut-1 glucose transporter,” *Arch. Biochem. Biophys.*, vol. 399, no. 2, pp. 206–211, Mar. 2002, doi: 10.1006/abbi.2002.2758.

[190] Y. Skreb and A. B. Fischer, “Toxicity of nickel for mammalian cells in culture,” *Zentralbl. Bakteriol. Mikrobiol. Hyg. [B]*, vol. 178, no. 5–6, pp. 432–445, Jan. 1984.

[191] S. A. Mookerjee, A. A. Gerencser, D. G. Nicholls, and M. D. Brand, “Quantifying intracellular rates of glycolytic and oxidative ATP production and consumption using extracellular flux measurements,” *J. Biol. Chem.*, vol. 292, no. 17, pp. 7189–7207, Apr. 2017, doi: 10.1074/jbc.M116.774471.

[192] S. A. Mookerjee, D. G. Nicholls, and M. D. Brand, “Determining Maximum Glycolytic Capacity Using Extracellular Flux Measurements,” *PLOS ONE*, vol. 11, no. 3, p. e0152016, Mar. 2016, doi: 10.1371/journal.pone.0152016.

[193] E. Mullarky and L. C. Cantley, “Diverting Glycolysis to Combat Oxidative Stress,” in *Innovative Medicine*, Tokyo, 2015, pp. 3–23, doi: 10.1007/978-4-431-55651-0_1.

[194] Z. Salloum, E. A. Lehoux, I. Catelas, and M.-E. Harper, “Effects of cobalt and chromium ions on glycolytic flux and the stabilization of hypoxia-inducible factor-1α in macrophages in vitro.,” *Journal of Orthopaedic Research*, In Press.

[195] “ToxinSensorTM Chromogenic LAL Endotoxin Assay Kit Kit - GenScript.” https://www.genscript.com/kit/L00350-ToxinSensor_sup_TM_sup_Chromogenic_LAL_Endotoxin_Assay_Kit.html (accessed Oct. 24, 2019).

[196] M.-A. Ferko and I. Catelas, “Effects of metal ions on caspase-1 activation and interleukin-1β release in murine bone marrow-derived macrophages,” *PLOS ONE*, vol. 13, no. 8, p. e0199936, Aug. 2018, doi: 10.1371/journal.pone.0199936.

[197] S. A. Mookerjee, R. L. S. Goncalves, A. A. Gerencser, D. G. Nicholls, and M. D. Brand, “The contributions of respiration and glycolysis to extracellular acid production,” *Biochim. Biophys. Acta*, vol. 1847, no. 2, pp. 171–181, Feb. 2015, doi: 10.1016/j.bbabio.2014.10.005.

[198] J. Traba, P. Miozzo, B. Akkaya, S. K. Pierce, and M. Akkaya, “An Optimized Protocol to Analyze Glycolysis and Mitochondrial Respiration in Lymphocytes,” *J. Vis. Exp. JoVE*, no. 117, Nov. 2016, doi: 10.3791/54918.

[199] A. Serguienko *et al.*, "Metabolic reprogramming of metastatic breast cancer and melanoma by let-7a microRNA," *Oncotarget*, vol. 6, no. 4, pp. 2451–2465, Dec. 2014.

[200] M. A. Fath, A. R. Diers, N. Aykin-Burns, A. L. Simons, L. Hua, and D. R. Spitz, "Mitochondrial electron transport chain blockers enhance 2-deoxy-D-glucose induced oxidative stress and cell killing in human colon carcinoma cells," *Cancer Biol. Ther.*, vol. 8, no. 13, pp. 1228–1236, Jul. 2009, doi: 10.4161/cbt.8.13.8631.

[201] "Thermo Scientific/Pierce, Instructions: Coomassie (Bradford) Protein Assay Kit (catalog no. 23200)." Thermo Scientific/Pierce.

[202] N. Romero, P. Swain, A. Neilson, and B. P. Dranka, "Improving Quantification of Cellular Glycolytic Rate Using Agilent Seahorse XF Technology." Agilent Technologies, Inc., Mar. 01, 2017.

[203] "Seahorse XF Buffer Factor Protocol Quick Reference Guide," p. 24.

[204] R. J. Mailloux and M.-E. Harper, "Glucose regulates enzymatic sources of mitochondrial NADPH in skeletal muscle cells; a novel role for glucose-6-phosphate dehydrogenase," *FASEB J.*, vol. 24, no. 7, pp. 2495–2506, Mar. 2010, doi: 10.1096/fj.09-151803.

[205] D. Kong *et al.*, "Glucose Stimulation of Hypothalamic MCH Neurons Involves KATP Channels, Is Modulated by UCP2, and Regulates Peripheral Glucose Homeostasis," *Cell Metab.*, vol. 12, no. 5, pp. 545–552, Nov. 2010, doi: 10.1016/j.cmet.2010.09.013.

[206] R. J. Mailloux *et al.*, "Glutathionylation State of Uncoupling Protein-2 and the Control of Glucose-stimulated Insulin Secretion," *J. Biol. Chem.*, vol. 287, no. 47, pp. 39673–39685, Nov. 2012, doi: 10.1074/jbc.M112.393538.

[207] D. P. Jones *et al.*, "Glutathione measurement in human plasma: Evaluation of sample collection, storage and derivatization conditions for analysis of dansyl derivatives by HPLC," *Clin. Chim. Acta*, vol. 275, no. 2, pp. 175–184, Jul. 1998, doi: 10.1016/S0009-8981(98)00089-8.

[208] L. H. Lash and D. P. Jones, "Distribution of oxidized and reduced forms of glutathione and cysteine in rat plasma," *Arch. Biochem. Biophys.*, vol. 240, no. 2, pp. 583–592, Aug. 1985, doi: 10.1016/0003-9861(85)90065-7.

[209] L. Manna, L. Valvo, and P. Betto, "Determination of oxidized and reduced glutathione in pharmaceuticals by reversed-phase high-performance liquid chromatography with dual

electrochemical detection," *J. Chromatogr. A*, vol. 846, no. 1, pp. 59–64, Jun. 1999, doi: 10.1016/S0021-9673(99)00427-6.

[210] C. N.-K. Adjeitey, R. J. Mailloux, R. A. deKemp, and M.-E. Harper, "Mitochondrial uncoupling in skeletal muscle by UCP1 augments energy expenditure and glutathione content while mitigating ROS production," *Am. J. Physiol. - Endocrinol. Metab.*, vol. 305, no. 3, pp. E405–E415, Aug. 2013, doi: 10.1152/ajpendo.00057.2013.

[211] A. B. Thrush *et al.*, "Lower Mitochondrial Proton Leak and Decreased Glutathione Redox in Primary Muscle Cells of Obese Diet-Resistant Versus Diet-Sensitive Humans," *J. Clin. Endocrinol. Metab.*, vol. 99, no. 11, pp. 4223–4230, Nov. 2014, doi: 10.1210/jc.2014-1726.

[212] Z. Salloum, "Effects of Metal Ions Released from Implants on Energy Metabolism in Macrophages," University of Ottawa, Ottawa, ON, 2020.

[213] L. C. Davies, C. M. Rice, E. M. Palmieri, P. R. Taylor, D. B. Kuhns, and D. W. McVicar, "Peritoneal tissue-resident macrophages are metabolically poised to engage microbes using tissue-niche fuels," *Nat. Commun.*, vol. 8, no. 1, Dec. 2017, doi: 10.1038/s41467-017-02092-0.

[214] A. Guentsch *et al.*, "PHD2 Is a Regulator for Glycolytic Reprogramming in Macrophages," *Mol. Cell. Biol.*, vol. 37, no. 1, Dec. 2016, doi: 10.1128/MCB.00236-16.

[215] J. V. den Bossche, J. Baardman, and M. P. J. de Winther, "Metabolic Characterization of Polarized M1 and M2 Bone Marrow-derived Macrophages Using Real-time Extracellular Flux Analysis," *JoVE J. Vis. Exp.*, no. 105, pp. e53424–e53424, Nov. 2015, doi: 10.3791/53424.

[216] S. A. Mookerjee, A. A. Gerencser, D. G. Nicholls, and M. D. Brand, "Quantifying intracellular rates of glycolytic and oxidative ATP production and consumption using extracellular flux measurements," *J. Biol. Chem.*, vol. 292, no. 17, pp. 7189–7207, Apr. 2017, doi: 10.1074/jbc.M116.774471.

[217] H. Arnott, M.-E. Harper, and I. Catelas, "Effects of cobalt, chromium and nickel ions on oxidative energy metabolism in murine bone marrow-derived macrophages," *34th Annual Meeting of the Canadian Biomaterial Society*, Victoria, BC, Canada, 2018.

[218] I. Catelas, H. Arnott, K. Wilson, E. A. Lehoux, and M.-E. Harper, “Effects of Cobalt Ions on Energy Metabolism in Murine Bone Marrow-Derived Macrophages,” *Orthopaedic Research Society (ORS) 2019 Annual Meeting*, Austin, TX, USA, 2019.

[219] “Agilent Seahorse XF Instruments Overview and Selection Guide | Agilent.” https://www.agilent.com/en/products/cell-analysis/seahorse-xf-instruments-selection-guide (accessed Nov. 13, 2019).

[220] B. A. Fensterheim *et al.*, “The TLR4 Agonist Monophosphoryl Lipid A Drives Broad Resistance to Infection via Dynamic Reprogramming of Macrophage Metabolism,” *J. Immunol.*, vol. 200, no. 11, pp. 3777–3789, Jun. 2018, doi: 10.4049/jimmunol.1800085.

[221] S. Pavlou, J. Lindsay, R. Ingram, H. Xu, and M. Chen, “Sustained high glucose exposure sensitizes macrophage responses to cytokine stimuli but reduces their phagocytic activity,” *BMC Immunol.*, vol. 19, no. 1, p. 24, Jul. 2018, doi: 10.1186/s12865-018-0261-0.

[222] P. Leroy, A. Nicolas, C. Thioudellet, T. Oster, M. Wellman, and G. Siest, “Rapid liquid chromatographic assay of glutathione in cultured cells,” *Biomed. Chromatogr.*, vol. 7, no. 2, pp. 86–89, Mar. 1993, doi: 10.1002/bmc.1130070208.

[223] L. A. Ridnour, R. A. Winters, N. Ercal, and D. R. Spitz, “[22] Measurement of glutathione, glutathione disulfide, and other thiols in mammalian cell and tissue homogenates using high-performance liquid chromatography separation of N-(1-pyrenyl)maleimide derivatives,” in *Methods in Enzymology*, vol. 299, Academic Press, 1999, pp. 258–267.

[224] V. Sutariya, D. Wehrung, and W. J. Geldenhuys, “Development and Validation of a Novel RP-HPLC Method for the Analysis of Reduced Glutathione,” *J. Chromatogr. Sci.*, vol. 50, no. 3, pp. 271–276, Mar. 2012, doi: 10.1093/chromsci/bmr055.

[225] M. Afzal, A. Afzal, A. Jones, and D. Armstrong, “A Rapid Method for the Quantification of GSH and GSSG in Biological Samples,” in *Oxidative Stress Biomarkers and Antioxidant Protocols*, D. Armstrong, Ed. Totowa, NJ: Humana Press, 2002, pp. 117–122.

[226] D. Lipsa, C. Cacho, P. de Leva, J. Barrero-Moreno, and P. Aguar, “Development of a HPLC-UV method for the simultaneous determination of intracellular glutathione species in human cells,” 2015, doi: 10.4172/2155-9872.1000259.

[227] J. Sian, D. T. Dexter, G. Cohen, P. G. Jenner, and C. D. Marsden, “Comparison of HPLC and Enzymatic Recycling Assays for the Measurement of Oxidized Glutathione in Rat

Brain," *J. Pharm. Pharmacol.*, vol. 49, no. 3, pp. 332–335, doi: 10.1111/j.2042-7158.1997.tb06807.x.

[228] D. J. Langton *et al.*, "Accelerating failure rate of the ASR total hip replacement," *J. Bone Joint Surg. Br.*, vol. 93-B, no. 8, pp. 1011–1016, Aug. 2011, doi: 10.1302/0301-620X.93B8.26040.

[229] A. Hartmann *et al.*, "Metal ion concentrations in body fluids after implantation of hip replacements with metal-on-metal bearing--systematic review of clinical and epidemiological studies," *PloS One*, vol. 8, no. 8, p. e70359, 2013, doi: 10.1371/journal.pone.0070359.

[230] V. J. Rasquinha, C. S. Ranawat, J. Weiskopf, J. A. Rodriguez, A. K. Skipor, and J. J. Jacobs, "Serum metal levels and bearing surfaces in total hip arthroplasty," *J. Arthroplasty*, vol. 21, no. 6 Suppl 2, pp. 47–52, Sep. 2006, doi: 10.1016/j.arth.2006.05.005.

[231] E. A. Phillips, G. R. Klein, H. E. Cates, S. M. Kurtz, and M. Steinbeck, "Histological Characterization of Periprosthetic Tissue Responses for Metal-on-Metal Hip Replacement," *J. Long. Term Eff. Med. Implants*, vol. 24, no. 1, 2014, doi: 10.1615/JLongTermEffMedImplants.2014010275.

[232] S. M. Horowitz, S. B. Doty, J. M. Lane, and A. H. Burstein, "Studies of the mechanism by which the mechanical failure of polymethylmethacrylate leads to bone resorption," *J. Bone Joint Surg. Am.*, vol. 75, no. 6, pp. 802–813, Jun. 1993, doi: 10.2106/00004623-199306000-00002.

[233] R. S. Bockman, "Prostaglandin production by human blood monocytes and mouse peritoneal macrophages : Synthesis dependent on in vitro culture conditions," *Prostaglandins*, vol. 21, no. 1, pp. 9–31, Jan. 1981, doi: 10.1016/0090-6980(81)90192-1.

[234] M. Stubbs, A. V. Kühner, E. A. Glass, J. R. David, and M. L. Karnovsky, "METABOLIC AND FUNCTIONAL STUDIES ON ACTIVATED MOUSE MACROPHAGES," *J. Exp. Med.*, vol. 137, no. 2, pp. 537–542, Jan. 1973.

[235] L. Liu *et al.*, "Proinflammatory signal suppresses proliferation and shifts macrophage metabolism from Myc-dependent to HIF1α-dependent," *Proc. Natl. Acad. Sci.*, vol. 113, no. 6, pp. 1564–1569, Feb. 2016, doi: 10.1073/pnas.1518000113.

[236] S. Galván-Peña and L. A. J. O'Neill, "Metabolic reprograming in macrophage polarization," *Front. Immunol.*, vol. 5, p. 420, 2014, doi: 10.3389/fimmu.2014.00420.

[237] A. J. Freemerman *et al.*, "Metabolic reprogramming of macrophages: glucose transporter 1 (GLUT1)-mediated glucose metabolism drives a proinflammatory phenotype," *J. Biol. Chem.*, vol. 289, no. 11, pp. 7884–7896, Mar. 2014, doi: 10.1074/jbc.M113.522037.

[238] A. Bordbar *et al.*, "Model-driven multi-omic data analysis elucidates metabolic immunomodulators of macrophage activation," *Mol. Syst. Biol.*, vol. 8, p. 558, Jun. 2012, doi: 10.1038/msb.2012.21.

[239] D. Schubert, T. Soucek, and B. Blouw, "The induction of HIF-1 reduces astrocyte activation by amyloid beta peptide," *Eur. J. Neurosci.*, vol. 29, no. 7, pp. 1323–1334, Apr. 2009, doi: 10.1111/j.1460-9568.2009.06712.x.

[240] I. F. Scheiber and R. Dringen, "Copper accelerates glycolytic flux in cultured astrocytes," *Neurochem. Res.*, vol. 36, no. 5, pp. 894–903, May 2011, doi: 10.1007/s11064-011-0419-0.

[241] C. A. Janson and W. W. Cleland, "The inhibition of acetate, pyruvate, and 3-phosphogylcerate kinases by chromium adenosine triphosphate," *J. Biol. Chem.*, vol. 249, no. 8, pp. 2567–2571, Apr. 1974.

[242] M. G. Permenter, J. A. Lewis, and D. A. Jackson, "Exposure to nickel, chromium, or cadmium causes distinct changes in the gene expression patterns of a rat liver derived cell line," *PloS One*, vol. 6, no. 11, p. e27730, 2011, doi: 10.1371/journal.pone.0027730.

[243] G. L. Semenza, P. H. Roth, H. M. Fang, and G. L. Wang, "Transcriptional regulation of genes encoding glycolytic enzymes by hypoxia-inducible factor 1," *J. Biol. Chem.*, vol. 269, no. 38, pp. 23757–23763, Sep. 1994.

[244] S. E. Corcoran and L. A. J. O'Neill, "HIF1α and metabolic reprogramming in inflammation," *J. Clin. Invest.*, vol. 126, no. 10, pp. 3699–3707, 03 2016, doi: 10.1172/JCI84431.

[245] D. G. Hardie, F. A. Ross, and S. A. Hawley, "AMPK: a nutrient and energy sensor that maintains energy homeostasis," *Nat. Rev. Mol. Cell Biol.*, vol. 13, no. 4, pp. 251–262, Mar. 2012, doi: 10.1038/nrm3311.

[246] F. S. Sutterwala, S. Haasken, and S. L. Cassel, "Mechanism of NLRP3 inflammasome activation," *Ann. N. Y. Acad. Sci.*, vol. 1319, no. 1, pp. 82–95, Jun. 2014, doi: 10.1111/nyas.12458.

Appendix

CO_2 Contribution Factor (CCF)

In order to determine the EA coming from glycolysis through the production of lactate and H^+, contributions to EA from mitochondrial CO_2 production should be corrected for. Therefore, three CO_2 contribution factor (CCF) experiments were performed with no ions, 6-24 ppm Co^{2+}, 50-200 ppm Cr^{3+}, 12-96 ppm Ni^{2+} or 1 μg/mL LPS in BMDMs. The CCF experiment determines the contribution to EA from mitochondrial-derived CO_2 which produces H^+ and HCO_3 via the TCA-cycle. The experiments were performed as described for the ECAR experiments (above) with the exception that it follows a modified injection strategy [202] and the assay medium was supplemented with Sodium Pyruvate (Sigma-Aldrich) [202]. CCF experiments were also seeded at 90,000 BMDMs/well in tissue culture-treated polystyrene 96-well microplates (Seahorse XFe96 V3 PS Cell Culture Microplates; Agilent Technologies, Santa Clara, CA). The assay medium was prepared twice exactly as described for ECAR (above) with the addition of Sodium Pyruvate (1 mM final concentration; Sigma-Aldrich): half of the medium was prepared for Co^{2+} and Ni^{2+} samples with a final concentration of 2 mM HEPES and half of the medium was prepared for Cr^{3+} samples with a final concentration of 5 mM HEPES. During the assay oligomycin (1 μM final concentration; Sigma-Aldrich), CCCP (2.5 μM; Sigma-Aldrich) and, rotenone and antimycin A (1.5 μM each; Sigma-Aldrich) were injected sequentially.

CCF Supplemental Information

Supplementary Table 1: CO_2 Contribution Factor (CCF) results for experiments with Co^{2+}, Ni^{2+} and Cr^{3+}.

	Experiment #1		Experiment #2		Experiment #3	
Condition	Average CCF	Standard Deviation	Average CCF	Standard Deviation	Average CCF	Standard Deviation
0 ppm	0.44	0.08	0.94	0.08	0.79	0.11
6 ppm Co^{2+}	0.62	0.01	1.20	0.12	0.79	0.20
12 ppm Co^{2+}	0.59	0.05	0.80	0.28	0.90	0.22
18 ppm Co^{2+}	0.44	0.08	1.21	0.16	0.87	0.24
24 ppm Co^{2+}	0.38	0.15	1.08	0.04	0.84	0.19
12 ppm Ni^{2+}	0.50	0.05	1.07	0.13	0.70	0.28
24 ppm Ni^{2+}	0.56	0.15	1.20	0.13	1.40	0.79
48 ppm Ni^{2+}	0.72	0.02	1.36	0.23	1.73	0.53
96 ppm Ni^{2+}	0.66	0.09	1.59	0.20	1.13	0.60
Condition	Average CCF	Standard Deviation				
0 ppm	0.32	0.03				
50 ppm Cr^{3+}	0.29	0.03				
100 ppm Cr^{3+}	0.29	0.06				
150 ppm Cr^{3+}	0.34	0.02				
200 ppm Cr^{3+}	0.35	0.03				

The CCF values for Cr^{3+} had a low standard deviation and comparable values for all concentrations. Therefore, these conditions were not repeated in experiments #2 and #3. However, further investigation revealed that none of the values were within the expected range of 0.60-0.81, and reproducibility was a fundamental problem for the CCF assay as determined by the manufacturer (Agilent).